Altered Mitochondrial Dynamics in a Novel Cellular Model of Leber Hereditary Optic Neuropathy (LHON)

by

Kolitha Halangoda

B.Sc. (Hons.), Simon Fraser University, 2014

Thesis Submitted in Partial Fulfillment of the
Requirements for the Degree of
Master of Science

in the
Department of Biological Sciences
Faculty of Science

SIMON FRASER UNIVERSITY
Summer 2018

Approval

Name:	**Kolitha Halangoda**
Degree:	**Master of Science (Biological Sciences)**
Title:	**Altered Mitochondrial Dynamics in a Novel Cellular Model of Leber Hereditary Optic Neuropathy (LHON)**
Examining Committee:	**Chair: Leah Bendell** Professor
	Gordon Rintoul Senior Supervisor Associate Professor
	Claire Sheldon Supervisor Clinical Assistant Professor Ophthalmology and Neuro-Ophthalmology The University of British Columbia
	Damon Poburko Supervisor Assistant Professor Department of Biomedical Physiiology and Kinesiology
	Christopher Beh Internal Examiner Associate Professor Department of Molecular Biology and Biochemistry
Date Defended/Approved:	July 11, 2018

Ethics Statement

The author, whose name appears on the title page of this work, has obtained, for the research described in this work, either:

a. human research ethics approval from the Simon Fraser University Office of Research Ethics

or

b. advance approval of the animal care protocol from the University Animal Care Committee of Simon Fraser University

or has conducted the research

c. as a co-investigator, collaborator, or research assistant in a research project approved in advance.

A copy of the approval letter has been filed with the Theses Office of the University Library at the time of submission of this thesis or project.

The original application for approval and letter of approval are filed with the relevant offices. Inquiries may be directed to those authorities.

Simon Fraser University Library
Burnaby, British Columbia, Canada

Update Spring 2016

Abstract

Leber Hereditary Optic Neuropathy (LHON) is a disease that is caused by mutations in mitochondrial DNA resulting in vision loss due to retinal ganglion cell (RGC) degeneration. The exact pathophysiological mechanism causing RGC degeneration is poorly understood. This is partly due to a lack of a suitable model system. We created a novel cellular model for investigating mitochondrial dynamics in LHON by treating human dermal fibroblasts carrying the most prevalent G11778A LHON mutation with staurosporine (STSP). This treatment induced cytoplasmic protrusions resembling neurites. Mitochondrial movement was impaired in LHON fibroblasts compared to wild-type fibroblasts under conditions that induce oxidative phosphorylation (OXPHOS) but could not be attributed to reduced cytosolic ATP levels. Furthermore, LHON fibroblasts displayed altered mitochondrial network remodeling under conditions that induced OXPHOS. Our results demonstrate altered mitochondrial dynamics in LHON fibroblasts which may have implications in the pathogenesis of LHON in RGCs.

Keywords: LHON G11778A; fibroblasts; staurosporine; cell model; mitochondrial dynamics; ATP

Dedication

To my mom and dad, for all your sacrifices and hard work to provide me with a better future. Thank you for always being supportive in all my endeavours.

Acknowledgements

I would like to thank my senior supervisor, Dr. Gordon Rintoul, for granting me the opportunity to pursue my master's degree under his supervision, for providing support and guidance over the course of my degree and making graduate school an enjoyable experience. I would also like to thank Dr. Claire Sheldon and Dr. Damon Poburko for being part of my supervisory committee and for their invaluable feedback and advice. Thank you to Dr. Chris Beh for accepting to be my internal examiner and to Dr. Leah Bendell for agreeing to Chair my defence.

A big thank you goes to Bryce Pasqualotto who has spent countless number of hours training me in laboratory techniques, answering questions, troubleshooting equipment and software issues and editing my thesis. Thank you so much for your support as well as for making my time in the Rintoul lab so much more enjoyable. I also wish to extend my gratitude to former members of the Rintoul lab, Dr. Samineh Deheshi, Priye Iworima and Alexa Nelson for their support over the course of my degree.

I wish to convey my gratitude to Dr. Melanie Hart for being a mentor to me, for clearing the path to my journey into graduate studies and for the continuous support I received throughout the past few years.

I would like to acknowledge Ryan Thomas from the Kermode lab, Priyanka Aggarwal and Michael Chua from the Guttman lab, Asim Renyard from the Gries lab and Lydia BaRun Kim from the Poburko lab for their help, advice and friendship.

Furthermore, I am grateful to the Canadian Institute of Health Research and the Department of Graduate Studies at Simon Fraser University for the financial support I received over the course of my studies. I also wish to express my appreciation to our graduate program assistant Marlene Nguyen for her help and guidance.

Finally, I would like to thank my wonderful parents and my sister for their love, strength and support. And to Natasha Nawaratne, for encouraging me and being by my side through all my ups and downs.

Table of Contents

List of Figures

List of Acronyms

AD	Alzheimer's disease
ADP	Adenosine diphosphate
AIF	Apoptosis inducing factor
ALS	Amyotrophic lateral sclerosis
APP	Amyloid precursor protein
Ateam	Adenosine 5' triphosphate indicator based on epsilon subunit for analytical measurement
ATP	Adenosine triphosphate
Aβ	Amyloid beta
CFP	Cyan fluorescent protein
CMT	Charcot-Marie-Tooth disease
CPEO	Chronic progressive external ophthalmoplegia
CrP	Creatinine phosphate
DOA	Dominant optic atrophy
DRG	Dorsal root ganglion
DRP1	Dynamin related protein 1
EBV	Epstein-Barr virus
Endo-G	Endonuclease G
ERG	Electroretinogram
ERK 1/2	Extracellular signal-regulated kinase 1/2
ETC	Electron transport chain
FRET	Fluorescence resonance energy transfer
GPx	Glutathione peroxidase
GR	Glutathione reductase
hFIS1	Human fission protein 1
HTT	Huntingtin protein
KIF	Kinesin family protein
KSS	Kearns-Sayre syndrome
LC3	Microtubule-associated protein 1A/1B-light chain 3
LHON	Leber hereditary optic neuropathy
MELAS	Mitochondrial encephalomyopathy, lactic acidosis and stroke like episodes

MERFF	Myoclonic epilepsy and ragged red fibers
MFF	Mitochondrial fission factor
MFN	Mitofusin
MiD49/50	Mitochondrial dynamics protein
MiNA	Mitochondrial network analysis toolset
MIRO	Mitochondrial rho
MnSOD	Manganese-superoxide dismutase
mPTP	Mitochondrial permeability transition pore
mRNA	Messenger ribonucleic acid
mtDNA	Mitochondrial deoxyribonucleic acid
Mt-eYFP	Mitochondrially-targeted enhanced yellow fluorescent protein
NARP	Neuropathy, ataxia, and retinitis pigmentosa
NDUFA1	NADH:ubiquinone oxidoreductase subunit A1
NIX	NIP3-like protein X
NT2	Ntera-2/D1 human teratocarcinoma
OCT	Optic coherence tomography
OPA1	Optic atrophy protein 1
OXPHOS	Oxidative phosphorylation
PARL	Presenilin-associated rhomboid-like
PC-12	Rat pheochromocytoma cells
PD	Parkinson’s disease
PINK1	PTEN-induced kinase 1
PKC	Protein kinase C
PMB	Papillomacular bundle
PTEN	Phosphatase and tensin homolog
RGC	Retinal ganglion cells
RGC-5	661W mouse cone photoreceptor cell
RNFL	Retinal nerve fiber layer
ROS	Reactive oxygen species
SCLC	Small cell lung carcinoma
SOD2	Superoxide dismutase 2
sORF	Short open reading frame
STSP	Staurosporine
TRAK	Trafficking kinesin protein

tRNA	Transfer ribonucleic acid
VEP	Visual evoked potential
YME1L1	YME1 like 1 ATPase

Chapter 1. Introduction

1.1. Mitochondrion

Mitochondria are organelles in eukaryotic cells which convert fuels into ATP through the process of oxidative phosphorylation (Taanman, 1999). A mitochondrion contains an inner and outer membrane that separates it into two compartments; the intermembrane space and the matrix. The outer membrane separates the mitochondrion from the cytosol. The inner membrane is highly folded into cristae and is where the five enzyme complexes of the oxidative phosphorylation system are embedded (Taanman, 1999; McBride et al., 2006). Mitochondria form a functional reticulum whose steady-state morphology is regulated by dynamic fission, fusion and motility events (McBride et al., 2006). The mitochondrion has its own genome which is present within the mitochondrial matrix. In mammalian cells, each organelle generally contains several identical copies of mitochondrial DNA (mtDNA) (Michaels et al., 1982; Shuster et al., 1988). In addition to its primary role in ATP production, mitochondria also play important roles in calcium homeostasis (Vandecasteele et al., 2002), apoptosis (Wang and Youle, 2009), synthesis of steroids (Miller, 1995), synthesis of heme groups and iron-sulphur clusters (Ponka, 1999; Lill and Kispal, 2000), neurotransmitter metabolism (Schousboe et al., 2013), thermogenesis (Nedergaard and Cannon, 1992), and detoxification of ammonia in the urea cycle (Meijer et al., 1990).

1.1.1. Origin

Mitochondria evolved from free living bacteria through symbiosis within a host cell considered to be the predecessor of the modern eukaryotic cell. The presence of its own genome and own translation system, which is distinct from its host was what lead to the initial hypothesis that has now been confirmed by detailed characterization of the mitochondrial genome. The mitochondrial genome shows considerable variation in size, physical form, coding capacity, organization patterns and modes of expression across the eukaryotic domain (Gray, 2012). In some non-animal species additional proteins are encoded in mtDNA and in others many of the protein coding genes and tRNA genes are lost. Ribosomal RNA genes are among the few genes that were universally encoded by mtDNA across all eukaryotes and these genes were important in determining the

evolutionary origin of mitochondria (Gray, 2012). Detailed molecular, genetic and phylogenetic studies pointed to the α-proteobacteria as the specific bacterial lineage from within which they originated (Yang et al., 1985).This affiliation has been confirmed by subsequent studies which also pointed to the *Rickettsiales*, an order within *alphaproteobacteria* as being the closest relatives of mitochondria (Gray, 1998; Williams et al., 2007). Mitochondria have lost many of their original functions during evolution due to loss or transfer of genes from mitochondria to the nucleus. Many of the proteins of the mitochondrial ancestor have been replaced by host derived proteins with the exception of proteins involved in translation and energy conversion (Gabaldón and Huynen, 2007).

1.1.2. Mitochondrial Genome

Mitochondrial DNA of animal cells represent <1 % of the total cellular DNA (Clayton, 1982). The structure and gene organization of mtDNA is highly conserved among mammals. Human mitochondrial DNA is a closed circular, double stranded DNA molecule of approximately 16,569 base pairs in size and consists of 37 genes (Taanman, 1999). Out of the 37 genes, twenty two genes encode transfer RNAs and two specify ribosomal RNA while the remaining 13 genes encode polypeptides that are components of the oxidative phosphorylation mechanism (Schon, 2000).The mtDNA duplex is composed of a light and a heavy chain, distinguished on the basis of the G+T composition of the two strands (Kasamatsu and Vinograd, 1974). Two rRNAs, 14 tRNAs and 12 polypeptides are encoded by genes on the heavy strand. The light strand only codes for eight tRNAs and a single polypeptide (Taanman, 1999). The mitochondrial genome is quite compact in its organization. Except for a single regulatory region, the genes lack introns and intergenic regions are either absent or limited to a few bases (Wolstenholme, 1992). Overlapping genes and termination codons, generated post-transcriptionally by polyadenylation of the mRNAs, are some of the ways in which this compaction is achieved (Ojala et al., 1981). The previously held view that the mitochondrial genome only possesses 13 protein coding genes has been challenged by recent discoveries of novel peptides encoded by the mtDNA (Shokolenko and Alexeyev, 2015). Humanin and MOTS-c (mitochondrial ORF of the twelve S c) are two such peptides that are located within the mitochondrial 16s rRNA and 12s rRNA sequences respectively (Hashimoto et al., 2001; Guo et al., 2003; Ikonen et al., 2003; Lee et al., 2015). Humanin appears to enhance cellular and organismal protection from stress or

disease states whereas MOTS-c target to skeletal muscle and enhance glucose metabolism (Lee et al., 2016). The identification of these short open reading frames (sORFs) indicates a larger mitochondrial genetic repertoire than previously known.

The mitochondrial genome is self-replicating and the genetic code differs from the nuclear genetic code. For instance, the TGA codon, which is a termination codon in the nuclear genetic code translates to a tryptophan in mtDNA of most phylogenetic groups. The mitochondrial genetic code varies even among species (Anderson et al., 1981; Osawa et al., 1992). The AGR (R= A, G) specifies a stop codon in mtDNA of vertebrates but translates to a serine in echinoderms and arginine in mtDNA of yeast just as in the nuclear genetic code (Osawa et al., 1992). The mitochondria also possess a simplified decoding system where the 22 tRNA species encoded by human mtDNA are able to translate all 13 mitochondrial protein genes (Osawa et al., 1992).

Mitochondria rely upon nuclear encoded factors for its function. All except two ribosomal proteins are nuclear encoded as are some of the enzyme complexes of the OXPHOS system. Enzymes of the various catabolic pathways as well as components of the mitochondrial import machinery are encoded by nuclear DNA (Ryan and Jensen, 1995). These are all synthesized by cytosolic ribosomes, with a cleavable mitochondrial target sequence in the N terminal region for subsequent import into the mitochondria (Ryan and Jensen, 1995).

Mitochondrial DNA in humans is maternally inherited with little to no contributions of mtDNA from the paternal lineage (Giles et al., 1980; Case and Wallace, 1981). Recent studies have found that sperm-derived mitochondria are degraded inside the fertilized oocyte by the autophagic pathway and ubiquitin-proteasome-dependent proteolysis in mammals, including humans (Song et al., 2014).

1.2. Mitochondrial dynamics

Formerly thought of as rigid and solitary structures mitochondria are now known as dynamic organelles that migrate throughout the cell, fuse and divide and undergo regulated turnover (Chen and Chan, 2009). The processes of mitochondrial movement, fission, fusion and recycling are collectively termed mitochondrial dynamics. These dynamic processes allow mitochondria to respond and adapt to changes in the cellular

environment. Therefore, preserving mitochondrial dynamics is crucial for cellular health. The importance of mitochondrial dynamics is evident in all cells but none more so than neurons. Neurons are polarized cells that typically consist of the cell body (soma), a long axon and multiple dendrites. Each of these domains are structurally and functionally distinct and therefore the mitochondrial distribution in each domain varies (Sheng and Cai, 2012). Studies done on neurons have provided key insights into understanding mitochondrial dynamics and its importance in cellular health (Chen and Chan, 2009; Sheng and Cai, 2012; Schwarz, 2013).

1.2.1. Mitochondrial Movement

It is necessary for mitochondria to travel to regions of high energetic demand and this may require long-range movement in certain neurons that extend their axons up to millimeters, centimeters or even a meter in length. Presynaptic and postsynaptic terminals, active growth cones and nodes of Ranvier are areas within an axon that have a high ATP demand and therefore the density of mitochondria in these regions are much higher compared to other regions (Fabricius et al., 1993; Morris and Hollenbeck, 1993; Li et al., 2004). Despite the ability to be produced locally within axons, it is thought that most mitochondrial biogenesis as well as degradation of dysfunctional mitochondria takes place in the cell body (soma), which necessitates long-range movement of mitochondria (Sheng and Cai, 2012). Movement of mitochondria involves the interplay between the three different groups of proteins; the cytoskeletal elements, the molecular motor proteins and adaptor proteins. Components of the cytoskeleton such as microtubules and actin serve as the track on which mitochondria are transported. Microtubules are polarized structures made from the polymerization of α and β tubulin. α and β tubulin dimerize and align end to end to form a protofilament. Thirteen laterally associated protofilaments form a microtubule (Downing and Nogales, 1998). On one end of the microtubule is an exposed α subunit known as the minus end while the end with a β subunit exposed is the plus end (Chevalier-Larsen and Holzbaur, 2006). In axons of neurons, the microtubules are oriented with their minus ends directed towards the soma and plus ends directed towards the distal tips (Schwarz, 2013).

Kinesin superfamily proteins (KIFs) and cytoplasmic dynein are the main microtubule-based motor proteins that drive long distance transport of mitochondria and other membrane bound organelles (Sheng and Cai, 2012). Most KIFs move towards the

plus end of microtubules while cytoplasmic dynein move towards the minus end (Vale, 2003). Therefore, in the axon where microtubules have a uniform minus to plus arrangement from the soma to the distal synapses, KIFs drive transport away from soma (anterograde) whereas cytoplasmic dynein drive transport towards the soma (retrograde) (Martin et al., 1999; Hirokawa et al., 2010). Dendrites in comparison have a mixed polarity of microtubules and therefore both KIFs and dynein can move either to or away from the soma depending on the orientation of the microtubule that the motor is attached to (Hirokawa and Takemura, 2004). Members of kinesin-1 family (KIF5) drive anterograde transport of axonal mitochondria (Tanaka et al., 1998; Pilling et al., 2006). KIF5 consists of three different isoforms in mammals, namely KIF5A, KIF5B and KIF5C (Aizawa et al., 1992; Meng et al., 1997; Kanai et al., 2000). KIF5A and KIF5C are only expressed in neurons whereas KIF5B is expressed in most cell types (Kanai et al., 2000). KIF5 has an amino terminal motor domain and a carboxy terminal domain that either associates with kinesin light chains or with cargo or cargo adaptors (Seog et al., 2004). Cytoplasmic dynein is composed of two dynein heavy chains that function as the motor and several dynein intermediate chains, dynein light intermediate chains and dynein light chains (Oiwa and Sakakibara, 2005). The mechanism of how dynein binds to mitochondria is not well characterized but involves various other polypeptides (Sheng and Cai, 2012). Mitochondria are also capable of movement on actin filaments albeit over short distances using myosin motors (Langford, 1995). Actin filaments are present in growth cones, presynaptic terminals and dendritic spines (Sheng and Cai, 2012).

Mitochondria bind to motors via adaptor proteins and these adaptor proteins play a crucial role in regulating mitochondrial movement. The protein Milton is a well characterized adaptor protein involved in mitochondrial binding to Kif5 in *D.melanogaster* neurons (Stowers et al., 2002). Milton binds to mitochondria through mitochondrial rho (Miro), a RHO family GTPase that is present in the mitochondrial outer membrane (Glater et al., 2006). Thus, Kif5, Milton and Miro make up the anterograde transport system of mitochondria (Sheng and Cai, 2012). Mammals possess two Milton orthologues; TRAK1 (OIP106) and TRAK2 (GRIF1) and two MIRO orthologues; MIRO1 and MIRO2 all of which are important components in organelle trafficking (Brickley et al., 2005; Fransson et al., 2006). The Milton/Miro complex also interacts with Dynein and therefore is important for dynein-mediated transport as well (Schwarz, 2013).

1.2.2. Fission and Fusion

Mitochondrial fission and fusion are processes that are important for mitochondrial quality control. Mitochondrial quality control prevents the release of apoptotic factors from damaged mitochondria and contributes to cellular health. Mitochondrial fission is the process where a single mitochondrion divides into two or more daughter mitochondria. Mitochondrial fission in mammals is mediated by DRP1, which is a dynamin like GTPase present in the cytosol (Smirnova et al., 2001). The tail-anchored mitochondrial fission factor (Mff) and N-terminally anchored mitochondrial dynamics proteins of 49 and 51 kDa (MiD49 and MiD51) are mitochondrial outer membrane anchored receptor proteins that recruit Drp1 to the surface of the mitochondria to initiate fission (Gandre-Babbe and van der Bliek, 2008; Otera et al., 2010; Palmer et al., 2011). Another outer mitochondrial membrane anchored receptor of DRP1 is hFIS1(Yoon et al., 2003), which is an orthologue of Fis1p of budding yeast. Despite its crucial role in mitochondrial fission in budding yeast, evidence supporting the role of hFIS1 in mammalian mitochondrial fission is contentious (Otera et al., 2010; Koirala et al., 2013; Losón et al., 2013). Following the translocation to the mitochondrial surface, DRP1 polymerize and form a ring around the mitochondria that constrict and sever both inner and outer membranes splitting the mitochondrion into two daughter mitochondria (Youle et al., 2012). Fission serves the important function of maintaining a healthy supply of mitochondria in maturing and dividing cells (Youle et al., 2012). Furthermore fission can serve to isolate damaged mitochondria, which can then be targeted for degradation (Twig et al., 2008). Defects in Drp1 mediated mitochondrial fission result in the accumulation of mitochondria in the cell body and reduced dendritic mitochondrial content (Li et al., 2004). This suggests that it may not be possible for the highly interconnected mitochondria that are present in fission deficient neurons to be efficiently transported to distal neuronal processes (Sheng and Cai, 2012).

The process of mitochondrial fusion is mediated by three dynamin family members, Mitofusin 1 (MFN1) and Mitofusin 2 (MFN2) which span the outer membrane of the mitochondria and Optic atrophy protein 1 (OPA1) which is present in the intermembrane space (Song et al., 2009). Mitofusins mediate the fusion between the outer membranes of the mitochondria whereas OPA1 mediate inner membrane fusion (Meeusen et al., 2006; Song et al., 2009). Mitochondrial fusion enables mitochondrial contents to be mixed which allows for the maintenance of a healthy pool of mitochondria

through the mixing of proteins, mtDNA and metabolites between mitochondria (Chen and Chan, 2009). While it is necessary for mitochondria to move for fusion to occur it has also been shown that mutations or deletions in fusion protein MFN2 contribute to reduced motility of mitochondria, thus demonstrating an interaction between fusion and transport proteins (Baloh et al., 2007; Chen et al., 2007).

1.2.3. Mitophagy

Mitophagy is a form of autophagy that is specific for the removal of damaged mitochondria (Lemasters, 2005). Mitophagy serves as a quality control method for the removal of defective mitochondria. In addition, mitophagy is also required for steady-state turnover of mitochondria (Tal et al., 2007), regulation of mitochondrial number to match metabolic demand (Kissová et al., 2004) and during specific stages of cell development (Schweers et al., 2007). Mitophagy begins with mitochondrial fission (Westermann, 2010) which segregates defective mitochondria into smaller daughter mitochondria which are surrounded by an isolation membrane known as a phagophore (Seglen et al., 1996). Once the phagophore has enveloped and sealed its target the resulting double membrane bound vesicle is now known as an autophagosome (Kim et al., 2007). The autophagosomes then fuse with lysosomes and form autolysosomes in which the cargo gets degraded by the lysosomal hydrolases and recycled (Kim et al., 2007). Mitochondria are labelled prior to being targeted for mitophagy and this can occur via two methods: 1. Binding of the outer mitochondrial membrane protein NIP3-like protein X (NIX) to ubiquitin like protein LC3 (Microtubule-associated protein 1A/1B-light chain 3) on the isolation membrane that mediate mitochondrial isolation into an autophagosome (Youle and Narendra, 2011) 2. The PTEN-induced putative kinase protein 1 (PINK1) recruitment of cytosolic E3 ubiquitin ligase (Parkin) to depolarized mitochondria which then gets ubiquitinated by Parkin followed by mitophagy (Matsuda et al., 2010; Vives-Bauza et al., 2010). The latter pathway can also target the proteasomal degradation of MIRO which can serve to arrest movement of damaged mitochondria and assist in their clearance (Wang et al., 2011). The PINK1-parkin pathway promotes fission and /or inhibit fusion by downregulating MFN and OPA1 proteins which may prevent the fusion of damaged mitochondrial into those that are healthy (Deng et al., 2008; Yang et al., 2008). Furthermore, Parkin induces the ubiquitination of mitofusins MFN1 and MFN2, leading to their degradation in a proteasome and a AAA+ ATPase

p97-depedent manner upstream of mitophagy thereby preventing the re-fusion of damaged and healthy mitochondria (Tanaka et al., 2010; Youle and Narendra, 2011).

1.3. Mitochondrial dynamics and neurodegenerative disorders

Neurodegenerative diseases encompass a diverse group of disorders of the nervous system each characterized by the death of a neuronal subtype (Schon and Przedborski, 2011). These are often debilitating disorders with no effective treatments. The pathogenesis of a majority of neurodegenerative diseases has not been completely elucidated. However, a few underlying themes have emerged regarding their pathogenesis such as disrupted cellular quality control mechanisms, oxidative stress, neuroinflammation and impaired subcellular trafficking (Schon and Przedborski, 2011). Impaired mitochondrial function and dynamics have also been implicated in the progression of several neurodegenerative disorders.

Parkinson's disease (PD) is a neurodegenerative disease that results in the progressive loss of dopaminergic neurons. The induction of early Parkinson's disease-like phenotypes (Lewy neurites) by chronic treatment with low concentrations of the complex I inhibitor, rotenone in differentiated SH-SY5Y neuroblastoma cells produced a reduction in the dynamic movement of mitochondria in neurites (Borland et al., 2008). The buildup of α-synuclein which gives rise to Lewy bodies is a characteristic pathology in certain forms of Parkinson's disease (Braak et al., 2004). Over expression of α-synuclein is detrimental to the microtubule system and aggregates of α-synuclein impede movement of mitochondria (Borland et al., 2008). Mutations of the two genes PINK1 and Parkin are associated with autosomal recessive forms of Parkinsonism (Kitada et al., 1998; Valente et al., 2004). Knocking out either gene in fruit flies lead to severe mitochondrial dysfunction characterized by swollen mitochondria with disrupted cristae and both mutants show flight muscle and dopaminergic neuron degeneration (Greene et al., 2003; Clark et al., 2006; Yang et al., 2006). Therefore, interaction of mutant PINK1 and Parkin with proteins such as MIRO and MFN can lead to disrupted mitochondrial dynamics.

A growing body of evidence point towards mitochondrial dysfunction as a major contributing factor in the pathogenesis of Alzheimer's disease (AD). Abnormal

mitochondrial dynamics is considered to be an early event in the progression of the disease where the balance between fission and fusion is shifted towards fission (Bonda et al., 2010; Reddy et al., 2012). A mouse model of AD demonstrated a decrease in anterograde mitochondrial movement along with increased fission (Calkins et al., 2011) while another study showed a decrease in both anterograde and retrograde movement of mitochondria (Du et al., 2010). Mutations in the genes that encode amyloid precursor protein (APP) and presenilin-1 and 2 are known to be risk factors for AD. APP and its enzymatic cleavage product Amyloid Beta (Aβ), accumulate in mitochondrial membranes and cause structural and functional damage to mitochondria (Pagani and Eckert, 2011). The interaction of Mitochondrial Aβ with cylcophilin D, a component of mitochondrial permeability transition pore (mPTP) cause an increase in the opening of mPTP, leading to a disruption in Ca^{2+} balance and increased ROS production (Wang et al., 2014). Elevation of Ca^{2+} and oxidative stress activates p38 MAP Kinase, which phosphorylates kinesin and dynein causing detachment of mitochondria from the motor proteins (Hirokawa et al., 2010). Phosphorylated tau is another pathological feature of AD. Tau is a microtubule associated protein enriched in axons that play an important role in stabilizing axonal microtubules (Ebneth et al., 1998). Tau affects axonal transport if overexpressed, or when aggregates form or when isoform composition or phosphorylation state is significantly changed (Wang et al., 2014). Overexpression of tau retard plus end directed transport of mitochondria involving Kinesin (Ebneth et al., 1998). Both phosphorylated tau and Aβ peptides interact with dynamin related protein (DRP1) leading to increased mitochondrial fragmentation, impaired axonal transport of mitochondria and synaptic degeneration (Manczak et al., 2011; Manczak and Reddy, 2012).

Studies showed a direct link between impaired mitochondrial movement and degeneration of peripheral sensory and motor axons in Charcot-Marie-Tooth disease (CMT). A common inherited disorder of the nervous system, CMT causes muscle wasting, weakness, and sensory loss (Reilly et al., 2011). Type II CMT, characterized by diminished compound motor action potentials as a result of axonal loss, is commonly due to mutations in the outer mitochondrial membrane protein Mitofusin 2 (MFN2), (Kijima et al., 2004; Züchner et al., 2004; Lawson et al., 2005; Chung et al., 2006). MFN2, a dynamin family GTPase, together with its homolog MFN1 participates in the docking and tethering to neighboring mitochondria and subsequent outer membrane

fusion (Koshiba et al., 2004). Cultured dorsal root ganglion (DRG) neurons expressing mutant MFN2 protein showed accumulation of mitochondria in the proximal axonal segments with only a few mitochondria in the distal segments pointing towards a marked impairment of mitochondrial trafficking (Baloh et al., 2007). A qualitative defect in mitochondrial movement was demonstrated in MFN2 knocked out mouse embryonic fibroblasts as well as in an engineered MFN2 mutant fibroblast cell line (Chen et al., 2003; Neuspiel et al., 2005). It has been proposed that incomplete mitochondrial fusion in MFN2 mutants lead to the formation of tethered intermediates which then undergo fission leading to fragmented-tethered mitochondrial clusters whose transport is affected secondarily as a consequence (Baloh et al., 2007). An alternative hypothesis is that MFN2 has a regulatory role in the assembly of the molecular complex for the attachment to kinesin and dynein motor proteins (Baloh et al., 2007). MFN2 mutations associated with type II CMT also affect endoplasmic reticulum (ER) tubulation and tethering to mitochondria which can lead to altered ER-mitochondrial communications (de Brito and Scorrano, 2008; Schon and Przedborski, 2011).

Both vesicular and mitochondrial transport defects are emerging as key contributors to the pathology of Huntington's disease (Li et al., 2001; Gunawardena et al., 2003; Lee et al., 2004; Trushina et al., 2004). Altered mitochondrial transport has also been demonstrated in familial Amyotrophic lateral sclerosis (ALS) linked mouse models as well as in neurons from ALS patients (Sasaki and Iwata, 1996, 2007; Kong and Xu, 1998; Higgins et al., 2003). Disrupted mitochondrial dynamics were reported in other neurodegenerative diseases such as autosomal dominant distal hereditary motor neuropathy and autosomal dominant Perry Syndrome (Levy et al., 2006; Ishikawa et al., 2014). Despite growing evidence for disrupted mitochondrial dynamics in neurodegenerative disorders it is difficult to attribute impaired mitochondrial dynamics as the primary cause of these disorders. It is possible that disrupted mitochondrial dynamics is a consequence of general transport defects and is secondary to the main pathogenic event (Rintoul and Reynolds, 2010; Sheng and Cai, 2012).However, disrupted mitochondrial dynamics leads to local energy depletion, loss of Ca^{2+} buffering capacity and the release of apoptotic signals (Sheng and Cai, 2012) therefore it is difficult to rule out its contribution to neurodegeneration.

1.4. Mitochondrial Genetic Disorders

Diseases that are caused by mutations in the mtDNA or in nuclear encoded genes whose products are imported into mitochondria are defined as mitochondrial disorders (Falk and Sondheimer, 2010). Diseases associated with a mitochondrial DNA point mutation were first discovered in 1988 (Holt et al., 1988; Wallace et al., 1988a). Since then many mutations associated with mitochondrial diseases have been identified. At present, the minimal prevalence of mitochondrial disease is estimated to be 1 in 5000 (Falk and Sondheimer, 2010). There are no cures for mitochondrial diseases at present and treatment is limited to managing symptoms and antioxidant and vitamin cofactor cocktails (Falk and Sondheimer, 2010). Novel therapies are being developed with a few in the early clinical phase showing some promise (Lam et al., 2010; Yiu et al., 2013; Wan et al., 2016). These therapies can be broadly categorized into gene therapy, small molecule pharmaceuticals, new protein delivery and stem cell therapy (Nightingale et al., 2016). The pathogenic mutations can occur in protein synthesis genes of the mitochondria, mitochondrial protein encoding genes or nuclear encoded mitochondrial genes.

Kearns-Sayre syndrome (KSS) and chronic progressive external ophthalmoplegia (CPEO) is caused by mtDNA deletions and was one of the first mitochondrial diseases to be identified (Holt et al., 1988; Zeviani et al., 1988; Moraes et al., 1989). The most common deletion is a 4977 bp region in the mitochondrial DNA where seven protein encoding genes and five tRNA genes are lost (Shoffner et al., 1989). In patients, deleted mtDNA copies exist in a mixture with wild-type mtDNA termed heteroplasmy (Shoffner et al., 1989). The severity of the disease is determined by the distribution and proportion of mutant mtDNA (Moraes et al., 1995). Clinical signs include muscle weakness, lactic acidosis, pigmentary retinopathy, and cardiac conduction defects (Moraes et al., 1989). Deficiencies in complex I and decreased cytochrome c oxidase were reported in muscle tissue from patients with KSS/CPEO (Mita et al., 1989; Larsson et al., 1990). Mitochondrial protein synthesis is also affected as a result of the deletion of mitochondrial tRNA and rRNA genes (Bourgeron et al., 1993).

Myoclonic epilepsy and ragged red fibers (MERFF) is caused by an A to G substitution at nucleotide position 8344 in the mitochondrial *MT-TK* gene (encoding $tRNA^{Lys}$) in 80% of the cases (Shoffner et al., 1990; Silvestri et al., 1992; DiMauro and

Hirano, 2003). Patients with MERFF display myoclonus, generalized epilepsy, neuropathy, ataxia and dementia (Fukuhara et al., 1980). Hearing loss, short stature and optic atrophy are also commonly reported (DiMauro and Hirano, 2003). MERFF can be diagnosed by the presence of ragged red fibers in a muscle biopsy (Fukuhara et al., 1980). Patients are heteroplasmic and will develop the disease phenotype only if the proportion of mutant mtDNA is above a threshold (Shoffner et al., 1990). The onset of the disease is usually during childhood and clinical presentation can be variable even among family members (Boulet et al., 1992; DiMauro and Hirano, 2003). A deficiency in aminoacyl $tRNA^{Lys}$ leads to impairments in protein translation (Enriquez et al., 1995). The ensuing defect in protein synthesis in turn results in decreased respiratory chain activities particularly in complex I and complex IV (Wallace et al., 1988b; Bindoff et al., 1991).

Mitochondrial encephalomyopathy, lactic acidosis, and stroke-like episodes (MELAS) is a rare disease that results in nervous system and muscle dysfunction (Henry et al., 2017). Eighty percent of cases are caused by an A to G substitution at nucleotide position 3243 in the mitochondrial *MT-TL1* gene encoding $tRNA^{Leu}$ gene (Goto et al., 1992). Additional point mutations in the same gene or other mtDNA genes particularly *MT-ND5* can also cause the disease (DiMauro and Hirano, 2013). The clinical signs appear during early adulthood and patients experience vomiting, migraine, myopathy, seizures that result in transient hemiparesis or cortical blindness (DiMauro and Hirano, 2013). For the disease to manifest the amount of mutant mitochondrial DNA should be greater than 85% (Goto et al., 1990). Biochemical studies in transmitochondrial cytoplasmic hybrids (cybrids) carrying the most common 3243 mutation has revealed severe respiratory deficiency, reduced mitochondrial protein synthesis, decreased mitochondrial membrane potential and reduced amino acylation (King et al., 1992; James et al., 1996; Helm et al., 1999). Cybrids are cells that have been depleted of their endogenous mtDNA and repopulated by fusing with foreign mtDNA from enucleated mtDNA donors.

Dominant Optic Atrophy (DOA) is a disease that is primarily caused by mutations in *OPA1*, a nuclear encoded mitochondrial gene that encodes a dynamin-related guanosine triphosphatase (Delettre et al., 2000). Mutations in other OPA genes also give rise to X-linked or recessive optic atrophy (Lenaers et al., 2012). Loss of vision is the most common phenotype in patients with DOA and this is due to the degeneration of

retinal ganglion cells (RGCs) and the optic nerve. About 20% of DOA patients present with additional symptoms such as neurosensory hearing loss, ophthalmoplegia, myopathy, peripheral neuropathy, multiple sclerosis-like illness and cataracts (Lenaers et al., 2012). In humans, OPA1 localizes to inner membrane of the mitochondria and regulates mitochondrial fusion (Olichon et al., 2003). Studies have shown that cell lines (HeLa, COS) and patient fibroblasts carrying the OPA1 mutations are susceptible to apoptosis and also display a varying degree of mitochondrial respiratory defects due to reduced energetic coupling (Olichon et al., 2007; Chevrollier et al., 2008; Zanna et al., 2008). Furthermore, abnormalities in mitochondrial dynamics, distribution and disruption of mtDNA structural integrity were reported (Olichon et al., 2007; Zanna et al., 2008; Elachouri et al., 2011).

Mutations in mitochondrial protein encoding genes are mainly described in three diseases, Leber Hereditary Optic Neuropathy, Neurogenic muscle weakness, ataxia, and retinitis pigmentosa (NARP) and Leigh syndrome. Leber Hereditary Optic was one of the first diseases to be associated with a mitochondrial DNA point mutation (Wallace et al., 1988a) and will be the focus of this thesis.

Both NARP and Leigh syndrome share a common pathogenic T-G point mutation at nucleotide position 8993 in the mitochondrially-encoded ATPase 6 gene (Holt et al., 1990). The disease outcome depends on the proportion of mutant to healthy mtDNA copies in the body. A mutation load less than 75% can cause NARP while greater than 95% of mutant mtDNA can cause Leigh syndrome (Wallace, 1999). A T-C mutation at the same nucleotide position can also give rise to NARP and Leigh syndrome but has a milder phenotypic expression than the original and more common T-G point mutation (Santorelli et al., 1994; Fujii et al., 1998). The syndrome was coined NARP after the primary clinical features which are proximal neurogenic muscle weakness, with sensory neuropathy, ataxia and pigmentary retinopathy. The more severe and often fatal Leigh syndrome is a neurodegenerative disease of the brainstem and basal ganglia (Tatuch and Robinson, 1993) and clinical signs include, but are not limited to hypotonia, spasticity, movement disorders, cerebellar ataxia, peripheral neuropathy (Thorburn et al., 1993). Lymphoblasts and cybrids carrying the T8893G mutation showed a block in the ATP synthase F0 proton channel (Trounce et al., 1994). The mutation also caused ATP synthase assembly to be slowed and the assembled holoenzyme complex to be unstable (Nijtmans et al., 2001).

1.5. Leber Hereditary Optic Neuropathy

1.5.1. History

LHON is a mitochondrial disease, characterized by loss of vision due to the degeneration of retinal ganglion cells and their axons that comprise the optic nerve. The disease was first recognized by Dr. Albrecht von Graefe in 1858 but was described as a distinct clinical entity by the German ophthalmologist Theodore Leber in 1871 (Leber, 1871). He studied 15 individuals from 4 families and described the characteristic pattern of visual loss which was later confirmed in pedigrees from different populations (Bell, 1931; Imai and Moriwaki, 1936; Lundsgaard, 1944). These early studies identified some of the key features of LHON such as its gender bias, maternal transmission and the degeneration of optic nerve (Man et al., 2002), but it was initially mistaken to be X-linked in its genetics. It was not until 1988, when Wallace and colleagues determined that the maternal transmission was due to a mitochondrial DNA mutation (Wallace et al., 1988a). They discovered the first point mutation associated with LHON which was a G to A substitution at position 11778 (Wallace et al., 1988a) which converted a highly conserved arginine to histidine at codon 340 in the NADH subunit 4 of complex I (NADH dehydrogenase) of the electron transport chain. In 1991, a G to A point mutation at nucleotide position 3460 of mitochondrial DNA (mtDNA) was reported in three LHON independent pedigrees that converted an alanine to threonine at codon 52 in subunit 1 of complex I (Howell et al., 1991a; Huoponen et al., 1991). One year later a T to C mutation at nucleotide position 14484 was discovered that converted a methionine to a valine at codon 64 in subunit 6 of complex I (Johns et al., 1992; Mackey and Howell, 1992). The three mutations are now considered the primary pathogenic mutations that cause LHON since they occur in about 95% of LHON cases worldwide and each mutation alone has the ability to cause the disease (Mackey et al., 1996). Other rare mtDNA mutations continue to be identified (figure 1). Many of these rare mutations were reported in single patients that exhibit clinical features of LHON (Bi et al., 2016).

Genes	Gen Bank ID	Nucleotide position	AA change	Phenotype	Hom/Het	Reference
MT-ND1	ACT53094.1	m.3316G>A	A4T	LHON/NIDDM	Hom	Matsumoto et al., 1999 [122]
		m.3376G>A	E24K	LHON/MELAS	Hom/Het	Blakely et al., 2005 [123]
		m.3394T>C	Y30H	LHON/NIDDM	Hom	Brown et al., 1992 [124]
		m.3460G>A	A52T	LHON	Hom/Het	Huoponen et al., 1991 [30]
		m.3496G>T	A64S	LHON	Hom	Matsumoto et al., 1999 [122]
		m.3497C>T	A64V	LHON	Hom	Matsumoto et al., 1999 [122]
		m.3635G>A	S110N	LHON	Hom	Brown et al., 2001 [125]
		m.3700G>A	A112T	LHON	Hom	Fauser et al., 2002 [126]
		m.3733G>A	E143K	LHON	Hom/Het	Valentino et al., 2004 [127]
		m.4025C>T	T240M	LHON	Hom	Huoponen et al., 1993 [128]
		m.4136A>G	Y277C	LHON	Hom	Howell et al., 1991 [129]
		m.4160T>C	L286P	LHON	Hom	Howell et al., 1991 [129]
		m.4171C>A	L289M	LHON	Hom/Het	Kim et al., 2002 [130]
		m.4216T>C	Y304H	LHON/Insulin resistance	Hom	Johns and Berman, 1991 [131]
MT-CO1	ACT53096.1	m.6261G>A	A120T	LHON/Prostrate Cancer	Hom	Abu-Amero and Bosley et al., 2006 [132]
		m.7444 G>A	Ter-K	LHON/SNH/DEAF	Hom	Brown et al., 1992 [133]
		m.7623 C>T	T13I	LHON	Hom	Abu-Amero and Bosley et al., 2006 [132]
MT-CO2	ACT53097.1	m.7868C>T	L95F	LHON	Hom	Yang et al., 2009 [134]
MT-ND2	ACT53095.1	m.4640C>A	I57M	LHON	Hom	Brown et al., 2001 [125]
		m.4917A>G	N150D	LHON/AMD/Insulin resistance/NRTI-PN	Hom	Johns and Berman, 1991 [131]
		m.5244G>A	G259S	LHON	Het	Brown et al., 1992 [135]
MT-ND3	ACT53101.1	m.10237T>C	I60T	LHON	Hom	Horvath et al., 2002 [136]
MT-ND4	ACT53103.1	m.11253T>C	I165T	LHON	Hom	Kjer 1959 [137]
		m.11696G>A	V312I	LHON + Spastic Dystonia	Het	De Vries et al., 1996 [138]
		m.11778G>A	R340H	LHON	Hom/Het	Wallace et al., 1988 [6]
		m.11874C>A	T372N	LHON	Hom	Abu-Amero and Bosley et al., 2006 [132]
MT-ND4L	ACT53102.1	m.10543A>G	H25R	LHON	Het	Abu-Amero and Bosley et al., 2006 [132]
		m.10591T>G	F41C	LHON	Het	Abu-Amero and Bosley et al., 2006 [132]
		m.10663T>C	V65A	LHON	Hom	Brown et al., 2002 [139]
		m.10680G>A	A71T	LHON	Hom	Yang et al., 2009 [134]
MT-ND5	ACT53104.1	m.12782T>G	I149S	LHON	Het	Abu-Amero and Bosley et al., 2006 [132]
		m.12811T>C	Y159H	LHON	Hom	Huoponen et al., 1993 [128]
		m.12848C>T	A171V	LHON	Het	Mayorov et al., 2005 [140]
		m.13045A>C	M237L	LHON/MELAS/LS	Het	Liolitsa et al., 2003 [141]
		m.13051G>A	G239S	LHON	Hom	Howell et al., 2003 [142]
		m.13379A>C	H348P	LHON	Hom	Abu-Amero and Bosley et al., 2006 [132]
		m.13528A>G	T398A	LHON-Like	Hom	Batandier et al., 2000 [143]
		m.13637A>G	Q434R	LHON	Hom	Huoponen et al., 1993 [128]
		m.13708G>A	A458T	LHON/MS risk	Hom	Johns and Berman, 1991 [131]
		m.13730G>A	G465E	LHON	Het	Howell et al., 1993 [144]

Genes	Gen Bank ID	Nucleotide position	AA change	Phenotype	Hom/Het	Reference
MT-ND6	ACT53105.1	m.14568C>T	G36S	LHON	Hom	Besch et al., 1999 [145]
		m.14279G>A	S132L	LHON	Hom	Zhadanov et al., 2005 [146]
		m.14459G>A	A72V	LHON + Spastic Dystonia	Hom/Het	Jun et al., 1994 [147]
		m.14482C>G	M64I	LHON	Hom/Het	Howell et al., 1998 [148]
		m.14484T>C	M64V	LHON	Hom/Het	Brown, et al., 1992 [124]
		m.14495A>G	L60S	LHON	Het	Chinnery et al., 2001 [149]
		m.14498C>T	Y59C	LHON	Hom/Het	Wissinger et al., 1997 [150]
		m.14596A>T	I26M	LHON	Hom	De Vries et al., 1996 [138]
		m.14325T>C	N117D	LHON	Hom	Howell et al., 2003 [142]
		m.14729G>A	S132L	LHON	Hom	Zhadanov et al., 2005 [146]
MT-CYB	ACT53106.1	m.14831G>A	A29T	LHON	Hom	Fauser et al., 2002 [126]
		m.14841A>G	N32S	LHON	Het	Yang et al., 2009 [134]
		m.15257G>A	D171N	LHON	Hom	Johns and Berman, 1991 [131]
		m.15674T>C	S310P	LHON	Hom	Abu-Amero Bosley et al., 2006 [132]
		m.15773G>A	V343M	LHON	Hom	La Morgia et al., 2008 [151]
		m.15812G>A	V356M	LHON	Hom	John et al., 1991 [152]
MT-CO3	ACT53100.1	m.9438G>A	G78S	LHON	Hom	Johns and Neufeld 1993 [153]
		m.9738G>T	A178S	LHON	Hom	Johns and Neufeld 1993 [153]
		m.9804G>A	A200T	LHON	Het	Johns and Neufeld 1993 [153]
MT-ATP6	ACT53099.1	m.8836A>G	M104V	LHON	Hom	Abu-Amero Bosley et al., 2006 [132]
		m.9016A>G	I164V	LHON	Het	Povalko et al., 2005 [154]
		m.9101 T>C	I192T	LHON	Hom	Puomila et al., 2007[17]
		m.9139G>A	A205T	LHON	Hom	La Morgia et al., 2008 [151]

Figure 1 **comprehensive list of genes/mutations involved in LHON** (Koilkonda and Guy, 2011)

1.5.2. Epidemiology

LHON is the most commonly occurring mitochondrial genetic disease (Man et al., 2002; Sadun et al., 2011). In the North East of England, 1:8,500 individuals carry a pathogenic LHON mutation and 1:31,000 suffer from vision loss due to LHON in the region (Y-W-Man et al., 2003; Gorman et al., 2015). The prevalence of vision loss due to LHON is 1: 39,000 in the Netherlands and 1:50,000 in Finland (Spruijt et al., 2006; Puomila et al., 2007). However, disease prevalence is underestimated due to inadequate diagnosis or misdiagnosis. Although considered as a rare disease, the minimum prevalence for the LHON mtDNA mutations is reported to be about 15:100,000 similar to many autosomally inherited neurological disorders (Sadun et al., 2011). The three primary mutations account for 95% of LHON cases (Yu-Wai-Man et al., 2008). The G11778A mutation is the most prevalent in Northern European and Asian populations (Mackey et al., 1996; Mashima et al., 1998; Jia et al., 2006) whereas the T14484C is the most common mutation among French Canadians (87%) (Macmillan et al., 1998).

1.5.3. Penetrance

Ninety five percent of those who lose vision do so by the age of 50 and vision loss is more frequent in young adults in their second and third decade of life (Man et al., 2002). Penetrance for the disease is higher for men than for women (Man et al., 2002). Penetrance refers to the proportion of people with a given genotype who exhibit the phenotype associated with that genotype. As mentioned, an interesting feature of LHON is that only 50% of males and 10% of females who harbor one of the 3 primary mutations actually develop the optic neuropathy (Seedorff, 1985; Brown and MD, 1994; Nikoskelainen, 1994) The penetrance is variable even within the same family of homoplasmic mutation carriers (Chalmers and Harding, 1996; Howell and Mackey, 1998). Of the indexed patients carrying the 11778 mutation only 50% had a history of affected relatives whereas this proportion was 71% and 100% for patients carrying the 3460 and 14484 mutations respectively (Riordan-Eva et al., 1995). Another study showed that a family harboring the 11778 mutation consisted of a low penetrance branch where none of the 24 male descendants was affected and a high penetrance branch where 12 of 18 males were affected (Howell and Mackey, 1998). Incomplete penetrance and gender bias shows that optic neuropathy in LHON cannot be explained by a single pathophysiological mechanism and may involve additional genetic or environmental factors that modulate the phenotypic expression of LHON (Yu-Wai-Man et al., 2008). Subtle anatomical, hormonal and physiological variations between males and females could also contribute to the gender bias (Yu-Wai-Man et al., 2008).

1.5.4. Clinical features

Patients experience painless subacute loss of central vision in one eye followed by the other with a median inter-eye delay of six to eight weeks (Harding et al., 1995). The sequential loss of vision is more common (75%) but vision loss can also occur simultaneously in both eyes (25%) (Harding et al., 1995). Large and dense cecocentral scotomas on visual fields are the characteristic field defects associated with LHON due to the involvement of the papillomacular bundle (PMB) (Newman et al., 2006). Visual acuity is reduced to 20/200 or less by 4-6 weeks following onset of symptoms (Newman et al., 1991). Color perception is impaired (dyschromatopsia) but pupillary light reflexes are preserved due to relative sparing of melanopsin-containing RGCs (Newman et al., 2006; Moura et al., 2013). These are thought to be more resistant to metabolic insult

from mitochondrial dysfunction compared with other RGCs (La Morgia et al., 2010; Moura et al., 2013). Fundoscopy examination during or preceding acute stages show swelling of the retinal nerve fiber layer (RNFL) around the optic disc (termed “pseudoedema”), optic disc hyperemia, circumpapillary telangiectatic blood vessels and vascular tortuosity of the central retinal vessels (Man et al., 2002). However, in 20-40% of cases in the acute phase, the optic disc can look entirely normal which can delay diagnosis (Riordan-Eva and Harding, 1995; Yu-Wai-Man et al., 2014).

During the chronic phase the disc hyperemia, circumpapillary telangiectasias (spider veins) and pseudoedema (swelling of the optic nerve head resembling edema) disappear but is accompanied by optic disc pallor and cupping of the optic disc as a result of the death of RGCs (Mashima et al., 2003; Newman, 2005). The optic atrophy is more severe on the temporal side which includes the PMB, but extends to other quadrants leading to diffuse optic atrophy (Barboni et al., 2010). The unique feature of LHON is the exclusive involvement of the optic nerve with preferential loss of the small fibers that constitute the PMB (Sadun et al., 2000). Further characterization of fundus changes using optical coherence tomography (OCT), show thickening of the RNFL, first in the temporal and inferior quadrants, then the superior and nasal quadrants (Barboni et al., 2010). RNFL thickening can be attributed to axonal swelling from impaired mitochondrial function and axonal transport (Carelli et al., 2004a). During the chronic phase, the macula thinning precedes the thinning of the RNFL (Zhang et al., 2014). Both macula and RNFL thickness can be used as markers for monitoring the progression of the disease using OCT (Zhang et al., 2014). LHON patients also show abnormalities in visual evoked potentials (VEPs) and electroretinograms (ERGs) due to optic nerve degeneration and RGC loss (Dorfman et al., 1977; Salomão et al., 2004; Ziccardi et al., 2013).

Spontaneous visual recovery has been reported several years after disease onset. Studies have shown that the extent of visual recovery varies depending on the patient’s mutational status. Patients carrying the 14484 mutation have the best prognosis while those carrying 11778 have the worst (Stone et al., 1992; Johns et al., 1993). A younger age of onset also has a more favorable prognosis (Oostra et al., 1994; Pezzi et al., 1998). In addition to vision loss, cardiac arrhythmias and neurological abnormalities such as postural tremor, peripheral neuropathy, nonspecific myopathy, movement disorders were reported to be more common in LHON patients compared to

controls. (Bower et al., 1992; Meire et al., 1995; Nikoskelainen et al., 1995; Mashima et al., 1996). However, these are rarely considered clinically significant (Yu-Wai-Man et al., 2009). A small number of LHON pedigrees have shown severe neurological deficits such as spastic dystonia, ataxia and juvenile onset encephalopathy. These are known as “LHON plus” syndromes and have been linked to various mtDNA mutations in isolated pedigrees from Holland, Australia and North America (Howell et al., 1991b; Jun et al., 1994; De Vries et al., 1996; Gropman et al., 2004).

There have been documented cases of LHON carriers who also suffer from a demyelinating syndrome that is clinically and radiologically identical to multiple sclerosis (Harding et al., 1992; Kellar-Wood et al., 1994; Olsen et al., 1995; Jansen et al., 1996). The disease was named Harding syndrome after the author who first reported the cases (Harding et al., 1992). A significant minority of LHON carriers that mostly included Caucasian females carrying the G11778A mutation were diagnosed with the disease posing the question as to whether autoimmunity maybe involved in the pathophysiology of LHON (Harding et al., 1992; Vanopdenbosch et al., 2000). Antibodies to the optic nerve protein tubulin have been found to be higher among LHON carriers compared to controls (Smith et al., 1995). However other studies have not found a significant association between LHON and either class I or class II histocompatibility complex (MHC) genotypes (Govan et al., 1994; Chalmers et al., 1996b). The disease showed features such as female predominance, multiple episodes of vision loss and lengthy inter-eye delay of vision loss that were not typical of LHON (Pfeffer et al., 2013). Therefore the association between LHON and multiple sclerosis might be due to chance (Pfeffer et al., 2013). More evidence is needed to validate whether autoimmunity has a role in LHON.

1.5.5. Mitochondrial genetic factors

In addition to housing the primary pathogenic LHON mutations, the multi-copy mitochondrial genome may contribute to disease penetrance in three other ways: 1. by modifying the amount of mutant vs wild-type mitochondrial genotypes that may occur as a mixture in a cell or tissue known as heteroplasmy, 2. by adjusting the cellular quantity of mtDNA, known as copy number, 3. by adding secondary mtDNA mutations acting in synergy with the primary mutations (Bianco et al., 2017). The penetrance or the severity

of most mitochondrial neurologic diseases is influenced by the proportion of mutant versus wild-type mtDNA (Schon et al., 2012).

Heteroplasmy

A majority of LHON patients and family members only harbor mutant copies of mtDNA in their cells, termed homoplasmy (Yen et al., 2006). Only 10-15% of LHON carriers contain a mixture of mutant and wild-type mtDNA termed heteroplasmy (Smith et al., 1993; Harding et al., 1995; Y-W-Man et al., 2003). In 167 genealogically unrelated LHON families the prevalence of heteroplasmy was 5.6%, 40% and 36.4% for the 11778, 3460 and 14484 LHON mutations respectively (Jacobi et al., 2001). Heteroplasmy is thought to influence the inheritance and penetrance of LHON. Offspring born to mothers with less than 80% mutated mtDNA in their blood cells are less likely to be symptomatic compared to offspring born to mothers with 100% mutated mtDNA (homoplasmic) in their blood cells (Chinnery et al., 2001). The risk of blindness is also considered to be minimal if the mutational load is less than 60% (Chinnery et al., 2001). However, Jacobi et al. (2001) reported a male LHON patient with 26% blood mutation load despite a positive correlation between level of mutant mtDNA and disease expression. This is most likely due to the variation in the distribution of mutant mtDNA in different tissues as a result of random segregation of mutant and wild-type mtDNA during embryogenesis (Jacobi et al., 2001). This was clearly demonstrated in a report by Howell et al. (1994) where the mutant mtDNA level was 33% in the leukocytes compared with 95% and 100% in the optic nerve and retina in autopsied material from a heteroplasmic patient carrying 11778 mutation. There has been contradicting evidence regarding the proportion of mutant mtDNA in successive generations, where some studies show an increase (Smith et al., 1993; Howell et al., 1994) while others show a decrease (Howell et al., 2000; Kaplanová et al., 2004). Other studies have found no major shift in heteroplasmy showing no selection of either mtDNA genotype (Puomila et al., 2002). Therefore it has been proposed that segregation of mtDNA is a stochastic process governed by random genetic drift and that LHON mutations behave more like neutral polymorphisms staying at a stable heteroplasmic level (Lagerström-Fermér et al., 2001; Puomila et al., 2002).

Mitochondrial DNA copy number

An increase in mitochondrial biogenesis is commonly observed in mitochondrial diseases as a way of compensating for mitochondrial dysfunction (DiMauro and Schon, 2003). In a mouse model expressing ragged red fibres, an increase in mitochondrial mass help maintain total ATP production in skeletal muscle despite reduced respiratory chain function (Wredenberg et al., 2002). A few reports exists that show an increase in mitochondrial DNA content in blood cells from patients with LHON (Yen et al., 2002; Iommarini et al., 2012), and also in unaffected carriers (Nishioka et al., 2004) compared with controls. Treating HIV infected LHON carriers with anti-retroviral drugs which reduce mtDNA content resulted in the induction of optic neuropathy (Mackey et al., 2003). Furthermore, the differentiation of neuronal Ntera-2/D1 (NT2) human teratocarcinoma cybrids carrying the homoplasmic 11778 mutation showed increased oxidative stress and a threefold reduction in the mtDNA: nuclear DNA ratio (Wong et al., 2002). A comprehensive study by Giordano et al. (2014) involving three large pedigrees and 39 independent LHON families demonstrated a positive correlation between mitochondrial biogenesis and incomplete penetrance in LHON. In this study the unaffected mutation carriers had a significantly higher copy number, mitochondrial mass and higher capacity for activating mitochondrial biogenesis under metabolic demand compared to their affected relatives and control individuals. Similar findings were reported by Bianco et al. (2017) in a study of a heteroplasmic cohort carrying either the 11778 or 3460 LHON mutation. The study reported significantly higher mtDNA copy numbers in carriers compared to those affected implicating mtDNA copy number as a risk factor in the penetrance of the disease. The increase in mtDNA copy number occurs regardless of whether a carrier is homoplasmic or heteroplasmic for a primary LHON mutation. This could explain why there are homoplasmic individuals who are unaffected and heteroplasmic individuals who are affected. Increase in mtDNA copy number is evidence for increased mitochondrial biogenesis which may serve as a compensatory response to mitochondrial dysfunction in LHON carriers (Bianco et al., 2017).

Haplogroups

Features of mitochondrial DNA such as high mutation rate, maternal inheritance and zero recombination has resulted in the sequential accumulation of polymorphisms along radiating maternal lineages as women migrated out of Africa 150,000 years ago resulting in continent specific polymorphisms (Wallace et al., 1999). The clustering of a

number of stable polymorphisms together in a specific combination is referred to as a haplogroup (Yu-Wai-Man et al., 2008). Individuals of European ancestry belong to one of nine haplogroups: H, I, J, K, T, U, V, W and X (Torroni et al., 1996; Hofmann et al., 1997). A meta-analysis of 3613 subjects from 159 European pedigrees showed an influence of mtDNA background on vision loss in individuals carrying the three primary mutations (Hudson et al., 2007a). A greater risk of visual failure was observed when 11778 and 14484 mutations are present in individuals belonging to haplogroup J and when the 3460 mutation is present in haplogroup K. The risk of vision loss was significantly lower if 11778 and the 14484 mutations are present in haplogroup H (Howell et al., 2003; Hudson et al., 2007a). Haplogroups H, J and K, have in common, a non-synonymous, polymorphic substitution in the MT-CYB gene which codes for cytochrome b, the only mitochondrially encoded subunit of complex III. With recent findings on the existence of stable respiratory chain supercomplexes, such as the one between a complex I monomer and complex III dimer, it is speculated that the substitution associated with the haplogroup affects the stability of these supercomplexes which in turn modulate the biochemical consequences of the LHON mutation (Dudkina et al., 2005; Carelli et al., 2006; Hudson et al., 2007a). Consistent with the hypothesis, a cybrid line carrying the 11778 mutation from a haplogroup J background had lower oxygen consumption and a longer doubling time compared to non-haplogroup J cell lines (Vergani et al., 1995). In contrast, patients of haplogroup J background carrying the 11778 mutation showed no further impairment of mitochondrial oxidative metabolism in their brain and skeletal muscle compared to patients of non haplogroup J background carrying 11778 mutation using 31P-Magnetic Resonance Spectroscopy (31P-MRS) measurements (Lodi et al., 2000). A study in South-East Asian LHON pedigrees also found no association between specific mtDNA haplogroups and risk of vision loss (Tharaphan et al., 2006). Therefore, the evidence for the influence of haplogroups on visual loss in LHON is still inconclusive and requires further research.

1.5.6. Nuclear genetic factors

Bu and Rotter (1991, 1992) proposed that a recessive X-linked gene can act in combination with the primary LHON mutation to give rise to the optic neuropathy. This model can also be used to explain the male predominance, where simultaneous inheritance of a primary mutation and the X-linked susceptibility allele can give rise to

the optic neuropathy in males whereas females will be affected if they are homozygous at the susceptibility locus or heterozygous with skewed X chromosome inactivation in affected female carriers (Man et al., 2002). An initial study by Vilkki et al (1991) involving 6 LHON pedigrees showed that the probability of developing the optic neuropathy was linked to the DXS7 locus of the chromosome X through linkage analysis. However, other studies that followed were not able to find evidence in support of an X-linked susceptibility locus (Sweeney et al., 1992; Chalmers et al., 1996a; Oostra et al., 1996; Pegoraro et al., 1996; Handoko et al., 1998). These early studies, however did not take into account mtDNA heteroplasmy and also used non-informative markers. Hudson et al. (2005) performed a more comprehensive linkage analysis study using 100 European LHON families and identified a DXS8090 (166)-DXS1068 (258) region of the chromosome X that is linked to the onset of LHON. This high risk nuclear haplotype increased the risk of visual failure ~35 fold for the 11778 and 14484 mutations but not for 3460 (Hudson et al., 2005). Furthermore, the effect of the nuclear haplotype on vision loss was more significant than the mtDNA haplotype J in 11778 and 14484 mutation carriers (Hudson et al., 2005). Further evidence in support of an X-linked susceptibility gene came from the identification of a region Xq25-Xp27.2 in a Brazilian LHON family (Shankar et al., 2008) and two microsatellites (DXS6803 and DXS984) in chromosome X in Chinese male LHON patients (Ji et al., 2010) which conferred susceptibility to LHON. Another study by Hudson et al (Hudson et al., 2007b) indicated the susceptibility of estrogen receptor related genes in chromosome X to LHON. The presence of an X-linked susceptibility gene is still controversial and requires further validation.

The presence of other autosomal nuclear modifiers cannot be ruled out. Investigation of oxidative stress and apoptosis pathways lead to the identification of EPHX1 (Epoxide Hydrolase 1) and TP53 (Tumor Protein p53) genes that were associated with an early onset of visual loss in patients carrying the 11778 mtDNA mutation (Ishikawa et al., 2005). A genomic region containing six genes, including PARL, OPA1 was identified for their role as potential modifiers in a genome-wide linkage analysis in patients from Thailand (Phasukkijwatana et al., 2010). Two single nucleotide polymorphisms (SNPs) were identified in the PARL gene (presenilin-associated rhomboid like) that conferred susceptibility to LHON (Phasukkijwatana et al., 2010). PARL regulates OPA1 in the apoptosis pathway (Cipolat et al., 2006). However this association between the PARL SNPs and LHON could not be replicated in a Chinese

population (Zhang et al., 2010) which might suggest that these susceptibility genes maybe specific to certain ethnic backgrounds (Kirches, 2011). OPA1 is a pathogenic gene for autosomal dominant optic atrophy which shares clinical features with LHON (Carelli et al., 2004a). The OPA1 gene was found to be significantly downregulated in LHON patients in a genome-wide expression assay in LHON patients (Abu-Amero et al., 2010). The influence of these modifier genes may account for incomplete penetrance of LHON, further emphasizing the multifactorial nature of the disease.

1.5.7. External factors

Tobacco and Alcohol

Scientists have also investigated the role of environmental factors in the etiology of LHON. Environmental factors are thought to contribute to incomplete penetrance in LHON. Studies have shown that tobacco smoking and alcohol consumption, increase the risk of vision loss in LHON carriers (Riordan-Eva et al., 1995; Charlmers and Harding, 1996; Tsao et al., 1999; Sadun et al., 2003), but there has also been conflicting evidence showing no association between vision loss and smoking or drinking based on exposure levels before the onset of visual loss (Kerrison et al., 2000). The largest study to date involving 196 affected and 206 unaffected LHON carriers from 125 pedigrees found a strong association between smoking and vision loss in LHON carriers (Kirkman et al., 2009). The study also showed a trend towards visual failure with heavy intake of alcohol. A study by Giordano et al (Giordano et al., 2015), showed a reduction in mtDNA content and ATP when fibroblasts from LHON patients and LHON carriers were exposed to cigarette smoke condensate compared to healthy controls. However, the authors report that cells from unaffected carriers were more efficient at scavenging ROS compared to cells from affected patients. Other reports of nutritional deprivation, exposure to industrial toxins, antiretroviral drugs, the antibiotic ethambutol, psychological stress and acute illness have been implicated in triggering the onset of visual loss in LHON (Yu-Wai-Man et al., 2008). Although the evidence is not conclusive we cannot rule out the contribution of environmental factors as a secondary etiological factor in disease progression in LHON.

Light Stress

RGCs are constantly exposed to visible light and ultraviolet (UV) radiation. Studies have shown that long term exposure to light in the UV and blue regions of the spectrum can induce photochemical damage to the retinal layers (Rapp et al., 1990; Smith et al., 2005; Xie et al., 2017). UV radiation has been implicated in the pathogenesis of age related macular degeneration (AMD) (Young, 1988; Beatty et al., 2000). UV radiation induces cyclophilin D translocation to the inner mitochondrial membrane which leads to mitochondrial depolarization, opening of the mitochondrial permeability transition pore and release of cytochrome C and subsequent apoptosis (Ji et al., 2012; Jandova et al., 2013). Light exposure can also elevate ROS production due to photo-oxidation reactions which can promote lipid peroxidation resulting in damage to the retina (van Kuijk, 1991). However UV light below 400nm is absorbed by the cornea and the lens hence the UV damage is minimal to the retinal layers (Boulton et al., 2001). More and more studies have shown that the blue region (400-500nm) of the visible spectrum is more phototoxic to the retinal layers (Seiler et al., 2000; Seko et al., 2001; Glickman, 2002; King et al., 2004). Blue light is more easily transmitted (Algvere et al., 2006) and can be absorbed by biologic chromophores such as cytochrome C oxidase, flavins and flavoproteins that are in abundance in mitochondria (Boulton et al., 2001). Isolated, light-exposed mitochondria have been shown to release reactive oxygen species that include, singlet oxygen, superoxide and hydroxyl radicals (Godley et al., 2005). The high energy blue light will have a greater impact on the RGC axons compared to more external layers partly due to the higher density of mitochondria in this region (Wood et al., 2008). The chromophores in the mitochondria of the RGC axons will absorb most of the high energy light and reduce the energy that reaches the outer layers of the retina. Carotenoid pigments present in the macula offer additional protection to the photoreceptor layer and therefore RGC axons are the most susceptible to photochemical damage (Wood et al., 2008). In healthy cells the energy might be insufficient to cause cell death but in cells that are compromised such as in the case of LHON, the high energy visible light may serve as an additional stressor. Wood et al. (2008) showed that continuous visible light exposure is slightly but significantly harmful to cultured RGC-5 cells and even more harmful to energetically compromised RGC-5 cells. Despite the susceptibility of RGCs in LHON, a certain class of RGCs, known as melanopsin containing RGCs (mRGCs) are relatively spared from degeneration (La Morgia et al., 2010). These blue light absorbing mRGCs are thought to be protected from light damage

due to the presence of the melanopsin photopigment (La Morgia et al., 2010). High energy light especially in the blue region of the spectrum can therefore exacerbate the conditions within RGCs that contain mutant mitochondria that might trigger a cascade of events leading to death of RGCs.

1.5.8. Pathophysiology

Bioenergetic defect

Most of the initial research focused on the respiratory activity of complex I and ATP production was due to the occurrence of the three primary mutations in subunits of complex I. In order to study the effect of the three primary LHON mutations on cellular bioenergetics, researchers measured the oxygen consumption of whole cells, mitochondrial respiration with complex I substrates and performed complex I enzyme activity assays. Epstein-Barr virus (EBV) transformed lymphoblasts and cells depleted of their original mitochondria and repopulated with disease mitochondria known as transmitochondrial hybrids (cybrids) were used extensively for these biochemical studies.

A study on the complex I activity in lymphoblasts and cybrids harboring the 3 primary LHON mutations revealed a 79% reduction in 3460 mutation and a 20% reduction in the 11778 mutation and no change in complex I activity in cells carrying the 14484 mutation (Brown et al., 2000). Other studies were able to show a reduction in complex I activity in the 3460 mutation but not in the 11778 and 14484 mutations (Carelli et al., 1999, 2004b; Cock et al., 1999). Therefore, a dysfunction of complex I at the level of enzyme activity has not been found consistently in cybrids and lymphoblasts carrying all three primary LHON mutations.

The same study by Brown et al. (2000) measured the respiratory function of lymphoblasts and cybrids which revealed a reduction in the maximal respiration rate at 20-28% in the 3460 mutation, a 30-36% reduction in the 11778 and 10-15% in the 14484 mutation. Defective respiratory function was also observed *in vivo* by 31 phosphorous magnetic resonance spectroscopy (^{31}P-MRS) studies. ^{31}P-MRS is a non-invasive spectroscopic technique that allows the relative quantification of the various phosphate-containing small molecules, which contribute to the ability of cells to drive ATP-consuming biochemical reactions (Kirches, 2011). Changes of the energy reserve

available to re-phosphorylate ADP, are reflected by peaks for creatinine phosphate (CrP). In LHON patients carrying the 11778 mutation these parameters were reduced in the brain and skeletal muscle (Cortelli et al., 1991; Barbiroli et al., 1995; Carelli et al., 1997). This shows that despite the absence of significant changes in the complex I enzyme activity ND4 mutants show a reduced energy conserving function. Another study showed a decrease of CrP and a corresponding increase of ADP for the 3460 mutation only in the occipital lobe tissue of the brain and not in skeletal muscle (Lodi et al., 2002). These results implicate a decrease in OXPHOS, playing a role in the pathophysiological mechanism of LHON. Furthermore, the reduced energy conserving function observed in non-retinal neural tissue might also help explain the other clinical abnormalities seen in rare cases of LHON.

A few studies have shown that despite the decrease in complex I activity and respiratory rate in cells harboring the common 11778 or the 3460 mutations, the energy availability in cells and the complex I linked ATP production was normal (Yen et al., 1998; Cock et al., 1999). In an *in vitro* study using cybrids, an impairment of complex I-driven ATP synthesis was shown for all three pathogenic LHON mutations but the total cellular ATP content did not show any significant reduction (Baracca et al., 2005). The more or less unchanged total cellular ATP levels can be attributed to compensatory ATP production by glycolysis which can mask any impairment in ATP production via OXPHOS. Human cells produce ATP via glycolysis and mitochondrial OXPHOS. Tumor cells and certain primary cell such as fibroblasts produce majority of the total ATP yield through glycolytic breakdown of glucose to lactate and only a minimal amount of pyruvate is oxidized to CO_2 and water (Ghelli et al., 2003). To overcome the reliance of cells on glycolysis, scientists replaced glucose with galactose as the main carbon source in the culture media. The production of pyruvate via glycolytic metabolism of glucose yields 2 net ATP whereas the glycolytic metabolism of galactose yields no net ATP, forcing cells to turn to mitochondrial OXPHOS to satisfy their energy requirements (Aguer et al., 2011). In a study by Zanna *et al.* (2005) it was shown that cybrids carrying all three primary LHON mutations showed a dramatic decrease in ATP in galactose media compared to control cybrids only 3 hours after switching to galactose media. Cybrids carrying the 11778 mutation also showed growth impairment in glucose-free galactose media. These findings show that all 3 primary pathogenic LHON mtDNA mutations can cause a certain degree of bioenergetic defect; however a bioenergetic

defect by itself is not sufficient to explain the pathogenesis of LHON. Features of LHON such as, higher risk of RGC degeneration in male than in female mutation carriers, selective vulnerability of RGCs and sparing of other energetically demanding cells such as photoreceptors cannot be explained by bioenergetic failure. Therefore, other factors such as reactive oxygen species, apoptosis, or nuclear genetic factors have been investigated for their involvement in the pathogenesis of LHON.

Oxidative stress

Reactive oxygen species (ROS) are generated as by-products of normal oxidative metabolism. Complex I and III have been shown to be responsible for much of the superoxide anions generated by mitochondria (Raha and Robinson, 2001). Therefore, it is possible that a defect in complex I could lead to an increase in the superoxide anion generation. Initial studies on 11778/ND4 mutant cybrid cells showed increased sensitivity to H_2O_2 exposure compared to control cybrids (Wong and Cortopassi, 1997). The cell mortality was Ca^{2+}-dependent and was partially reversed by Ca^{2+} withdrawal from the media or by treatment with Cyclosporine A, a known inhibitor of the mitochondrial permeability transition pore (mPTP). Oxele and Zwirner (1997) showed a ROS injury mediated telomere shortening in two LHON patients. In a later study scientists created an NT2 teratoma cybrid line that can be differentiated into neuron morphology using retinoic acid, in order to develop a more realistic model for LHON. A significant increase in ROS production was observed in 11778 and 3460 cybrids in the differentiated state (Wong et al., 2002). Haroon et al.(2007) were able to show a slight increase in ROS levels in the same cybrids (NT2 cybrids carrying the 11778 mutation) in the undifferentiated state that became more pronounced following the addition of an external oxidant. Other reports have also shown evidence for the increase in ROS production in all 3 LHON cybrids (Carelli et al., 2002a; Beretta et al., 2004).

The role of oxidative stress is further highlighted by studies showing evidence for reduced antioxidant defenses in LHON cell models. LHON cybrids, especially those carrying 3460 and 11778 mutations showed decreased activities of glutathione reductase (GR), glutathione peroxidase (GPx) and Mn-superoxide dismutase (MnSOD) (Carelli et al., 2002a). Floreani et al. (2005) showed a fast increase in the oxidized form of glutathione (GSSG), when 143B.TK- osteosarcoma cybrids carrying any one of the three primary LHON mutations were grown in galactose. Another study using NT2-

derived LHON cybrids with the 11778 mutation was found to contain lower levels of total glutathione per mg cellular protein compared to controls following differentiation with retinoic acid to enhance OXPHOS dependency (Schoeler et al., 2007).

An animal model generated using ribozyme mediated knockdown of SOD2 showed reduced MnSOD expression and an increase in mitochondrial ROS levels (Qi et al., 2003a). The animals also developed optic neuropathy similar to the histopathology of LHON. In another study by Qi and colleagues, 143B.TK- cybrids carrying the 11778 mutation were transduced with adeno-associated viral vector to overexpress SOD2 which resulted in a decrease in superoxide production and enhanced cell survival (Qi et al., 2007).

Patients and carriers of LHON have been shown to have reduced α-tocopherol/lipid ratio in their plasma due to increased free radical generation and consumption of α-tocopherol (Klivenyi et al., 2001). Increased ROS generation also resulted in reduced uptake of glutamate in LHON 143B.TK osteosarcoma cybrids (Beretta et al., 2004). These findings reveal a potential pathomechanism of LHON where the reduced clearance of glutamate from the synaptic cleft by retinal Müller astroglial cells can lead to excitotoxic injury to retinal ganglion cells (Beretta et al., 2004). In a mouse model that closely resembles LHON in humans, researchers discovered increased ROS production in synaptosomes which maintained stable ATP levels despite reduced complex I activity (Lin et al., 2012). These findings show that oxidative stress may play a bigger role than bioenergetic deficiency in LHON pathophysiology. However, results are not conclusive and other factors have been implicated in LHON pathophysiology such as apoptosis, nuclear genetic factors and environmental factors.

Apoptosis

The painless and non-inflammatory loss of RGCs prompted researchers to look into the role of apoptosis in the pathophysiology of LHON (Howell, 1997, 1999). FAS stimulation enhanced apoptosis in cybrids bearing the 3460 and 11778 mutations compared to wildtype cybrids (Danielson et al., 2002). Activation of caspase-3, increased DNA fragmentation (laddering) and enhanced annexin-V staining, confirmed the mode of cell death as apoptosis. It was proposed that complex I dysfunction leads to an increased probability of mitochondrial permeability transition pore (MPTP) opening which in turn can stimulate apoptosis (Fontaine et al., 1998; Danielson et al., 2002).

Although FAS-mediated cell death does not necessarily involve mitochondria, the prolonged opening of MPTP could enhance sensitivity of FAS-mediated apoptosis of LHON cybrids.

Cybrids carrying one of the three primary LHON mutations undergo increased apoptotic cell death compared to control cybrids when switched to galactose media as observed by chromatin staining and DNA laddering (Ghelli et al., 2003). The bioenergetic deficiency of LHON cybrids is exposed in galactose media which increases their susceptibility to apoptosis (Ghelli et al., 2003). In addition to rapid apoptosis, a decline in ATP was also observed in LHON cybrids carrying one of the three primary mutations compared to control cybrids when grown in galactose media (Zanna et al., 2003, 2005). The release of cytochrome c, apoptosis inducing factor (AIF) and endonuclease G (endo-G) from the mitochondria into the cytosol pointed to apoptosis as the cause of cell death (Zanna et al., 2005). Apoptosis occurred, independent of caspase activation due to ATP decline which is required for the formation of a functional apoptosome. However, AIF and endo-G release was sufficient to execute apoptosis (Zanna et al., 2005).

1.5.9. Tissue Specificity

Although the LHON mutation is present in every cell in the body, the RGCs are the only affected cells in most cases. The reason for this tissue specificity is unknown but it is speculated that the micromorphologic architecture of retinal nerve fiber layer (RNFL), optic nerve head and optic nerve plays a role in its pathogenesis. The axons of retinal ganglion cells travel through the retinal nerve fiber layer towards the optic nerve head where they take a sharp turn and exit through a small opening in the sclera and pass through the lamina cribrosa, a perforated collagen plate (Yen et al., 2006; Kirches, 2011). The mechanical compression at this point is thought to restrict axoplasmic flow, causing a buildup of mitochondria in the prelaminar axon sections (Minckler et al., 1976; Holländer et al., 1995; Howell, 1999).

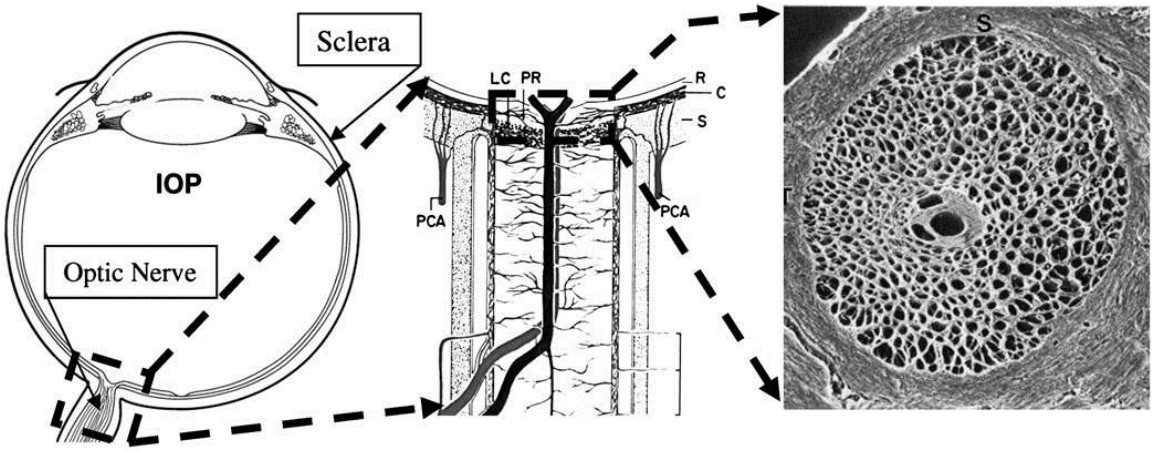

Figure 2 **Anatomy of the Optic nerve head and lamina cribrosa** (Eilaghi et al., 2010)**.**
The optic nerve composed of retinal ganglion cell axons exit the eye at the optic nerve head (pictured in the left panel and magnified in middle panel) where it must first pass through the lamina cribrosa (LC)(pictured in the middle and magnified frontal view on the right).
Note: Used with permission.

RGCs send out axons of about 5 cm length to connect the retina with the brain (Curcio and Allen, 1990). RGCs are highly polarized cells in terms of their mitochondrial distribution and myelination. Histological and Immunohistochemical studies revealed that the post-laminar portion of the RGC axons were wrapped in myelin sheaths (Barron et al., 2004) whereas the pre- and intra-laminar regions were unmyelinated and had a higher mitochondrial density compared to the post-laminar region (Andrews et al., 1999; Barron et al., 2004). Since saltatory action potential conduction is not possible in the pre-laminar region, there is a greater demand for ATP by the Na+/K+ ATPase in order to maintain the excitability of the axolemma compared to myelinated fibers in the post laminar regions (Kirches, 2011). Therefore it is imperative that mitochondria are trapped within those regions that are incapable of saltatory conduction (Kirches, 2011). The uneven mitochondrial distribution therefore reflects the local energy demand of the different axonal regions of the RGCs rather than the previously inferred axoplasmic stasis (Bristow et al., 2002). However, it is possible that this gradient of mitochondria distribution may be affected early on by LHON mutations (Kirches 2011). Mitochondrial biogenesis is a process that takes place in the cell body of RGCs from where they get transported to energy dependent locations such as the varicosities of the RNFL, the prelaminar and laminar regions, nodes of Ranvier in the post-laminar region and the synaptic terminals (Hollenbeck, 1996; Wang et al., 2003). The transport of mitochondria along the axon is itself an ATP-dependent process (Ochs and Hollingsworth, 1971; Sabri

and Ochs, 1972). The LHON mutations could result in impaired mitochondrial movement that could contribute to local energy deprivation at the unmyelinated portion of the RGC axons (Kirches, 2011). The small fibers of the papillomacular bundle are the initial targets of LHON degeneration and the susceptibility can be explained by their high surface area to volume ratio which limits their ability to compensate through increased mitochondrial biogenesis and transport (Sadun et al., 2000; Pan et al., 2012). A reduction in mitochondrial motility will also impact mitochondrial dynamics such as fission and fusion which is necessary for exchange of contents among mitochondria to avoid critical loss of components, such as mtDNA (Kirches, 2011). An exchange of components (mtDNA, RNA, soluble proteins, small molecules) between migrating mitochondria is important for the maintenance of a pool of functional mitochondria (Kirches, 2011). Histopathalogical studies of LHON nerves showed clumps of mitochondria in spared axons in the retrolaminar portion of the optic nerve, accumulations of multi-vesicular bodies and debris, and cytoskeletal changes that suggest impaired axonal transport (Sadun A, Kashima Y, Wurdeman A, Dao J, Heller K, 1994). The selective vulnerability of RGCs could therefore be due to a combination of factors which include high metabolic rate, atypical morphology and mitochondrial distribution.

1.5.10. Disease models

Although the clinical and genetic aspects of LHON are well known, little progress has been made in understanding the pathophysiological mechanism(s) of LHON. This is partly due to the impracticality of harvesting and experimenting on target tissue i.e. optic nerve, from LHON carriers and patients. Instead scientists have had to rely on other cell models to understand the pathomechanism of the disease. Until recently no animal models existed for the disease. Lymphoblasts, fibroblasts and transmitochondrial hybrids (cybrids) were the most commonly used cell models in LHON research but new cell and animal models have also been developed in the recent years. A virally transformed rat retinal ganglion cell line known as RGC-5 was the only retinal ganglion cell line in existence until recent evidence showed these cells were a misidentified mouse photoreceptor cell line (Van Bergen et al., 2009; Krishnamoorthy et al., 2013). As a result use of RGC-5 has been restricted in the study of the biology and mechanism of death of RGCs.

Lymphoblasts

The source for lymphoblast cell cultures are cells from peripheral blood samples which are immortalized by Epstein Barr virus (EBV) (Jankauskaitė et al., 2017). They divide rapidly and provide researchers with a constant supply of starting material for experimentation. Lymphoblasts harboring LHON mutations have been used to screen growth impairments, measure complex I driven ATP synthesis and OXPHOS enzyme activity in glucose free galactose media (Brown et al., 2000; Van Bergen et al., 2015) as well as to screen for oxidative and nitrosative stress (Falabella et al., 2016). However lymphoblast cultures do come with limitations such as sensitivity to factors such as temperature, pH, growth media, serum and length of time in culture (Jankauskaitė et al., 2017). In addition, lymphoblasts cultures are heterogenous and transformation with EBV can affect cell metabolism (Jankauskaitė et al., 2017). For these reasons the lymphoblast cell line is not ideal for biochemical and cellular studies.

Fibroblasts

Fibroblasts cultures overcome some of the limitations associated with lymphoblasts. They are derived from skin biopsies and are easy to grow in culture. Fibroblasts are primary cells and will closely mimic normal cellular physiology and metabolism. Fibroblast cell cultures have been used for mitochondrial proteome analysis (Tun et al., 2014), investigating the influence of environmental factors such as alcohol and tobacco smoke (Kerrison et al., 2000; Kirkman et al., 2009; Giordano et al., 2015) and in metabolic studies (Cock et al., 1995; Giordano et al., 2014). However, fibroblasts are non-neuronal, mitotic and primarily glycolytic in contrast to the neuronal, post-mitotic retinal ganglion cells that rely primarily on OXPHOS for their energy requirements. Furthermore, factors such as morphology, organelle trafficking and topology are different between the fibroblasts and RGCs. Therefore, caution must be exercised when extrapolating results from fibroblasts studies.

Cybrids

The transmitochondrial cytoplasmic hybrid (cybrid) model has been extensively used for LHON studies. Cybrids are created by depleting cells of their native mtDNA and fusing them with foreign mtDNA from enucleated cells or cytoplasts. In yeast, the process is known as cytoduction where nuclear fusion deficient cells are mated with strains of opposite mating type which yield hybrids that retain the nuclear composition of

one parent and cytoplasmic (mitochondrial) composition from the other (Zakharov and Yarovoy, 1977). The cell model was introduced by King and Attardi (1989) where mtDNA from osteosarcoma cells were depleted by long term exposure to sub-lethal concentrations of ethidium bromide and the resulting cells were known as ρ0 (rho-0) cells. The ρ0 cells were then repopulated with mtDNA from enucleated cells of a cell line chosen to be the mtDNA donor (Kirches, 2011). In addition to osteosarcoma cells other tumor cell lines such as teratoma or neuroblastoma lines have been used in cybrid construction and blood platelets have been used as mtDNA donor cells as they do not require enucleation (Kirches, 2011). The advantage to using cybrids in LHON studies is that they allow detection of cell physiology resulting from mitochondrial dysfunction and eliminate the influence of the nuclear background of the patient. The cybrid model has contributed much to our current understanding of LHON. Cybrids carrying one of the three primary LHON mutations have been used in complex I activity assays (Vergani et al., 1995; Brown et al., 2000), for measuring ATP production (Baracca et al., 2005) as well to investigate oxidative stress (Floreani et al., 2005) and apoptosis (Ghelli et al., 2003; Zanna et al., 2005). Furthermore, cybrids carrying one of the three primary LHON mutations have been used in studies investigating glutamate toxicity (Beretta et al., 2004), hormonal effects (Giordano et al., 2011), transcriptomic analysis (Danielson et al., 2005) and the influence of mitochondrial haplogroups on disease expression (Brown et al., 1997; Carelli et al., 2002c). Despite their utility in LHON studies, cybrids also have many disadvantages. The multi-step cybridization procedure can cause cellular stress resulting in changes in gene expression. A study by Danielson et al. (2005) showed transcriptomic changes between unfused control cells, ρ0 cells and cybrids. The cybridization process is also time-consuming and cybrids require long term selection. In addition, the ρ0 are derived from immortalized cells and therefore have a tumor nuclear background. Thus, it is difficult to know how much of the knowledge obtained from studying cybrids can be applied to LHON pathogenesis.

Animal models

Animal models are difficult to engineer for mitochondrial diseases due to technical limitations. However using different approaches, a few animal models resembling LHON have been generated in the recent years (Koilkonda and Guy, 2011). The first animal model for LHON was made by intravitreous injection of rotenone, a complex I inhibitor, into mice (Zhang et al., 2002). Histological analysis showed thinning

of the RGC layer similar to RGC degeneration in LHON. Following this, Qi et al.(2003b) designed a ribozyme to degrade the mRNA of NDUFA1, a nuclear encoded subunit gene of complex I. The ribozymes were delivered using the AAV vector into the vitreous cavity and resulted in loss of RGCs that resembled the histopathology of LHON. There was also marked reduction of complex I activity and oxidative stress. Another mouse model was created by the same group using ribozymes directed against mitochondrial superoxide dismutase (SOD2) mRNA, which also resulted in optic neuropathy with striking similarity to LHON histopathology (Qi et al., 2003a). The intraocular injection of an AAV overexpressing SOD2 mitigated RGC and axonal loss in the mouse model and also increased cell viability in a LHON cybrid model grown in galactose media. These studies point to antioxidant genes as targets in developing therapeutic agents. However, these animal models represent a more severe complex I defect whereas certain primary LHON mutations (e.g. 11778) only show a minor reduction in complex I activity. In order to develop a more representative animal model Qi et al. (2007) designed a synthetic mutant ND4 subunit gene which was injected to the mouse visual system. The mutant ND4 subunit gene contained an arginine to histidine substitution at amino acid 340 which is representative of the ND4 mutation in LHON. The treatment resulted in the swelling of the optic nerve head followed by optic nerve atrophy and loss of RGCs. Ultrastructural analysis revealed elevated ROS followed by apoptosis of RGCs. Injection of synthetic wildtype ND4 revealed no evidence of pathology. Therefore the mouse model was comparable to the human disease (Koilkonda and Guy, 2011). More recently, Lin et al. (2012) created a mouse model that harbors a mitochondrial mutation that resulted in optic atrophy that closely modeled LHON pathology. The murine model contains a mutation at G13997A, which causes the same amino acid substitution (proline to leucine at amino acid position 25) as reported in a human ND6 G14600A optic atrophy and Leigh syndrome family (Lin et al., 2012). A multistep approach was used in the generation of the mouse model. First, LMTK murine fibroblasts were mutagenized and mutant mtDNA species were enriched by depletion-reamplification and cloning. Following glucose-galactose selection, clones with partial respiratory defect were selected and their mtDNA sequenced. The clone for the proline to leucine (P25L) substitution at amino acid position 25 was picked, enucleated and fused to a female mouse embryonic stem cell line. These were then injected into blastocysts, after which the females harboring the mutation were backcrossed for over 10 generation resulting in the ND6 13997G>A mouse model. Investigation of mitochondrial function in the

synaptosomes of this mouse model revealed that oxidative stress plays a bigger role in the pathophysiology than bioenergetic defect (Lin et al., 2012).

1.6. Objectives and Rationale

The absence of a suitable model system has been a major barrier in our understanding of the disease pathophysiology. In this study, we created a new disease model for studying LHON that will help answer some of the questions that current models are unable to answer. We created a fibroblast cell model system that resembles neuronal morphology that will enable the study of mitochondrial trafficking as current cell models do not allow for the study of mitochondrial dynamics due to their highly reticulated mitochondrial networks.

Objective 1: Investigate the changes to the cell morphology of dermal fibroblasts treated with a broad spectrum kinase inhibitor, staurosporine at sub lethal concentrations.

Staurosporine (STSP) is a natural alkaloid isolated from the bacterium *Streptomyces staurosporeus*. Although it is best known as a high affinity protein kinase C (PKC) inhibitor, STSP's inhibitory actions are not limited to PKC but extend to over 250 protein kinases making it a broad spectrum kinase inhibitor (Karaman et al., 2008). The non-selective nature of STSP inhibition of protein kinases is thought to be due to its binding to the ATP-binding site on the catalytic domain common to all protein kinases (Rüegg et al., 1989). One of first observed effects of staurosporine was cytotoxicity which has led to its use as a common apoptosis-inducing agent. Changes to the phosphorylation state of proteins have been shown to be an important trigger of programmed cell death induced by different agents (Baxter and Lavin, 1992; Uckun et al., 1992). STSP has been shown to induce caspase-3/7 dependent apoptosis (Jiang et al., 2013). Another yet unexplained effect of staurosporine has been its ability to induce cytoplasmic protrusions that resemble neurites in a range of different cell types when administered in sub-lethal concentrations.

Among the different cell lines known to demonstrate STSP dependent changes in cell morphology include, 3Y1, COS7, HepG2, H1299 (Kohno et al., 2015). STSP has been shown to differentiate neuronal precursor cell lines, PC-12 (Hashimoto and Hagino, 1989), NB-1 (Morioka et al., 1985), SHSY5Y (Shea and Beermann, 1991) and RGC-5

cells (Frassetto et al. 2006). Differentiation with STSP causes RGC-5 cells to stop dividing, express ion channels and assume neuronal morphology (Thompson and Levin 2010). The neurites in these differentiated neural precursor cells immunostain for neuron specific proteins such as microtubule-associated protein 2 (MAP2), tau, growth associated protein (GAP-43) (Jalava, Akerman, and Heikkila 1993; Rasouly et al. 1994; Thompson and Levin 2010). The mechanism of how STSP induces morphological changes has not been elucidated. Attempts to induce similar phenotypic changes with other specific kinase inhibitors have either failed or have only been partially successfully (Frassetto et al. 2006). Therefore, the effects are thought to be either a result of different levels and specificities of protein kinase inhibition or effects on other cellular processes independent of kinase inhibition. However, it has been established that the process is not related to induction of apoptosis (Kohno et al. 2015; Thompson and Levin 2010).

The extension of processes in response to STSP treatment is rapid, occurring within seconds to minutes after STSP addition and is time- and concentration dependent although concentrations above 1 uM have been shown to be cytotoxic (Frassetto et al., 2006; Galkina et al., 2010; Kohno et al., 2015). The chemical induction of processes in human dermal fibroblasts containing LHON mutation will be useful for studying mitochondrial dynamics in LHON cells.

Hypothesis 1: Low concentrations of staurosporine induce cytoplasmic protrusions in both LHON and wild-type dermal fibroblasts.

Following the creation of the cell model, we investigated and compared the mitochondrial movement in the processes of wild-type and LHON cells in glucose media and glucose-free, galactose media. The glucose-free, galactose media forces glycolytic cells such as fibroblasts to rely on OXPHOS to satisfy their energy demands.

Objective 2: Compare the mitochondrial motility/trafficking in the staurosporine induced processes of wild-type versus G11778A LHON fibroblasts

The movement of mitochondria from their sites of biogenesis to distant regions of the cell is especially important for cells such as neurons that have a high ATP demand in regions such as the nodes of Ranvier and synaptic terminals (Carelli, Ross-Cisneros and Sadun 2004). The movement of mitochondria requires ATP, a portion of which the mitochondria themselves provide (Ochs and Hollingsworth 1971, Sabri and Ochs 1972).

If LHON mitochondria are defective in their movement, it is likely to have an impact on the health of RGCs. Mitochondria trafficking defects have been shown in neurodegenerative diseases such as Charcot-Marie tooth disease (Baloh et al. 2007), Parkinson's disease (Chan et al., 2011; Wang et al., 2011), Huntington's (Trushina et al. 2004), Perry Syndrome (Levy et al., 2006; Ishikawa et al., 2014) etc. This necessitates more extensive research into the role of mitochondrial dynamics in pathogenesis of LHON. Our fibroblast cell model will allow investigation of mitochondrial movement more easily due to their newly acquired morphology.

Hypothesis 2: The mitochondrial movement is decreased in LHON fibroblasts compared to wildtype fibroblasts during metabolic stress (glucose free, galactose media)

Objective 3: Compare the mitochondrial network morphology in staurosporine treated wild-type and G11778A LHON fibroblasts under glycolytic and OXPHOS conditions

The net mitochondrial ultrastructure is determined by the balance between fission and fusions reactions (Koopman et al., 2013). Furthermore, mitochondrial morphology is linked to mitochondrial function and metabolism during healthy and pathological conditions including neurodegeneration (Knott et al., 2008; Willems et al., 2009; Court and Coleman, 2012). An elongated, tubular and highly branched mitochondrial morphology promotes the health of the active mitochondrial population and are more efficient at generating energy whereas punctate, discrete or fragmented mitochondrial morphology promote their distribution, mitophagy and apoptosis (Mishra and Chan, 2016). Under normal physiological conditions mitochondria maintain a balance between fission and fusion but during metabolic stress such as OXPHOS, hypoxia, nitrogen starvation, this balance can be shifted leading to altered mitochondrial morphology (hyper-fused or fragmented). Therefore mitochondrial morphology can serve as an indicator to detect changes to the mitochondrial dynamics.

Hypothesis 3: The mitochondrial morphology in STSP-treated LHON fibroblasts is different from that of wild-type under OXPHOS conditions

Chapter 2. Materials and Methods

2.1. Cell culture

2.1.1. Cell harvest

Skin biopsies were performed on a male diagnosed with the G11778A mitochondrial mutation and age and sex matched control. Both males were in their early twenties and non-smokers. The male patient was homoplasmic for the G11778A mutation as determined by RFLP analysis (Johns, 1990). A 3mm diameter skin punch was performed by Dr. C. Sheldon (MD PhD) at the Eye Care Center, Vancouver General Hospital. The skin punches were divided and plated in a 12 well plate with 1 ml of complete fibroblast media (CFM) added to each well. Each well was covered with a 18 mm diameter round glass coverslip to facilitate the outgrowth of cells. The cells were incubated at 37^0 C and 5% CO_2 for 3 weeks with media changes every 7 days. Fibroblasts were then aliquoted in cryovials with 10% DMSO (dimethyl sulfoxide), 50% Fetal Bovine Serum and 40 % CFM and frozen in liquid nitrogen. Prior to experimentation, fibroblasts aliquots were thawed and seeded into T75 flasks with 10 ml CFM.

2.1.2. Cell growth conditions

Complete Fibroblast media (CFM) was made by combining Dulbecco's Modified Eagle Medium (DMEM) and 5% Fetal Bovine Serum (FBS) and supplemented with 1% antibiotic (penicillin and streptomycin) solution (Gibco). The solution was sterile filtered using vacuum filtration.

DMEM (Gibco) contains low glucose (5.6 mM), L-glutamine, 110mg/L sodium pyruvate and pyridoxine hydrochloride. DMEM provides essential amino acids, vitamins and inorganic salts for the growth of mammalian cells. In order to make CFM with galactose, a premade glucose free DMEM (GF-DMEM) solution was used, and supplemented with 10mM galactose.

Characterized Fetal Bovine Serum (Hyclone) contains approximately 90 mg/dl glucose and is made from a fraction of fetal cow's blood with proteins and growth factors

which facilitate fibroblast growth. For CFM with galactose, FBS which had previously undergone a dialysis procedure to filter out smaller molecules such as glucose, was used. The final concentration of glucose in the dialyzed FBS was approximately 1.4mg/dl. The methodology for cell culture conditions were adapted from the procedure described by Rossignol et al. (2004).

Fibroblasts grow in monolayers and are said to be confluent when they cover the entire surface of the well. Once 80% confluency is achieved the fibroblasts were split and seeded, a process known as passaging. First the fibroblasts were trypsinized with 5ml of 0.25% EDTA-trypsin (Invitrogen) for 1 minute at 37^0 C. This helps break down extracellular matrix proteins and cell adhesion molecules in order to loosen the cells and get them into solution for harvesting. The concentration of cells is then estimated using a hemocytometer. The fibroblasts were then diluted to a concentration of 25,000 cells/ml and seeded into a 12 well plate at 1 ml per well. Extra fibroblasts were used for re-seeding T75 flasks and grown for a week before passaging again. Due to the finite replicating capacity and senescence associated with increasing passages of primary cells grown in culture known as the Hayflick limit (Hayflick, 1965), only fibroblasts that were passaged 8 times or less were used for experimentation. A complete change in media was performed 24 hours after seeding, where wells were given either CFM (glucose-fed) or CFM-Gal media (galactose-replacement).

2.1.3. Staurosporine (STSP) treatment

Twenty-four hours after the media change the fibroblasts were treated with either staurosporine (Cayman Chemical) dissolved in ethyl acetate to a final concentration of 750 nM or an equal concentration of ethyl acetate alone (vehicle control). The plates were incubated for another 24 hours at 37°C and 5% CO_2. Following the 24-hour incubation, the media was aspirated from each well, washed once with fresh media and replaced with fresh media (STSP treatment termination). Half the coverslips were imaged 1-hour after the treatment termination while the other half was imaged 24 hours after treatment termination to determine if any changes observed in response to STSP treatment are transient or persistent.

2.2. Labelling cells and nuclei

In order to study the morphology of the fibroblasts following staurosporine (STSP) treatment, the coverslips were treated with the fluorescent dye H_2DCFDA (2', 7'-dichlorodihydrofluorescin diacetate) (Molecular Probes®). H_2DCFDA readily diffuses into cells and can be used for labelling entire fields of cells. Upon entering cells, the non-fluorescent DCFDA is de-acetylated by cellular esterases and oxidized by ROS into DCF (2',7'-dichlorofluorescein) in the presence of Fe^{2+} (Rothe and Valet, 1990) which is a highly fluorescent compound with an excitation and emission spectra of 498 nm and 522 nm respectively. The H_2DCFDA was diluted in glucose free HBSS (see 2.4 below) to a final concentration of 2.5 µM and added to the wells after removal of media and then incubated for 30 minutes at 37°C. After the incubation, the coverslips were rinsed twice with glucose free HBSS and imaged in 500 µL of either HBSS or HBSS-Gal.

To measure cell viability of STSP treated fibroblasts, the cells were co-stained with Hoechst 33342 (Molecular Probes®). Hoechst 33342 is a cell permeable DNA stain that is excited by UV light (~350nm) and emits blue fluorescence at 460-490 nm (Latt and Stetten 1976) and is a derivative of bis-benzimidazole. Due to its ability to bind to adenine-thymine (A-T) regions of DNA, Hoechst is used for staining nuclei of living or fixed tissue (Portugal and Waring, 1988). 1.5 µM of Hoechst was added to each well and incubated for 30 minutes along with H_2DCFDA at 37^0 C and 5% CO2. The coverslips were rinsed twice as mentioned above an imaged in 500 µM of either HBSS or HBSS-Gal.

2.3. Labelling mitochondria

A mitochondrially-targeted enhanced yellow fluorescent protein (mt-eYFP) (gifted by Roger Tsien) was used for real time visualization of mitochondria in STSP treated fibroblasts. The construct contains a COX-IV mitochondrial targeting sequence preceding the eYFP coding region cloned into a pcDNA3 mammalian expression vector. The eYFP has an excitation peak of 514 nm and an emission peak of 527 nm.

The cells were transfected with mt-eYFP using Lipofectamine® LTX and PLUS reagent a day after they were passaged at a density of 25,000 cells/ ml. The protocol is as follows. A mastermix consisting 100 µl of DMEM (or GF-DMEM), 0.5 µg of mt-eYFP

plasmid, 0.5 µl of PLUS reagent and 1.25 µl of LTX per well, was prepared and incubated at room temperature for 30 minutes to facilitate the formation of Lipofectamine: DNA complexes. Following the incubation, 100 µL of the mastermix was added to each well containing 400 µl of CFM or CFM-GAL. The plates were incubated for 6 hours at 37^0 C and 5% CO_2. After 6 hours, the transfection was terminated by changing the media with fresh CFM or CFM-GAL. After 24 hours, the transfected fibroblasts were treated with 750 nM STSP and incubated for another 24 hours at 37^0 C and 5% CO_2. The media was then changed following a single rinse in fresh media and imaged either 1-hour or 24-hour after STSP treatment termination.

2.4. Fluorescence microscopy

Fluorescence imaging was performed on a Nikon Eclipse TE 2000E2 inverted microscope with barrier filter attachments for specification of excitation and emission wavelengths. A Sutter instrument Lambda-LS Xenon Arc lamp was used as a light source for the microscope and images were captured with an ORCA-AG digital CCD camera (Hamamatsu Photonics) mounted on the microscope. HCImage software (Hamamatsu Photonics) was used to operate the microscope and the camera and also for image processing.

HEPES Buffered Saline Solution (HBSS) was used as the imaging buffer which mimics physiological conditions of cells and lacks proteins that emit autofluorescence which can interfere when measuring epifluorescence of cells. HBSS contains 20 mM HEPES (4-(2-hydroxyethyl)-1 piperazineethanesulfonic acid), 137 mM NaCl, 5.4 mM KCl, 0.6 mM Na_2HPO_4, 0.6 mM KH_2PO_4, 0.9 mM $MgSO_4$, 1.4 mM $CaCl_2$, 10 mM $NaHCO_3$ and 5.6 mM glucose. The pH was adjusted to 7.4 at 21°C with NaOH or HCl. HEPES is a zwitterionic organic molecule which is used to buffer HBSS to physiological pH of cells when imaging in atmospheric CO_2. For HBSS with galactose (HBSS-Gal) 5.6 mM glucose was replaced with 10.0 mM galactose.

For characterizing the morphology and assessing cell viability of staurosporine-treated fibroblasts, four representative fields of the H_2DCFDA and Hoechst stained cells were captured from each coverslip at 100x magnification, at a binning of 1. All images were acquired at room temperature.

For movement analysis, time lapse movies of individual cells labelled with mt-eYFP were captured at a 400x magnification, a binning of 1 and at 37^0 C. Time lapse movies consisted of 26 successive images over a 2-min period. The movies were obtained 1-hour and 24-hour after STSP treatment termination.

2.5. Ratiometric Imaging of ATP

Ateam (Adenosine 5'- Triphosphate indicator based on Epsilon subunit for Analytical Measurement) is a fluorescence resonance energy transfer (FRET)-based indicator for ATP which is used for real time monitoring of ATP levels inside individual living cells (Imamura 2009). Ateam is composed of a ε subunit of the bacterial F_0F_1-ATP synthase and has a high specificity for ATP. The ε subunit links a monomeric super enhanced cyan fluorescent protein (mseCFP) to a monomeric yellow fluorescent protein (YFP) called cp173-mVenus. In the absence of ATP, the two fluorescent proteins are separated from one another, resulting in low FRET efficiency. The binding of ATP to the ε subunit causes a conformational change that brings the two fluorescent proteins closer together which increases FRET efficiency (Fig 3). The changes in FRET efficiency facilitate ratiometric imaging to determine relative ATP levels. A high cp173-mVenus/mseCFP emission ratio indicates a relatively high ATP level whereas a low cp173-mVenus/mseCFP emission ratio is an indicator for a relatively low ATP level.

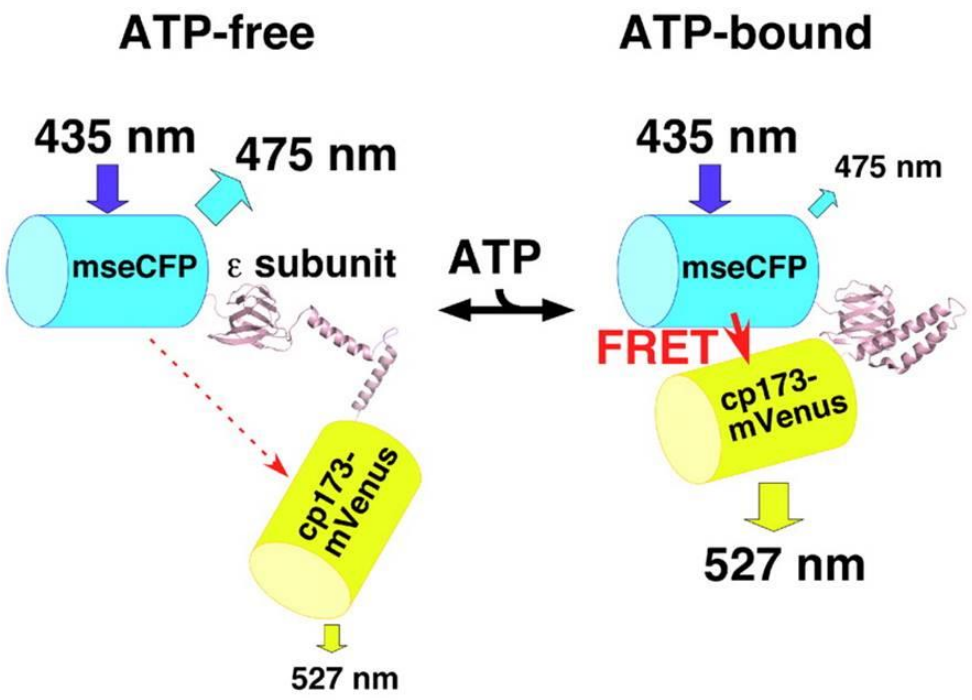

Figure 3 Schematic drawing of FRET-based ATP probe, Ateam. (AT1.03 probe)(Imamura et al., 2009)
Variants of CFP (mseCFP) and YFP (cp173-mVenus) connected by the ε subunit of *Bacillus subtilis* F_oF_1-ATP synthase. In an ATP-free state, the fluorophores are farther apart resulting in low FRET effieciency (left). In an ATP-bound state, the ε subunit retracts to draw the fluorophores close to each other resulting in high FRET efficiency.
Note: Used with permission.

The Ateam construct was provided by Dr. H Imamura in a pcDNA 3.1 plasmid vector for mammalian expression. The Ateam plasmid was transfected using Lipofectamine® LTX and PLUS reagent for measuring relative ATP levels. The transfection and staurosporine-treatment protocol was the same as for mt-eYFP labeling of mitochondria. The cells were visualized by exciting them at 436 nm wavelength and collecting the emissions at 535 nm (pseudocolored green) in one channel and 465 nm (pseudocolored blue) in the other channel. The exposure time was adjusted to avoid saturation in the regions with the highest intensity. Images of individual cells were captured at 400x magnification and a binning of 2 and the final image was generated by superimposing the images from the 2 channels.

2.6. Data Analysis

The number and length of cellular processes was measured using the NeuronJ plugin in ImageJ software (Meijering et al., 2004). Prior to loading NeuronJ, the multi-

channel images of H_2DCFDA and Hoechst stained fibroblasts are first split into their respective red, green and blue image components on ImageJ and only the green component displaying the H_2DCFDA stained fibroblasts are used for process tracing. The images are then saved following contrast enhancement and calibration. These images are then loaded in NeuronJ and each process that is equal to or greater in length than the diameter of the cell body and is less than or equal to half the width of the cell body is traced using the semi-automated tracing tool (fig 4&5). The neurites are labelled according to which cell they belong to. The measure tracings option will then generate a text file containing both individual neurite length measurements and combined and average neurite length measurement for the field. The cell counts in 100x magnification fields were obtained by using a custom-built macro in HCImage software.

For each captured cell expressing the Ateam plasmid, the fluorescence intensity for YFP (535 nm) and CFP (465 nm) emissions were obtained from three representative regions of the cell using HCImage software. Following background subtraction, the average cp173-mVenus/mseCFP emission ratio was calculated to determine the relative level of cellular ATP.

Mitochondrial movement analysis was performed using a custom built visual basic macro (Rintoul et al. 2003). Prior to running the macro, a fluorescence threshold was applied to identify mitochondrial pixels and distinguish from non-mitochondrial (i.e. background) fluorescence. Mitochondrial movement was detected by monitoring the changes in fluorescence activity of individual pixels between each successive frame. Any transition of a pixel from bright to dark or vice versa was scored as +1 and these were summated for a pair of successive images and divided by the total pixels (bright to dark+ dark to bright+ unchanged) to generate a movement ratio (fig 6). The mean movement ratio was calculated by averaging the movement ratio for each pair of successive images of a 26-frame time lapse movie.

Mitochondrial network morphology of each cell transfected with mt-eYFP captured at a 400x magnification and a binning of 1, was analyzed using Mitochondrial Network Analysis (MiNA) toolset (Valente et al., 2017) which uses a combination of different ImageJ macros. Briefly, after pre-processing the image to enhance contrast, the image is first converted to binary by thresholding where a foreground pixel is assigned the maximum value (255) and background pixels are assigned the minimum possible

value (0), the binary image is then converted to a skeleton that represents the features in the original image using a wireframe of lines one pixel wide (fig 7). All pixels within a skeleton are then grouped into three categories: end point pixels, slab pixels, and junction pixels (fig 8). The length of each branch and the number of branches are measured by how each pixel is defined and spatially related. MiNA recognizes only two distinct object types: individuals (no junctions) and networks (structures with at least one junction) (fig 8). Of the nine parameters computed by MiNA, we used four parameters which are 1. Mean number of individuals structures with no branches (puncta and rods) 2. Mean number of mitochondrial networks 3. Mean length of rods/ network branches 3. Mean number of branches per network.

Statistical analysis was performed using Graphpad Prism version 5.04 for Windows (GraphPad Software, San Diego California USA, www.graphpad.com) and SPSS Statistics (IBM analytics). A p value of less than 0.05 was considered to be statistically significant result represented by an asterisk in bar graphs.

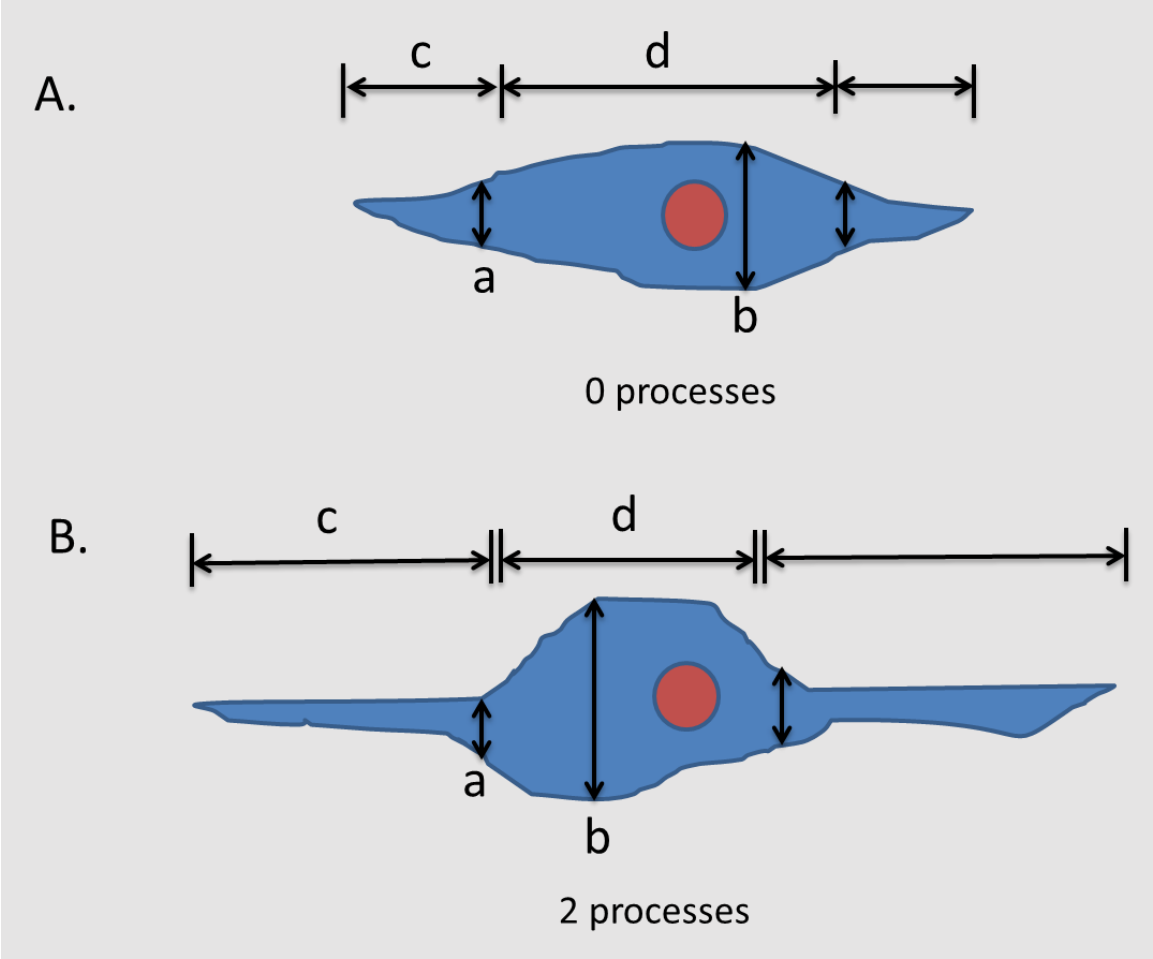

Figure 4 Identification of cellular processes.
A process is defined when its length (c) is equal to or greater in length than the diameter of the cell body (d) and width (a) is less than or equal to half the width of the cell body (b).

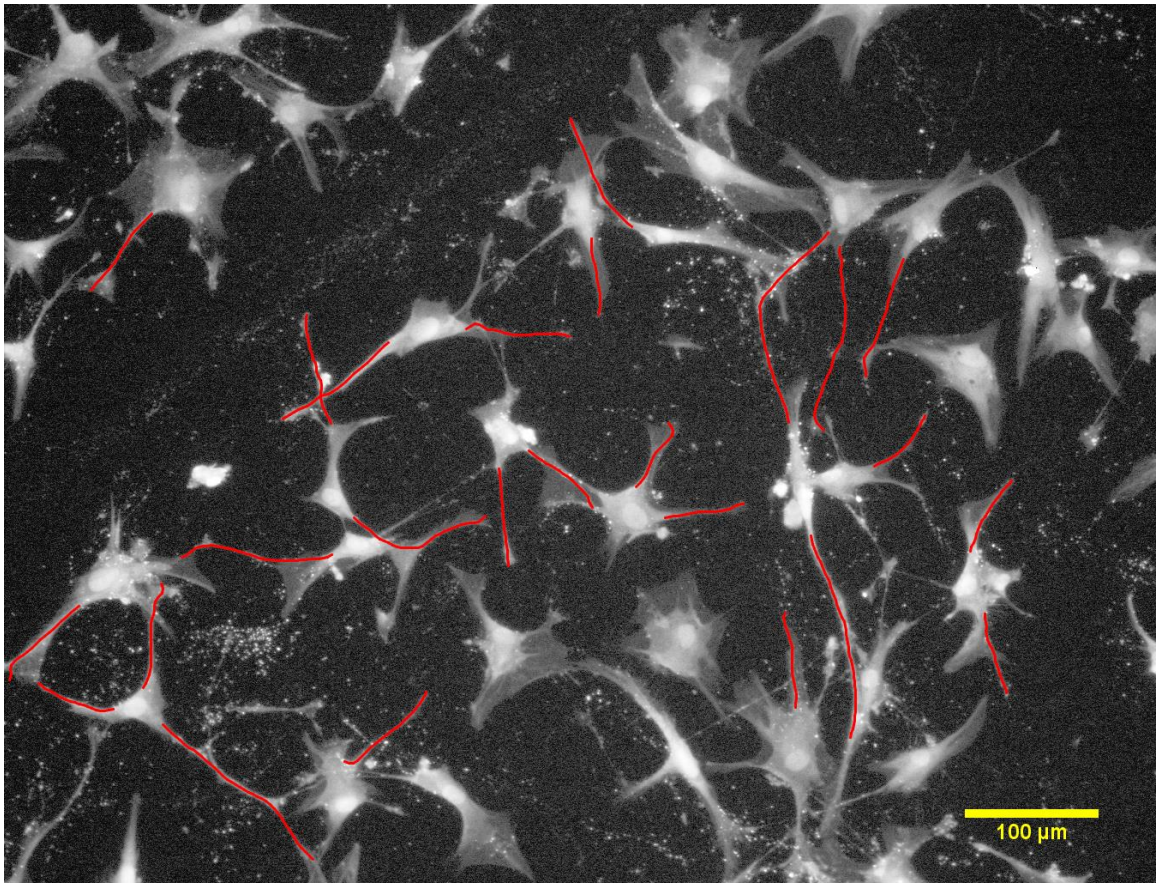

Figure 5 NeuronJ allows semi-automated tracing and quantification of elongated image structures

Neurite trace of a field containing STSP treated fibroblasts stained with H_2DCFDA

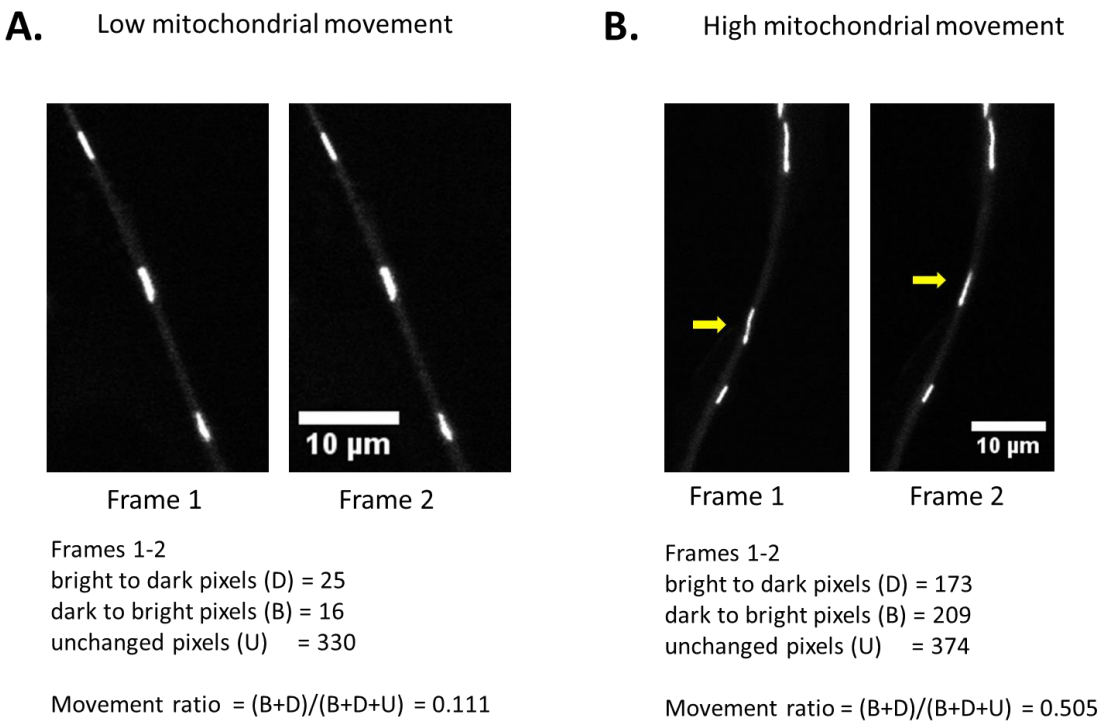

Figure 6 The mitochondrial movement macro allows quantification of bulk (non-directional) movement of mitochondria within cellular processes of STSP treated fibroblasts

A. Little to no movement of mitochondria correspond to only small changes in fluorescence (bright to dark, dark to bright) of mitochondrial pixels between successive frames resulting in a lower movement ratio. **B**. High mitochondrial movement correspond to greater changes in fluorescence of mitochondrial pixels between successive frames resulting in a higher movement ratio

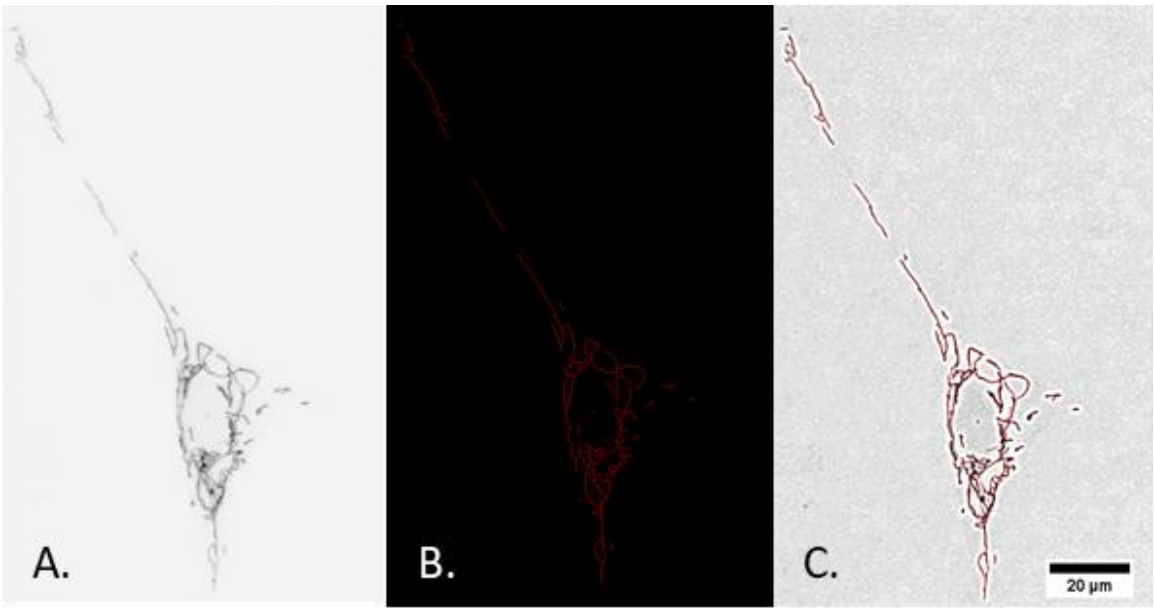

Figure 7 Mapping of the mitochondrial network of a STSP treated fibroblast transfected with mt-eYFP using MiNA.

Original image (A) is binarized and sketelonized (B) after pre-processing. The overlay of the skeletonized image on the original image (C)

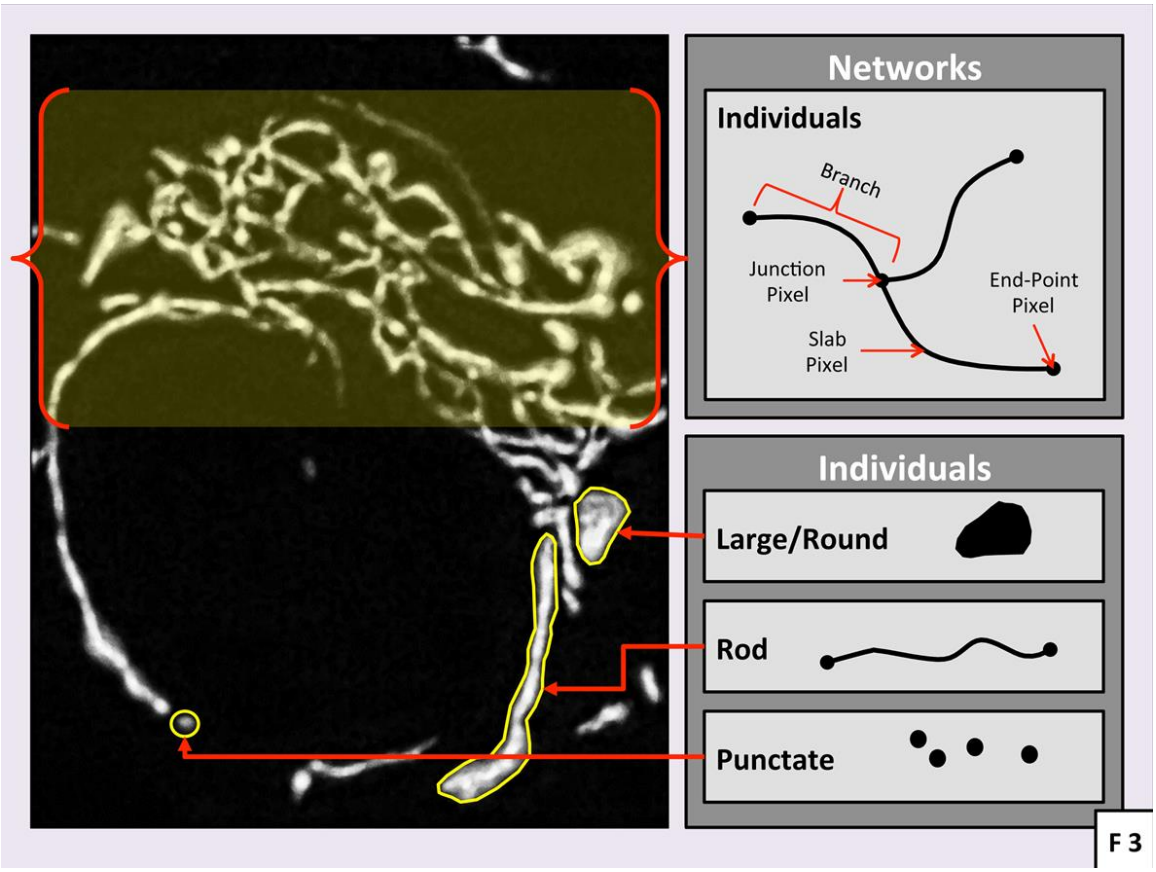

Figure 8 **MiNA recognizes common mitochondrial network features** (Valente et al., 2017)

MiNA recognizes two types of mitochondrial structures in a skeletonized image; individuals (puncta, rods, large round structures) and networks which are mitochondrial structures with at least a single junction pixel.
Note: Used with permission

Chapter 3. Results

3.1. Characterization of staurosporine treated fibroblasts

A typical fibroblast has fusiform morphology (figure 9A). Treatment with STSP causes the cell body to shrink. Furthermore, the presence of one or more cytoplasmic protrusions can be seen extending from the cell body (figure 9B).

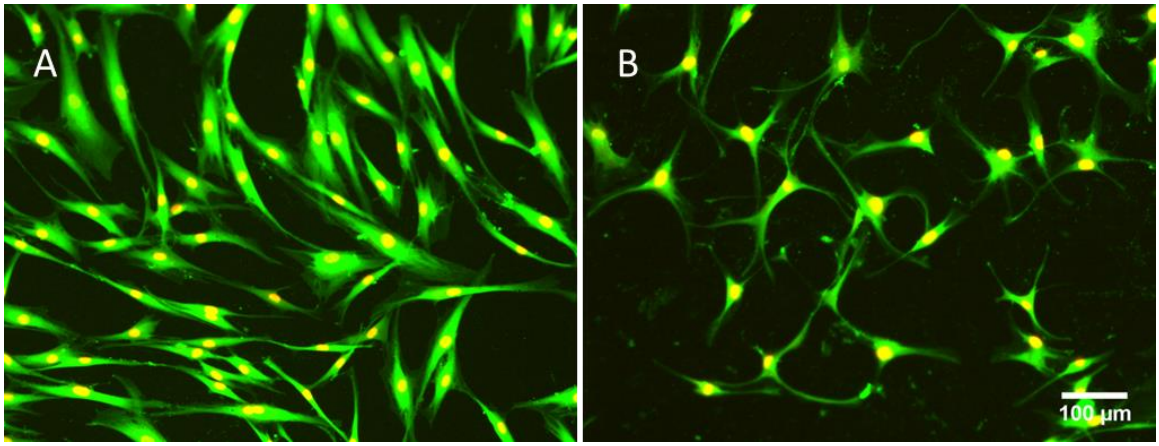

Figure 9 Staurosporine induces a neuron-like morphology in primary human fibroblasts

Human dermal fibroblasts were stained with H_2DCFDA fluorescent dye and Hoechst 33342 to label cell body and nuclei respectively. **A**. Vehicle-treated control fibroblasts exhibit a typical, fusiform morphology with two processes tapering from opposing sides of the cell body. **B**. 750 nM STSP-treated fibroblasts display multiple processes radiating from a more compact cell body.

The concentration-dependence of staurosporine-induced cytoplasmic protrusions was examined over a range of 500-1000 nM. The range was selected based on a study by Frassetto et al (2006) which showed that treatment with STSP from 316 nM to 1.78 µM for 24 hours induced a significant dose-dependent formation of neurites in RGC-5 cells. In the present study, a concentration of 750 nM staurosporine was found to be optimal for inducing cytoplasmic protrusions with minimal cytotoxicity (fig A.1, A.2 & A.3). The cell counts of STSP treated WT and LHON fibroblasts were compared in culture conditions that promoted primarily glycolytic metabolism (glucose media) and also under conditions that forced oxidative metabolism (galactose media) to assess whether there was a difference in cell viability between WT and LHON cells in response to STSP treatment. The cell counts for STSP treated WT and LHON cells were normalized to the mean cell counts of vehicle treated control WT and LHON cells cultured in parallel at the

same cell density. This was done to control for the known differences in the growth rates between WT and LHON cells. The concentration of 750 nM of staurosporine did produce a certain level of toxicity (~45% in LHON cells at 24 hours post STSP removal) but did not cause a significant difference in cytotoxicity between wild-type and LHON fibroblasts under conditions that promoted glycolysis or under conditions that induced OXPHOS (fig 10). In other words the toxicity was the same for both WT and LHON cells under the two different culture conditions. These results were consistent at both 1-hour and 24-hour after STSP removal.

We characterized the effect of STSP on fibroblast (WT and LHON) morphology based on number of processes per cell and average length of a process. The characterization was performed in both glycolytic conditions (glucose media) and in OXPHOS conditions (galactose media) to evaluate whether the changes observed are consistent under both metabolic conditions. Staurosporine-induced morphological changes were quantified by counting cellular processes or projections that are greater than or equal to the length of the cell body and are less than or equal to half the width of the cell body (fig 4). The definition of a process is slightly modified from the definition used by Frassetto et al (2006) to characterize STSP-treated RGC-5 cells. The proportion of cells that had one or more cellular processes was significantly higher for fibroblasts (WT and LHON) treated with 750nM STSP compared to vehicle-treated under conditions of primarily glycolytic metabolism (glucose media) 1-hour post STSP termination (χ^2, $p<0.0001$) (fig 11). The proportion of cells with processes was also significantly greater for fibroblasts (WT and LHON) treated with STSP compared to vehicle treated cells under conditions of primarily glycolytic metabolism 24 hours after STSP removal (χ^2, $p<0.0001$) (fig 12) which shows that the morphological changes persisted for at least 24 hours post STSP removal.

The same morphological changes were quantified in fibroblasts grown in glucose-free galactose media which forces cells to utilize OXPHOS for ATP generation. The proportion of cells that had one or more processes was significantly higher for fibroblasts (WT and LHON) treated with 750nM STSP compared to vehicle-treated under conditions that induce OXPHOS 1-hour post STSP termination (χ^2, $p<0.0001$) (fig 13). The proportion of cells with processes were also significantly greater for fibroblasts (WT and LHON) treated with STSP compared to vehicle treated under conditions that induce

OXPHOS 24 hours after STSP removal (χ^2, $p<0.0001$) (fig 14) demonstrating once again that the morphological changes persisted for at least 24 hours post STSP.

The mean length of processes was significantly greater in both WT and LHON fibroblasts that were treated with STSP compared to vehicle-treated WT and LHON fibroblasts under conditions of primarily glycolytic metabolism (glucose media) 1-hour post STSP removal (fig 15A). The mean length of processes was still significantly greater in STSP-treated WT and LHON fibroblasts compared to vehicle-treated WT and LHON 24 hours after STSP removal (fig 15B).

The mean process length was quantified for STSP-treated WT and LHON fibroblasts grown in galactose media which force cells to use OXPHOS for ATP generation. The mean process length was significantly greater in WT and LHON fibroblasts that were treated with STSP compared to vehicle-treated WT and LHON fibroblasts under conditions that induce OXPHOS 1-hour post STSP removal (fig 16A). The average process length was still significantly greater in STSP-treated WT and LHON fibroblasts compared to vehicle-treated WT and LHON fibroblasts 24 hours after STSP removal (fig 16B).

In summary, we observe a noticeable difference in the number of processes per cell, proportion of cells with processes and average length of a process in both WT and LHON fibroblasts in response to 750 nM STSP that was consistent under both glycolytic and OXPHOS conditions. Furthermore our results also show that the changes were persistent for up to 24 hour after STSP removal.

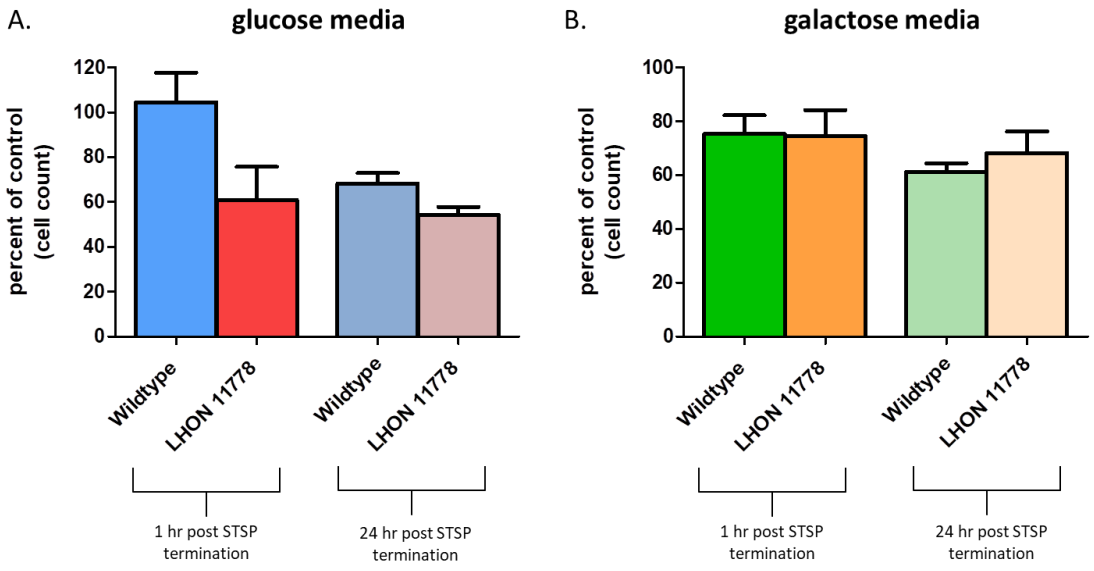

Figure 10 No difference in cell viability between wild-type and LHON fibroblasts in response to 750nM staurosporine

A. Wild-type (WT) and LHON 11778 (LHON) fibroblasts grown in glucose media (CFM) showed no significant difference in mean cell count (percent of control) both 1-hour post (WT 104.6% ±13.04 (SEM), 491 cells, LHON 60.80%±14.92, 277 cells, n=3, t(4)= 2.209, p>0.05) and 24-hour post (WT 68.34% ± 4.61, 450 cells, LHON 54.25% ± 3.59, 401 cells, n=3, t(4)= 2.413, p>0.05) STSP removal. **B**. WT and LHON fibroblasts grown in glucose free galactose media (CFM-GAL) showed no significant difference in cell survival both 1-hour post (WT 75.29% ± 7.02, 1044 cells, n=5, LHON 74.60% ± 9.63, 304 cells, n=5, t(9)=0.059, p>0.05) and 24-hour post (WT 61.21% ± 3.26, 1086 cells, LHON 68.29% ± 7.92, 768 cells, n=6, t(10)= 0.826, p>0.05) STSP removal. Cell viability was measured by averaging the counts of Hoechst stained nuclei in four representative 100x fields (4 replicates) per coverslip where n represents the number of coverslips which is then expressed as a percent of vehicle treated (0.04% ethyl acetate) controls. Data are presented as Means ± Standard Error of Mean.

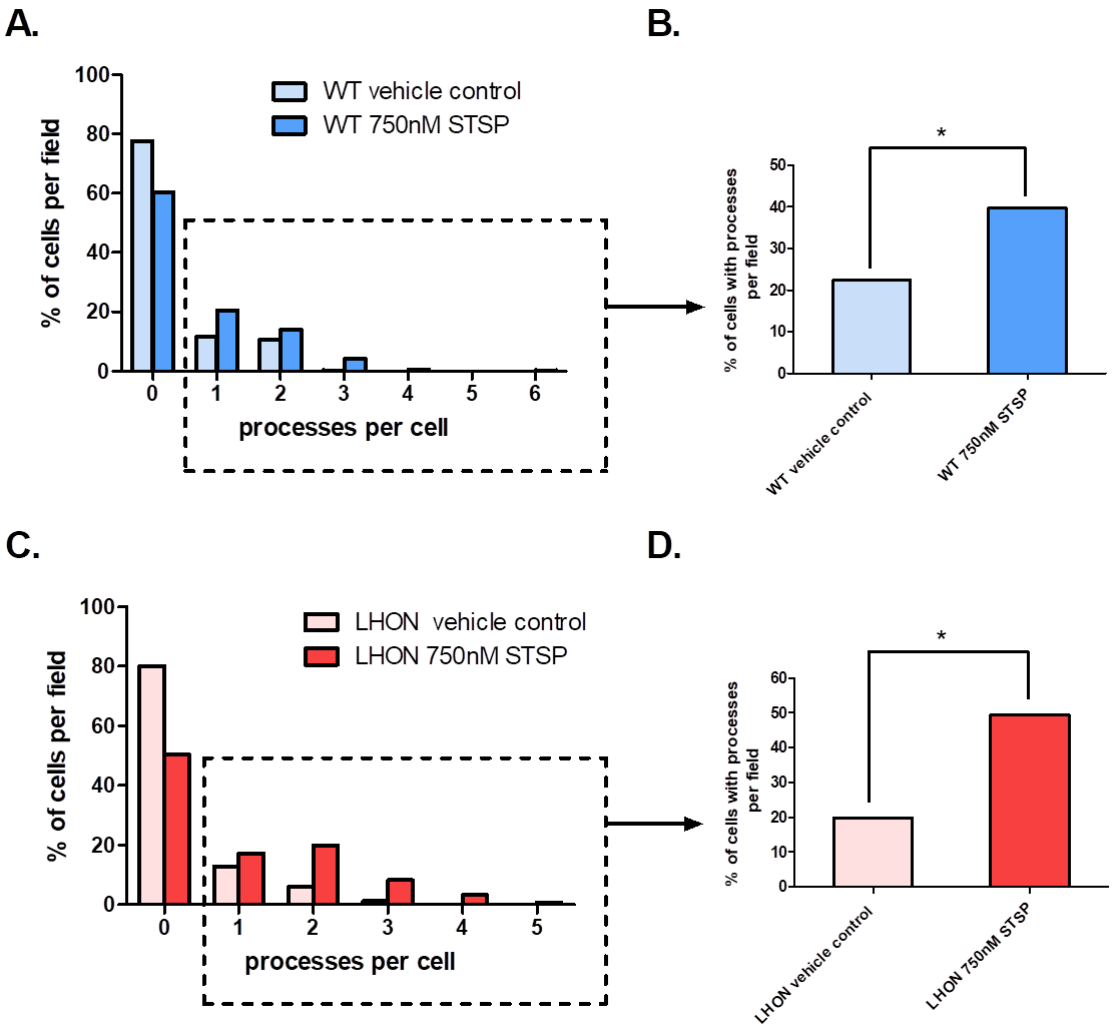

Figure 11 STSP treatment increases number of processes per cell in fibroblasts grown under conditions of primarily glycolytic metabolism 1-hour post STSP removal

A. Distribution of number of processes per cell in vehicle-treated and 750nM STSP treated WT fibroblasts 1-hour post STSP treatment termination in glucose media which promote energy production mainly via glycolysis. B. The percentage of cells with >0 processes per field is significantly greater in STSP treated WT cells (39.7%) (195 cells) compared to vehicle treated WT cells (22.4%) (70 cells), (χ^2 (1) = 26.01, p<0.0001). C. Distribution of number of processes per cell in vehicle-treated and 750nM STSP treated LHON fibroblasts 1-hour post STSP treatment termination in glucose media which promote glycolytic metabolism. D. The percentage of cells with processes is significantly greater in STSP treated LHON cells (49.5%) (137 cells) compared to vehicle treated LHON cells (19.9%) (84 cells), (χ^2 (1) = 67.79, p<0.0001).

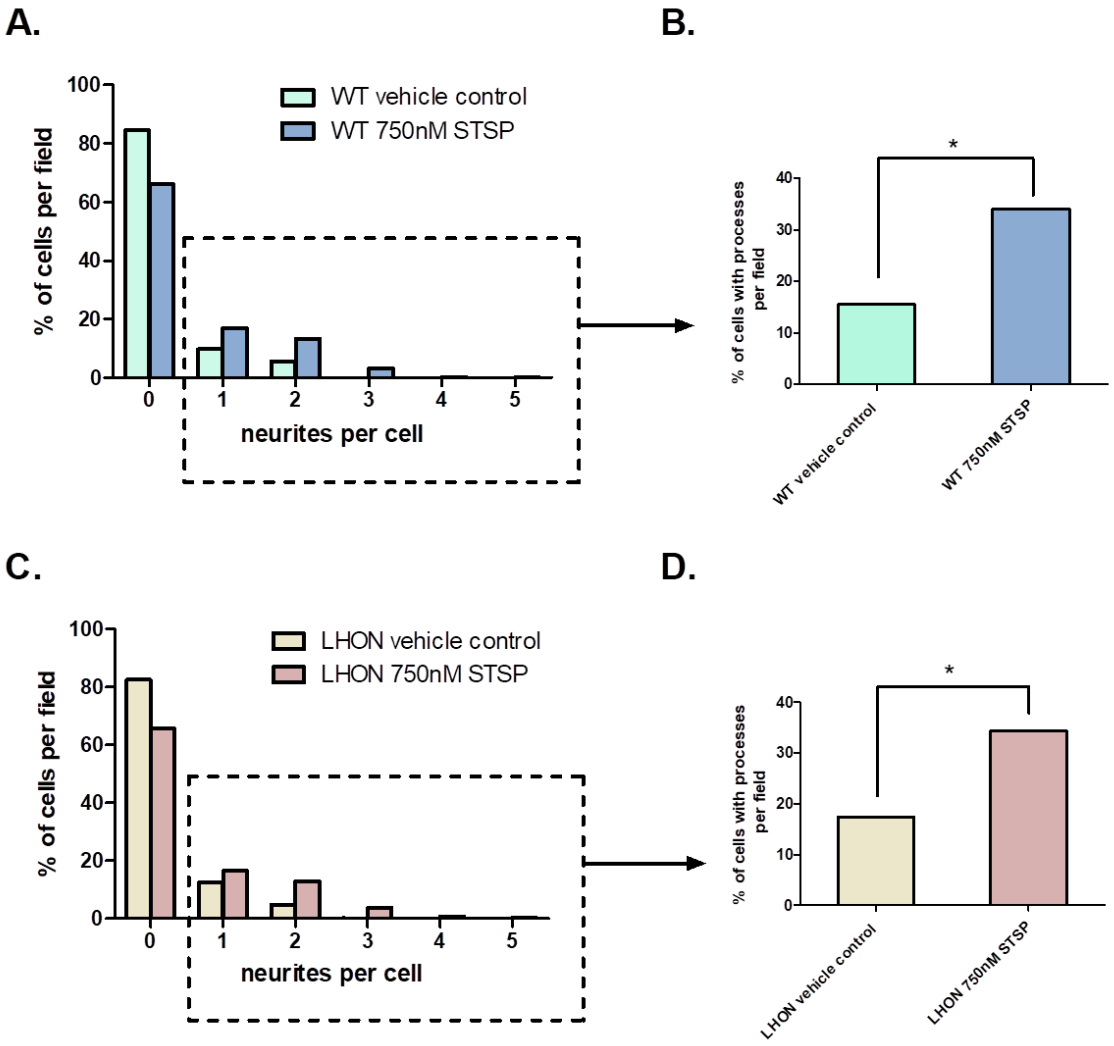

Figure 12 STSP treatment increases number of processes per cell in fibroblasts grown under conditions of primarily glycolytic metabolism 24 hours after STSP removal

A. Distribution of number of processes per cell in vehicle-treated and 750nM STSP treated WT fibroblasts 24-hour post STSP treatment termination in glucose media which promote mainly glycolytic metabolism. B. The percentage of cells with >0 processes per field is significantly greater in STSP treated WT cells (34%) (153 cells) compared to vehicle treated WT cells (15.5%) (68 cells), ($\chi 2$ (1) = 40.71, $p<0.0001$). C. Distribution of number of processes per cell in vehicle-treated and 750nM STSP treated LHON fibroblasts 24-hour post STSP treatment termination in glucose media. D. The percentage of cells with > 0 processes per field is significantly greater in STSP treated LHON cells (34.4%) (138 cells) compared to vehicle treated LHON cells (17.5%) (125 cells), ($\chi 2$ (1) = 40.99, $p<0.0001$).

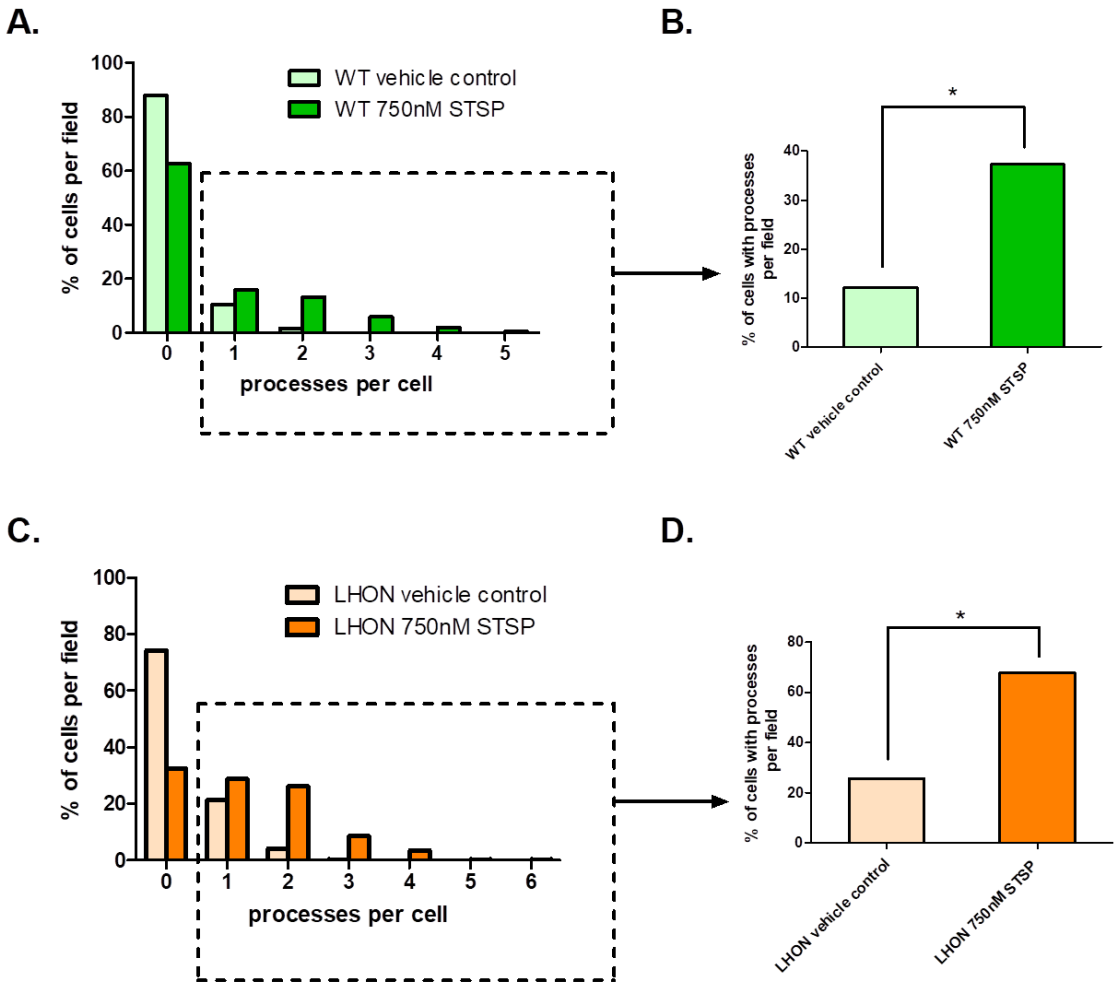

Figure 13 STSP treatment increases the number of processes per cell in fibroblasts grown under conditions that induce oxidative metabolism 1 hour after STSP removal

A. Distribution of number of processes per cell in vehicle-treated and 750nM STSP-treated WT fibroblasts 1-hour post STSP treatment termination in galactose media which induce oxidative metabolism. B. The percentage of cells with >0 processes per field is significantly greater in STSP treated WT cells (37.3%) (227 cells) compared to vehicle treated WT cells (12.2%) (112 cells), ($\chi 2$ (1) = 133.37, $p<0.0001$). C. Distribution of number of processes per cell in vehicle-treated and 750nM STSP treated LHON fibroblasts 1-hour post STSP treatment termination in galactose media which induce oxidative metabolism. D. The percentage of cells with > 0 processes per field is significantly greater in STSP treated LHON cells (67.7%) (212 cells) compared to vehicle treated LHON cells (25.8%) (129 cells), ($\chi 2$ (1) = 138.81, $p<0.0001$).

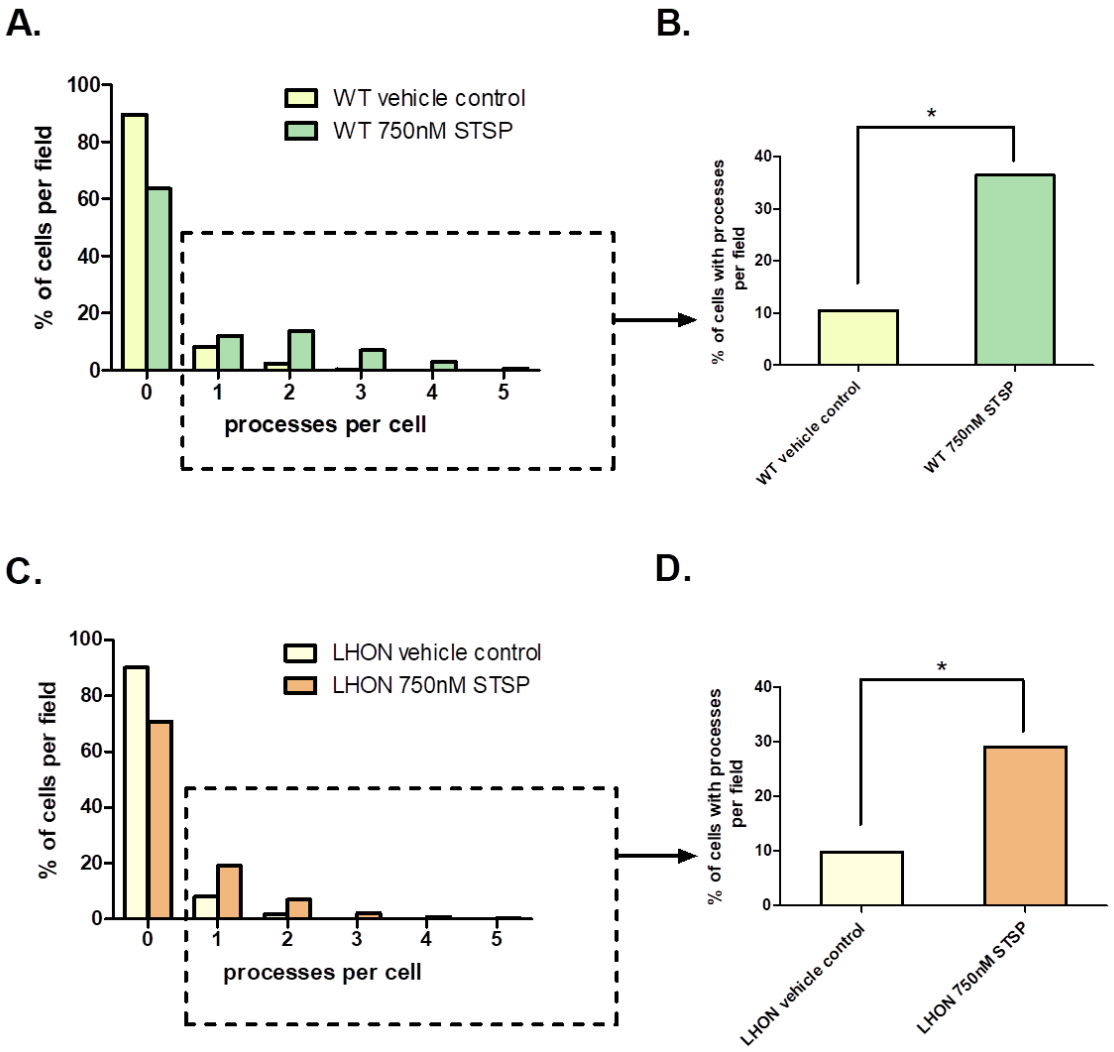

Figure 14 STSP treatment increases the number of processes per cell in fibroblasts grown under conditions that induce oxidative metabolism 24 hours STSP removal

A. Distribution of number of processes per cell in vehicle-treated and 750nM STSP treated WT fibroblasts 24-hour post STSP treatment termination in galactose media which induce oxidative metabolism. B. The percentage of cells with >0 processes per field is significantly greater in STSP treated WT cells (36.4%) (219 cells) compared to vehicle treated WT cells (10.6%) (113 cells), ($\chi 2$ (1) = 161.80, $p<0.0001$). C. Distribution of number of processes per cell in vehicle-treated and 750nM STSP treated LHON fibroblasts 24-hour post STSP treatment termination in galactose media which induce oxidative metabolism. D. The percentage of cells with > 0 processes per field is significantly greater in STSP treated LHON cells (29.1%) (218 cells) compared to vehicle treated LHON cells (9.9%) (133 cells), ($\chi 2$ (1) = 127.02, $p<0.0001$).

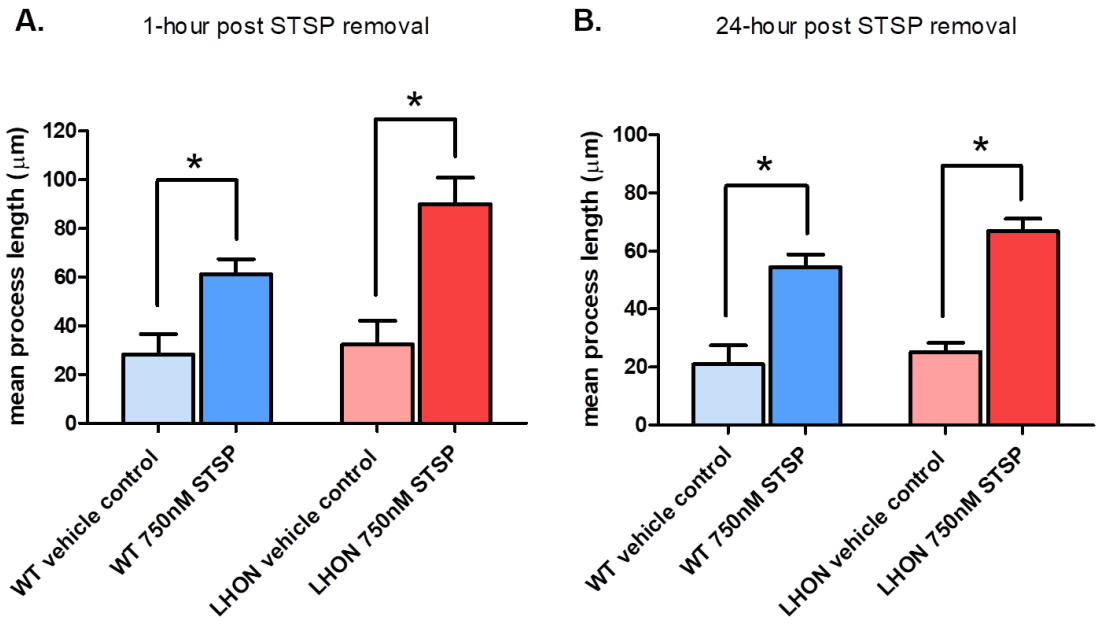

Figure 15 Staurosporine treatment causes an increase in process length in fibroblasts grown under conditions of primarily glycolytic metabolism

A. STSP-treated WT (61.11 ± 6.358 n=3, 491 cells) fibroblasts have a significantly greater mean process length compared to vehicle-treated WT (28.20 ± 8.470, n=3, 313 cells), (t (4) = 3.108, p = 0.0360) and STSP-treated LHON (90.07 ± 10.75, n=3, 277 cells) fibroblasts have a significantly greater mean process length compared to vehicle-treated LHON (32.30 ± 9.712, n=3, 423 cells) (t (4) = 3.989, p= 0.0163) **1-hour** post STSP removal. **B**. STSP-treated WT (54.54 ± 4.267, n=3, 450 cells) fibroblasts have a significantly greater mean process length compared to vehicle-treated WT (20.95 ± 6.624 n=3, 439 cells), (t (4) = 4.263, p= 0.0130) and STSP-treated LHON (66.79 ± 4.323 n=3, 401 cells) fibroblasts have a significantly greater mean process length compared to vehicle-treated LHON (25.31 ± 3.102 n=3, 790 cells) (t (4) = 7.797, p= 0.0015) **24-hour** post STSP removal. Mean process length was measured by dividing the total neurite length per field by the total cell count of the field in four representative 100x fields (4 replicates) and then taking the average of the four fields to get the mean neurite length per coverslip where n represents the number of coverslips. Data are presented as Means ± Standard Error of Mean.

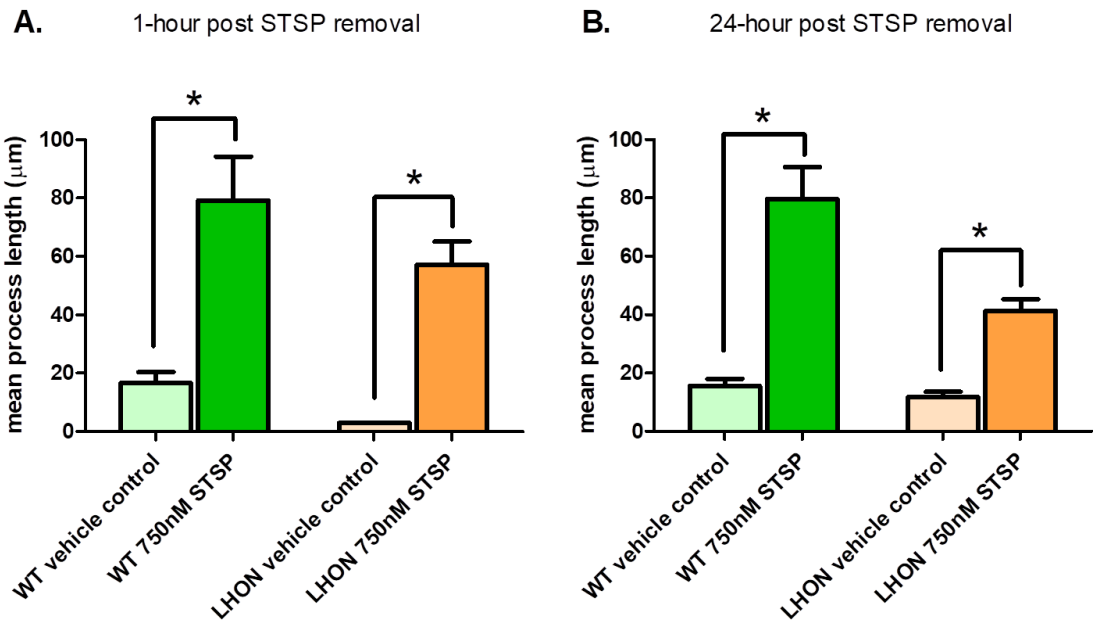

Figure 16 Staurosporine treatment causes an increase in process length in fibroblasts grown under conditions that induce oxidative metabolism

A. STSP-treated WT (79.21 ± 15.00, n=3, 609 cells) fibroblasts have a significantly greater mean process length compared to vehicle-treated WT (16.69 ± 3.705, n=3, 919 cells), (t (4) = 4.046, p= 0.0155) and STSP-treated LHON (57.17 ± 7.973 n=5, 1125 cells) fibroblasts have a significantly greater mean process length compared to vehicle-treated LHON (2.966 ± 0.1686 n=3, 380 cells) (t (6) = 5.099, p= 0.0022) **1-hour** post STSP removal. **B**. STSP-treated WT (79.60 ± 11.04 n=3, 601 cells) fibroblasts have a significantly greater mean process length compared to vehicle-treated WT (15.42 ± 2.558 n=3, 1070 cells), (t (4) = 5.665, p= 0.0048) and STSP-treated LHON (41.29 ± 3.989 n=5, 749 cells) fibroblasts have a significantly greater mean process length compared to vehicle-treated LHON (11.70 ± 1.873 n=6, 1342 cells) (t (9) = 7.123, p< 0.0001) **24-hour** post STSP removal. Mean process length was measured by dividing the total neurite length per field by the total cell count of the field in four representative 100x fields (4 replicates) and then taking the average of the four fields to get the mean neurite length per coverslip where n represents the number of coverslips. Data are presented as Means ± Standard Error of Mean.

3.2. Mitochondrial morphology in WT and LHON fibroblasts in response to STSP treatment

Staurosporine is a broad spectrum kinase inhibitor of both tyrosine and serine/threonine protein kinases. Therefore, STSP can inhibit cellular kinases such as protein kinase A (PKA), mitogen activated protein kinase (MAPK), 5' adenosine monophosphate-activated protein kinase (AMPK) that are involved in the regulation of mitochondrial morphology and dynamics (Chang and Blackstone, 2007; Pyakurel et al., 2015; Toyama et al., 2016). Therefore we decided to investigate the effect of STSP treatment on the mitochondrial network morphology in fibroblasts (WT and LHON) under

conditions that promote glycolytic metabolism (glucose media). Mitochondrial network characteristics were analyzed using the Mitochondrial Network Analysis toolset (MiNA) (Valente et al., 2017) and mitochondrial morphology and network features were compared between vehicle-treated and STSP-treated fibroblasts. The mitochondrial network was characterized based on four parameters which are; number of individual structures with no branches (puncta and rods), number of mitochondrial networks, mean length of rods/ network branches and mean number of branches per mitochondrial network. All mitochondrial network analyses were performed 24 hours post STSP removal.

The four parameters of the mitochondrial network that were tested were not significantly different between vehicle-treated and STSP-treated LHON fibroblasts in glucose media (fig 17). There were no significant differences between vehicle-treated and STSP-treated WT fibroblasts in number of individual mitochondria, number of networks and branches per network but the mean rod/branch length was significantly reduced for STSP-treated WT compared to vehicle-treated WT fibroblasts (fig 17C). This could be an indication that the mitochondria in WT cells are undergoing remodelling in response to STSP treatment.

Next, we investigated the effect of STSP treatment on the mitochondrial network morphology in both WT and LHON fibroblasts in galactose media which forces the fibroblasts to use their mitochondrial electron transport chain for ATP generation. There were no significant differences in mean rod/branch length and number of branches per mitochondrial network between vehicle-treated and STSP-treated WT fibroblasts (fig 18C&D). However, the number of individual mitochondria per cell and number of networks per cell were both lower in STSP-treated WT fibroblasts compared to vehicle-treated WT fibroblasts ($p < 0.05$) (fig 18A&B). Unlike in WT cells, there were no significant differences between vehicle-treated LHON fibroblasts and STSP-treated LHON fibroblasts in any of the parameters investigated (fig 18).

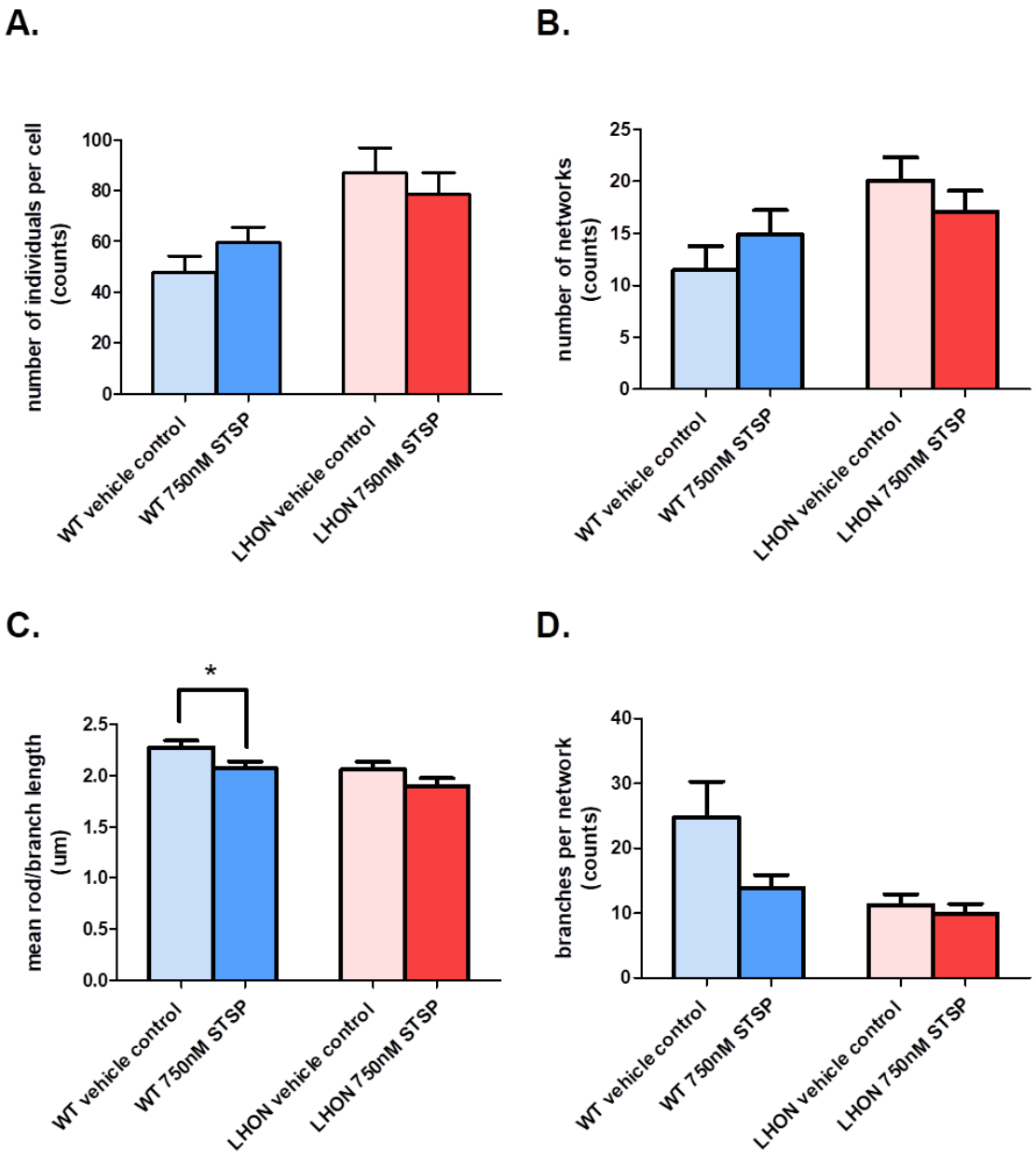

Figure 17 Staurosporine treatment caused a reduction in the mean rod/branch length in WT fibroblasts but did not change the mitochondrial network characteristics in LHON fibroblasts under glycolytic conditions

A. The number of individual mitochondria per cell was not significantly different between vehicle-treated (47.67 ± 6.509, n=9) and STSP-treated (59.56 ± 6.053, n=9) WT fibroblasts (t (16) = 1.338, $p > 0.05$). The number of individual mitochondria per cell was not significantly different between vehicle-treated (86.90 ± 10.080, n=10) and STSP treated (78.45 ± 8.675, n=11) LHON fibroblasts (t (19) = 0.6382, $p > 0.05$). **B.** The number of networks per cell was not significantly different between vehicle-treated (11.44 ± 2.340, n=9) and STSP treated (14.89 ± 2.324, n=9) WT fibroblasts (t (16) = 1.044, $p > 0.05$). The number of networks per cell was also not significantly different between vehicle-treated (20.10 ± 2.193, n=10) and STSP-treated (17.09 ± 1.998, n=11) LHON fibroblasts, (t (19) = 1.017, $p > 0.05$). **C.** The mean rod/branch length was significantly

greater for vehicle-treated fibroblasts (2.275 ± 0.065 µm, n=9) compared to STSP-treated fibroblasts (2.068 ± 0.070 µm, n=10) in WT fibroblasts ($t(17) = 2.169$, $p < 0.05$). The mean rod/branch length was not significantly different between vehicle-treated (2.060 ± 0.075 µm, n=10) and STSP-treated (1.896 ± 0.079 µm, n=11) LHON fibroblasts ($t(19) = 1.508$, $p > 0.05$. **D.** The mean number of branches per mitochondrial network was not significantly different between vehicle-treated (24.85 ± 5.462, n=8) and STSP-treated (13.89 ± 2.020, n=10) WT fibroblasts ($t(16) = 2.047$, $p > 0.05$). The mean number of branches per mitochondrial network was also not significantly different between vehicle-treated (11.28 ± 1.676, n=10) and STSP-treated (9.965 ± 1.47, n=11) LHON fibroblasts ($t(19) = 0.594$, $P > 0.05$). Mitochondrial network was analyzed using the MiNA toolset in fluorescent micrographs of mteYFP-labelled fibroblasts. Data are presented as Means ± Standard Error of Mean.

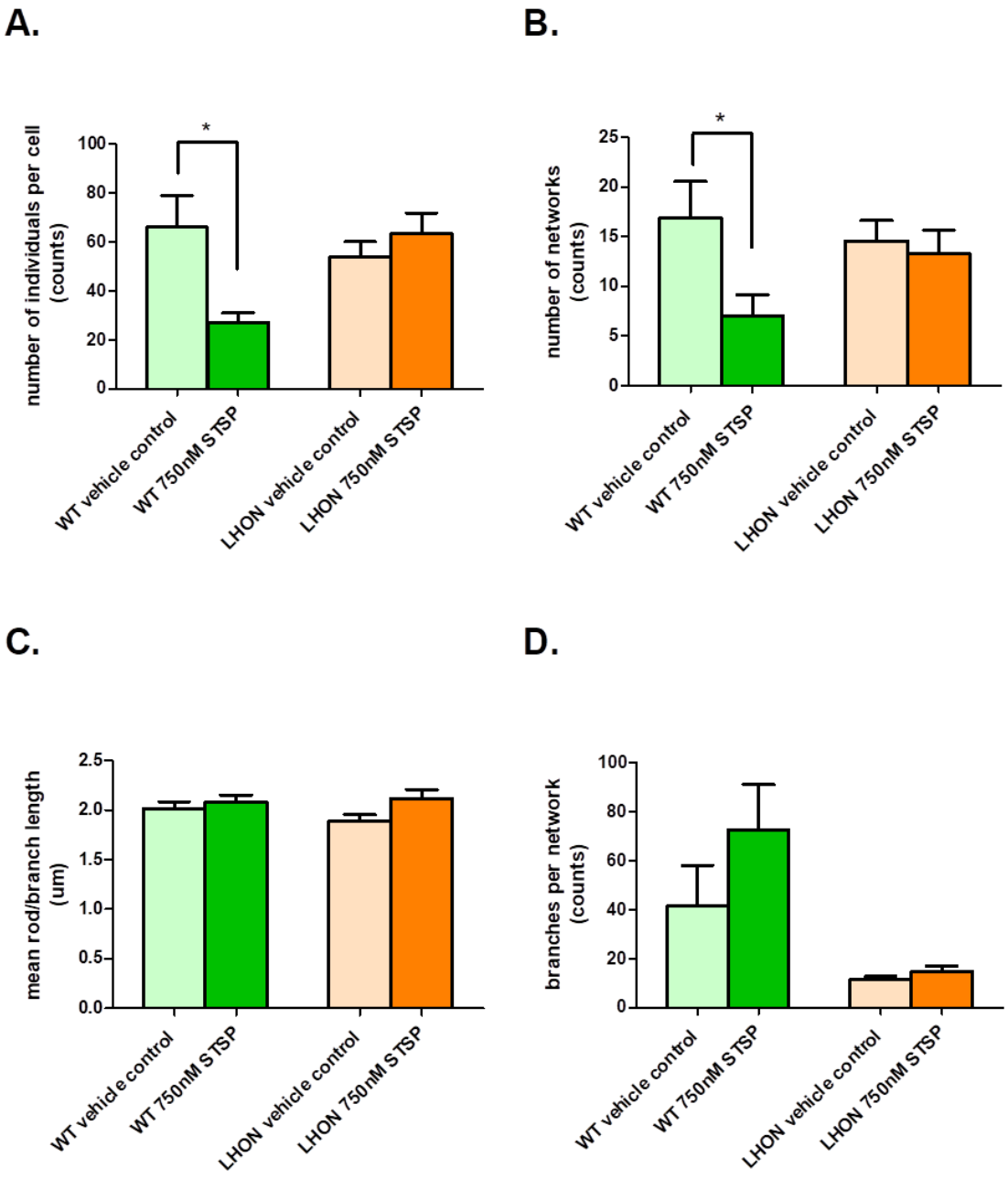

Figure 18 Staurosporine treatment caused a reduction in the number of individual mitochondria and number of mitochondrial networks in WT fibroblasts but did not change the mitochondrial network characteristics of LHON fibroblasts under OXPHOS conditions

A. The number of individual mitochondria per cell was significantly lower in STSP-treated (27.22 ± 3.722, n=9) compared to vehicle-treated (66.00 ± 13.00 n=12) fibroblasts in WT fibroblasts ($t(19) = 2.511$, $p < 0.05$). The number of individual mitochondria per cell was not significantly different between vehicle-treated (54.00 ± 6.207, n=12) and STSP-treated (63.33 ± 8.570, n=9) LHON fibroblasts ($t(19) = 0.906$, $p > 0.05$. B. The number of networks per cell was significantly lower in STSP treated (7.000 ± 2.155, n=10) compared to vehicle-treated (16.83 ± 3.739, n=12) WT cells ($t(20) = 2.159$, $p < 0.05$). The number of networks per cell was not significantly different between

vehicle-treated (14.58 ± 2.036, n=12) and STSP-treated (13.33 ± 2.315, n=9) LHON fibroblasts (t (19) = 0.405, p > 0.05). C. The mean rod/branch length per cell was not significantly different between vehicle-treated (2.015 ± 0.068 µm, n=12) and STSP-treated (2.083 ± 0.06808 µm, n=10) WT fibroblasts (t (20) = 0.692, p > 0.05). The mean rod/branch length per cell was also not significantly different between vehicle-treated (1.891 ± 0.064 µm, n=12) and STSP-treated (2.113 ± 0.095 µm, n=9) LHON fibroblasts (t (19) = 2.001, p > 0.05). D. The mean number of branches per mitochondrial network was not significantly different between vehicle-treated (41.57 ± 16.54, n=11) and STSP-treated WT (72.72 ± 18.51, n=10) fibroblasts (t (19) = 1.259, p > 0.05). The mean number of branches per mitochondrial network was also not significantly different between vehicle-treated (11.26 ± 1.557, n=11) and STSP-treated (14.76 ± 2.294, n=8) LHON fibroblasts (t (17) = 1.313, p > 0.05). Mitochondrial network was analyzed using the MiNA toolset in fluorescent micrographs of mteYFP-labelled fibroblasts. Data are presented as Means ± Standard Error of Mean.

3.3. Mitochondrial movement analysis in STSP-treated WT and LHON fibroblasts under conditions that promote different energy metabolic pathways

Following the characterization of the cellular and mitochondrial network morphology of STSP treated fibroblasts we investigated mitochondrial motility within STSP-induced processes in both WT and LHON fibroblasts in culture conditions in which cells primarily utilize glycolysis for ATP generation (glucose media) and in culture conditions that induce OXPHOS for ATP generation (galactose media). Mitochondrial movement analysis was performed 24 hours post STSP removal. The bulk movement of mitochondria within staurosporine induced processes of WT and LHON fibroblasts was quantified using the custom visual basic macro as described in the methods. The mean movement ratios of WT and LHON mitochondria were compared under glycolytic conditions (i.e. glucose) or conditions necessitating OXPHOS (i.e. galactose).

A two-way analysis of variance (2-way ANOVA) was conducted that examined the effect of mutational-status (presence or absence of LHON G11778A mutation) and energy metabolism on mitochondrial movement ratio 24 hours after STSP removal. In other words, we examined whether the effect of mutational-status (WT or LHON) on mitochondrial movement was influenced by the suppression or induction of OXPHOS (glucose or galactose media). There was no statistically significant interaction between the mutational status and energy metabolism on mitochondrial movement ratio, [F (1,104) = 1.539, p=0.218]. An analysis of simple main effects for the ATP-generating pathway (glycolysis or OXPHOS) was performed with statistical significance receiving a Bonferroni adjustment and being accepted at the p < 0.025 level. There was no statistically significant difference in the mitochondrial movement ratio between WT

(0.230 ± 0.066, n = 26) and LHON (0.216 ± 0.066, n = 26) cells grown under conditions where cells primarily utilize glycolysis (glucose media) F (1, 104) = 0.673, p = 0.414 (fig 19). In contrast, the mitochondrial movement ratio was significantly lower in LHON cells compared to WT cells grown in culture conditions that induced OXPHOS (galactose media) (fig 19). The analysis of simple main effects for mutational-status (WT or LHON) was also performed with statistical significance receiving a Bonferroni adjustment and being accepted at the $p < 0.025$ level. There was no statistically significant difference in mitochondrial movement ratio between WT cells grown in culture conditions where cells primarily utilize glycolysis for ATP generation (glucose media) (0.230 ± 0.066, n = 26) and culture conditions that induced OXPHOS (galactose media) (0.195 ± 0.067, n = 31), F (1, 104) = 4.642, p = 0.034 (fig 19). The movement ratio was significantly lower in LHON cells grown under conditions that induced OXPHOS (galactose media) compared to those grown under culture conditions that promote glycolysis (glucose media) (fig 19).

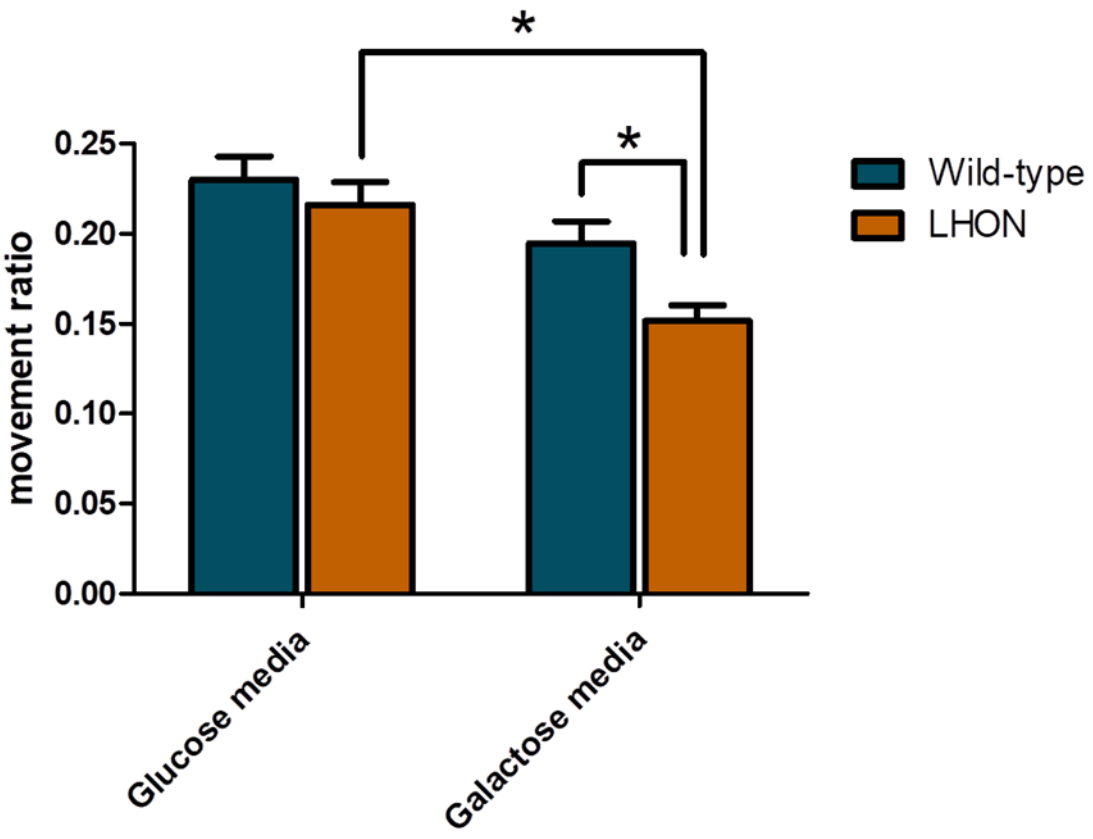

Figure 19 Mitochondrial movement decreases in staurosporine treated LHON fibroblasts in glucose free-galactose media

Mean mitochondrial movement ratio of wild type and LHON cells grown under culture conditions that promote glycolytic metabolism (glucose media) and under culture conditions that induce

OXPHOS (galactose media) 24 hours following STSP treatment removal (mean mitochondrial movement ratio ± SEM). The non-directional movement (bulk movement) of mitochondria was quantified using an excel macro and expressed as a movement ratio. Means that are significantly different are marked with an asterisk (Bonferroni correction). Mean movement ratio is significantly lower in LHON cells in media that induce OXPHOS (galactose media) (0.152 ± 0.038, n=24) compared to media that suppress OXPHOS (glucose media) (0.216 ± 0.066, n=26), $F (1, 104) = 14.074$, $p < 0.001$. The mean movement ratio is also significantly lower in LHON cells in media that induce OXPHOS (galactose media) (0.152 ± 0.038, n=24) compared to WT cells in media that induce OXPHOS (galactose media) (0.195 ± 0.067, n=31). $F (1, 104) = 6.721$, $p < 0.025$. Mitochondrial movement was quantified in time lapse images of mteYFP-labelled fibroblasts using a custom visual basic macro and expressed as a mean mitochondrial movement ratio. Data are presented as mean and standard deviation and n= number of cells.

3.4. Measuring relative ATP levels between STSP treated WT and LHON fibroblasts in growth media that promote different energy metabolic pathways

Mitochondrial trafficking is an ATP dependent process and the G11778A LHON mutation occurs in the machinery that generates the majority of ATP under OXPHOS conditions. In order to determine whether the decrease in the mitochondrial movement observed in LHON cells in media that induced OXPHOS was due to reduced ATP levels, we measured the intracellular ATP levels using the ATP sensitive FRET based probe, Ateam (Imamura et al., 2009). In the experimental conditions employed Ateam gives a minimum ATP/ADP value of 1.8 when cellular ATP is depleted by inhibition of glycolysis and OXPHOS by 2-deoxyglucose and potassium cyanide respectively and a maximum ATP/ADP value of 5.1 in fibroblasts (B. Pasqualotto unpublished data).

A 2-way ANOVA was conducted to examine the effect of the mutational status (WT or LHON) and ATP-generating pathway (glucose or galactose media) on the relative ATP/ADP. The interaction effect between mutational status and ATP-generating pathway on relative ATP/ADP was statistically significant at 24-hour post STSP removal, $F (1, 41) = 4.387$, $p = 0.042$. The analysis of simple main effects for energy metabolism 24-hour post STSP removal, was performed with statistical significance receiving a Bonferroni adjustment and being accepted at the $p < 0.025$ level. The data are mean and standard deviation, unless otherwise stated. There was no significant difference in ATP/ADP between WT (4.557 ± 0.539, n = 11) and LHON (5.009 ± 0.313, n = 15) cells grown in culture conditions where cells primarily use glycolysis for ATP generation (glucose media) $F (1, 41) = 3.792$, 0.058 (fig 20). The same was true for the ATP/ADP between WT (4.940 ± 0.888, n = 8) and LHON (4.644 ± 0.650, n = 11) cells in culture

conditions that induce OXPHOS (galactose media), F (1, 41) = 1.191, p = 0.281 (fig 20). The analysis of simple main effects for mutational-status 24-hour post STSP removal, was performed with statistical significance receiving a Bonferroni adjustment and being accepted at the $p < 0.025$ level. There was no significant difference in ATP/ADP between WT cells grown in culture conditions where cells utilize glycolysis for ATP generation (glucose media) (4.557 ± 0.539, n = 11) and in culture conditions that induce OXPHOS (galactose media) (4.940 ± 0.888, n = 8), F (1, 41) = 1.996, p = 0.165 and this was true for LHON cells grown in conditions of mainly glycolytic metabolism (5.009 ± 0.313, n = 15) and in culture conditions that induce OXPHOS (4.644 ± 0.650, n = 11), F (1, 41) = 2.468, p = 0.124.

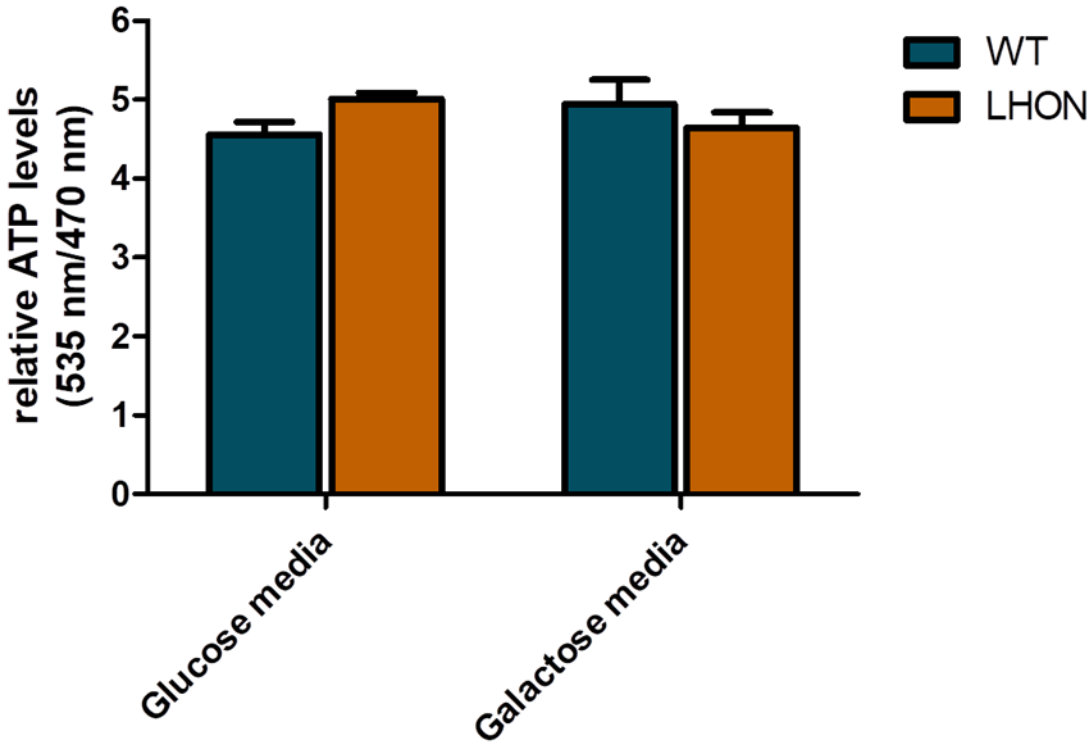

Figure 20 No changes in relative ATP levels between WT and LHON cells in media that suppress OXPHOS (glucose) and in media that induce OXPHOS (galactose)

Relative cytosolic ATP levels were measured using the Ateam construct which is a FRET-based indicator for ATP. Relative ATP levels (ATP/ADP) in WT and LHON cells in glucose and galactose media 24-hour- post STSP removal (mean ± SEM). No significant differences in relative ATP levels were found between WT and LHON fibroblasts in glucose and galactose media 24-hour post STSP removal (Bonferroni correction, $p > 0.025$).

3.5. Mitochondrial network characteristics between STSP-treated WT and LHON fibroblasts under culture conditions that promote different energy metabolic pathways

Since changes in mitochondrial morphology are associated with numerous disease states (Wang et al., 2008; Ong and Hausenloy, 2010; Rintoul and Reynolds, 2010; Galloway and Yoon, 2013) we compared the mitochondrial network characteristics in STSP-treated WT and LHON fibroblasts under glycolytic conditions and conditions that necessitate OXPHOS for ATP generation. The mitochondrial network was characterized based on four features; number of individual mitochondria per cell, number of mitochondrial networks per cell, rod/branch length per cell and mean number of mitochondrial networks per cell. A two way ANOVA was performed to determine the effect of mutational-status and energy metabolism on each of these parameters.

First, we examined the mean number of individual mitochondria per cell 24-hour (fig 21A) post STSP removal. There was no statistically significant interaction between mutational status and ATP-generating pathway for the mean number of individual mitochondria per cell, $F(1, 57) = 0.044$, $p = 0.835$. An analysis of simple main effects for the ATP-generating pathway was performed with statistical significance receiving a Bonferroni adjustment and being accepted at the $p < 0.025$ level. The data are mean and standard deviation unless otherwise stated. There was a statistically significant increase in mean number of individual mitochondria per cell in LHON compared to WT cells under conditions of mainly glycolytic metabolism (glucose media) (fig 21A). There was no statistically significant difference between WT (34.79 ± 24.48, $n=14$) and LHON (58.27 ± 30.91, $n=15$) cells under conditions that induce OXPHOS (galactose media) $F(1, 57) = 5.127$, $p = 0.027$ (fig 21A). The analysis of simple main effects for mutational status was also performed with statistical significance receiving a Bonferroni adjustment and being accepted at the $p < 0.025$ level. There was no statistically significant difference in the mean number of individual mitochondria per cell between WT cells grown under conditions of mainly glycolytic metabolism (51.40 ± 19.00, $n=15$) compared to WT cells grown under conditions that induce OXPHOS (34.79 ± 24.48, $n=14$), $F(1, 57) = 2.567$, $p = 0.115$ (fig 21A). Also, there was no statistically significant difference in mean individual mitochondria per cell between LHON cells grown under conditions of mainly glycolytic metabolism (77.88 ± 33.70, $n=17$) and LHON cells under conditions where OXPHOS is induced (58.27 ± 30.91, $n=15$), $F(1, 57) = 3.937$, $p = 0.052$.

Next, we examined the mean number of networks per cell 24-hour post STSP removal. The interaction effect between mutational status and ATP-generating pathway on mean individuals per cell was not statistically significant, $F(1, 57) = 0.038$, $p = 0.846$. The analysis of simple main effects for ATP-generating pathway was performed with statistical significance receiving a Bonferroni adjustment and being accepted at the $p < 0.025$ level. The data are mean and standard deviation, unless otherwise stated. The mean number of networks per cell was significantly higher in LHON cells compared to WT cells in conditions of mainly glycolytic metabolism (fig 21B). The mean number of individual networks per cell was not significantly different between WT cells (6.07 ± 4.89, $n=14$) and LHON cells (11.40 ± 6.84, $n=15$) in conditions that induce OXPHOS $F(1, 57) = 4.242$, $p = 0.044$ (fig 21B). The analysis of simple main effects for mutational status was also performed with statistical significance receiving a Bonferroni adjustment and being accepted at the $p < 0.025$ level. There was no statistically significant difference in mean number of networks per cell between WT cells grown in conditions of mainly glycolytic metabolism (11.27 ± 7.36, $n=15$) and conditions that induce OXPHOS (6.07 ± 4.89, $n=14$) $F(1, 57) = 4.032$, $p = 0.049$ (fig 21B).There was a statistically significant decrease in mean number of networks per cell in LHON cells grown in conditions that induce OXPHOS compared to LHON cells grown under conditions of mainly glycolytic metabolism (fig 21B).

A 2-way ANOVA was conducted to examine the effect of mutational-status and ATP-generating pathway on the mean rod/branch length of mitochondria 24-hour post STSP removal. There was no statistically significant interaction between mutational status and ATP-generating pathway $F(1, 59) = 1.154$, $p = 0.287$. The analysis of simple main effects for ATP-generating pathway was performed with statistical significance receiving a Bonferroni adjustment and being accepted at the $p < 0.025$ level. The data are mean and standard deviation, unless otherwise stated. The mean rod/branch length of mitochondria was not significantly different between WT (2.021 ± 0.224 µm, $n=16$) and LHON (1.908 ± 0.224 µm, $n=17$) in conditions of mainly glycolytic metabolism $F(1, 59) = 2.038$, $p = 0.159$ and was also not significantly different between WT (2.043 ± 0.186 µm, $n=15$) and LHON (2.054 ± 0.268 µm, $n=15$) in conditions that induce OXPHOS, $F(1, 59) = 0.015$, $p = 0.903$ (fig 21C). The analysis for simple main effects for mutational-status was performed with statistical significance receiving a Bonferroni adjustment and being accepted at the $p < 0.025$ level. There was no significant

difference in mean rod/branch length between WT cells grown in conditions of mainly glycolytic metabolism (2.021 ± 0.224 μm, n=16) and conditions that induce OXPHOS (2.043 ± 0.186 μm, n=15), $F(1, 59) = 0.074$, $p = 0.787$ (fig 21C). There was also no significant difference in mean rod/branch length between LHON cells grown in conditions of mainly glycolytic metabolism (1.908 ± 0.224 μm, n=17) and conditions that induce OXPHOS (2.054 ± 0.268 μm, n=15), $F(1, 59) = 3.260$, $p = 0.076$ (fig 21C).

A 2-way ANOVA was conducted to examine the effect of mutational-status and ATP-generating pathway on the mean number of branches per mitochondrial network 24-hour (fig 21D) post STSP removal. There was no statistically significant interaction between mutational-status and ATP-generating pathway on the number of branches per network, $F(1, 56) = 2.720$, $p = 0.105$. The analysis of simple main effects for ATP-generating pathway was performed with statistical significance receiving a Bonferroni adjustment and being accepted at the $p < 0.025$ level. The data are mean and standard deviation, unless otherwise stated. The mean number of branches per network was not significantly different between WT cells (28.69 ± 27.95, n=15).and LHON cells (15.31 ± 10.90, n=16) in conditions of mainly glycolytic metabolism, $F(1, 56) = 1.486$, $p = 0.228$ (fig 21D). The mean number of branches per network however was significantly greater for WT compared to LHON in conditions that induce OXPHOS (fig 21D). The analysis of simple main effects for mutational-status was performed with statistical significance receiving a Bonferroni adjustment and being accepted at the $p < 0.025$ level. There was a significant increase in the mean number of branches per network in WT cells in conditions that induce OXPHOS compared to conditions of mainly glycolytic metabolism (fig 21D) but was not significantly different between LHON cells grown in conditions of mainly glycolytic metabolism (15.31 ± 10.90, n=16) and conditions that induce OXPHOS (28.35 ± 23.32, n=14), $F(1, 56) = 1.362$, $p = 0.248$ (fig 21D).

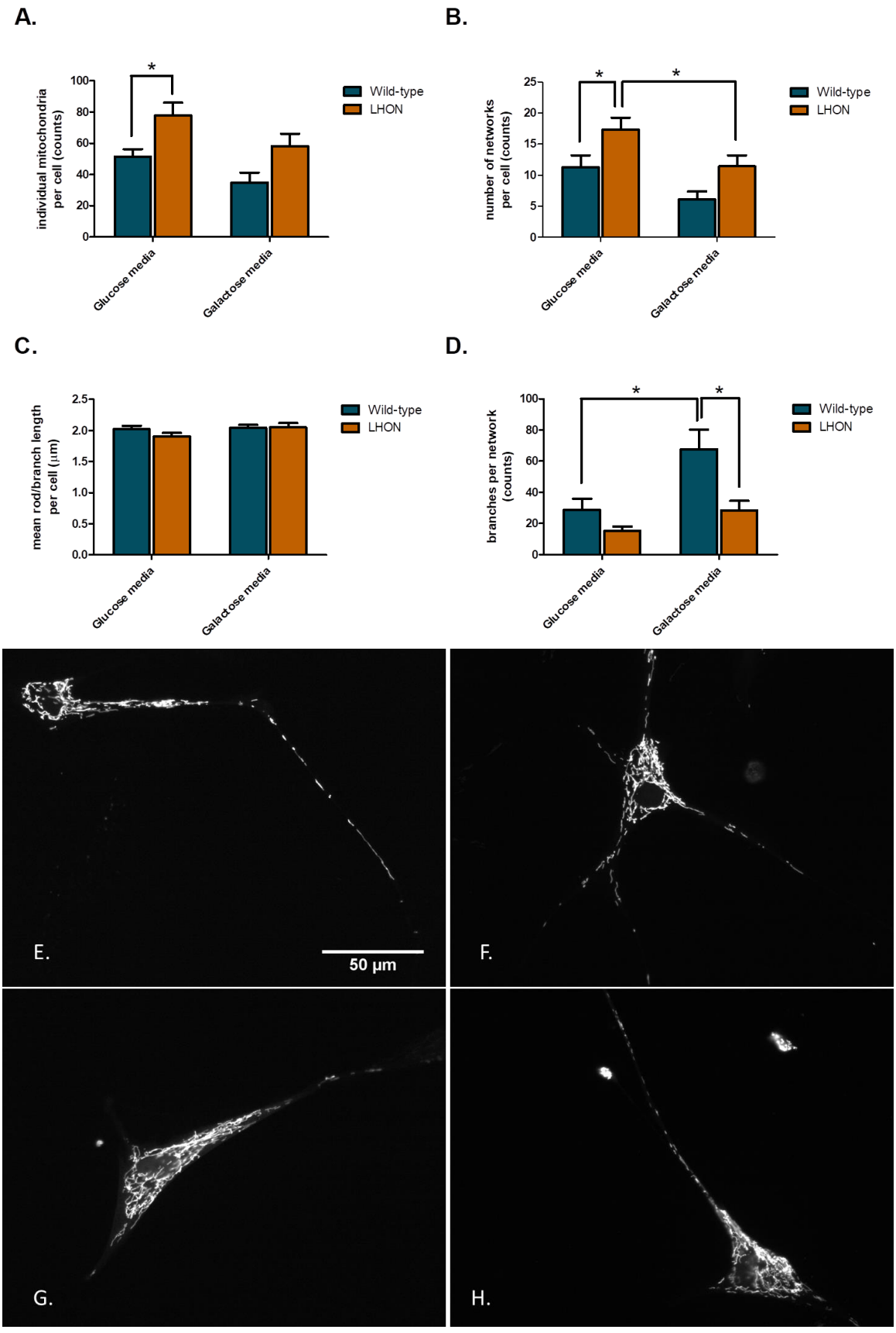
A.
B.
C.
D.
individual mitochondria per cell (counts)
number of networks per cell (counts)
mean rod/branch length per cell (μm)
branches per network (counts)
Wild-type
LHON
Glucose media
Galactose media
*
E.
F.
G.
H.
50 μm

Figure 21 The degree of mitochondrial networking is higher in galactose media compared to glucose media

Mitochondrial network analysis toolset (MiNA) was used for analyzing the mitochondrial network characteristics in fluorescent micrographs of mt-eYFP transfected WT and LHON fibroblasts under glycolytic and OXPHOS conditions 24 hours post STSP removal. **A.** Mean number of individual mitochondria per cell in WT and LHON cells under glycolytic (glucose media) and OXPHOS (galactose media) conditions (mean number of individual mitochondria ±. SEM). Means that are significant are marked with an asterisk (Bonferroni correction). Mean number of individual mitochondria per cell is significantly greater in LHON cells (77.88 ± 33.70, n=17) compared to WT (51.40 ± 19.00, n=15) cells under glycolytic conditions, $F(1, 57) = 7.176$, $p = 0.010$. **B.** Mean number of mitochondrial networks per cell in WT and LHON mitochondria under glycolytic and OXPHOS conditions (mean number of networks per cell ± SEM). Mean number of mitochondrial networks per cell is significantly greater in LHON cells (17.29 ± 8.05, n=17) compared to WT cells (11.27 ± 7.36, n=15) under glycolytic conditions, $F(1, 57) = 5.972$, $p = 0.018$. The mean number of networks per cell was also significantly greater in LHON cells under glycolytic conditions (17.29 ± 8.05, n=17) compared to LHON cells under OXPHOS conditions (11.40 ± 6.84, n=15), ($F(1, 57) = 5.711$, $p < 0.020$). **C.** Mean rod/branch length in WT and LHON mitochondria under glycolytic and OXPHOS conditions (mean rod/branch length ± SEM). There were no significant differences in mean rod/branch lengths between WT and LHON cells under glycolytic or OXPHOS conditions ($p > 0.025$). **D.** Mean number of branches per mitochondrial network in WT and LHON cells under glycolytic and OXPHOS conditions (mean branches per network ± SEM). The mean number of branches per network is significantly greater in WT cells under OXPHOS conditions (67.75 ± 48.11, n=15) compared to WT cells under glycolytic conditions (28.69 ± 27.95, n=15), $F(1, 56) = 12.281$, $p = 0.001$. The mean number of mitochondrial branches per network was also significantly greater in WT cells (67.75 ± 48.11, n=15) compared to LHON cells (28.35 ± 23.32, n=14) under OXPHOS conditions $F(1, 56) = 12.062$, $p = 0.001$. The data are mean and standard deviation and n = number of cells. **E-H**: fluorescent micrographs of representative mt-eYFP transfected WT fibroblast grown under glycolytic conditions (**E**), LHON fibroblast grown under glycolytic conditions (**F**), WT fibroblast grown under OXPHOS conditions (**G**), LHON fibroblast grown under OXPHOS conditions (**H**).

Chapter 4. Discussion

LHON is a disease that primarily affects tissue of the CNS and to understand its pathogenesis we need a model system that closely resembles RGCs. Here we show that exposure to the broad-spectrum kinase inhibitor STSP for 24 hours at a concentration of 750nM induced the development of cytoplasmic protrusions in fibroblasts resembling neurites in terms of their morphology. Fibroblasts typically consist of a reticulated mitochondrial network which makes the study of mitochondrial movement in these cells a challenge. The change in morphology allowed for the detection and quantification of mitochondrial movement along the processes, a phenomenon routinely observed in neurons. Fibroblasts carrying the G11778A LHON mutation showed a reduced mitochondrial movement under culture conditions that forced cells to rely on OXPHOS for ATP generation (galactose media) compared to culture conditions which mainly induce glycolytic metabolism (glucose media). The mitochondrial movement of fibroblasts carrying the G11778A LHON mutation was also lower compared to wild-type fibroblasts in forced OXPHOS culture conditions which may implicate an impairment in mitochondrial movement in LHON cells when the energy dependence is switched to OXPHOS which is the primary ATP generating pathway in RGCs and other neurons. The relative cytosolic ATP levels were not reduced in STSP-treated LHON fibroblasts under OXPHOS conditions. Furthermore, LHON cells displayed altered mitochondrial network remodeling where the number of branches per mitochondrial network was lower compared to WT cells under OXPHOS conditions.

4.1. Characterization of STSP treated fibroblasts

Human dermal fibroblasts can take variety of different forms in culture but typically exhibit a fusiform morphology (Abercrombie, 1978; Ravikanth et al., 2011). Treatment with 750 nM STSP for 24 hours induced morphological changes to the fibroblasts characterized by a smaller cell body and appearance of one or more cellular protrusions (fig 9). The morphology was similar to that of cultured cortical neurons which have multiple long thin projections radiating from a central soma/cell body. The morphological changes occurred without any significant differences in mortality between wild-type and LHON G11778A fibroblasts in two different growth media (fig 10). This showed that the two cell types demonstrated similar survival rates to staurosporine

treatment independent of growth media. Staurosporine is a commonly used apoptosis inducing agent, however its ability to induce the formation of cytoplasmic protrusions in a variety of cell lines has been widely reported (Jalava et al., 1993; Rasouly et al., 1994; Frassetto et al., 2006; Thompson and Levin, 2010; Murmann et al., 2014; Kohno et al., 2015). Studies have shown that these two processes are independent of each other and that the morphological changes are not part of the apoptotic cascade (Frassetto et al., 2006; Murmann et al., 2014). Differentiation by STSP also causes certain cell types (e.g. RGC-5) to become post-mitotic (Frassetto et al., 2006). Therefore, it is possible that the 25-45% reduction in cell counts observed for STSP-treated WT and LHON fibroblasts (fig 10) was due to lack of cell division as opposed to cytotoxicity or a combination of both. However, without further testing, no conclusions can be drawn regarding the lower cell density in STSP-treated cell populations.

The percentage of cells with processes as defined in the methods is significantly greater in fibroblasts that were treated with STSP compared to vehicle controls. This was consistent for both 1-hour and 24 hours post STSP removal in both glucose and galactose media. A study by Murmann et al (2014) reported that process formation by STSP is reversible in small cell lung carcinoma (SCLC) cells and process retraction occurred within two to three hours of STSP removal. Even though a direct comparison between the 1-hour and 24-hour post STSP removal was not performed, our results indicate that the percentage of cells with processes was lower after 24-hours compared to 1-hour after STSP removal. However, the percentage of cells with processes was still significantly greater 24 hours after STSP removal in STSP treated fibroblasts compared to vehicle controls indicating that the effect is largely plastic (i.e. persistent) in nature as opposed to elastic (i.e. transient). The mean length of processes per field was also significantly greater in STSP treated fibroblasts compared to vehicle controls both 1-hour and 24-hours post STSP removal. The increase in mean process length was consistent in both glucose and galactose media. The concentrations of STSP used for inducing process formation depend on the cell type and its sensitivity to STSP. A 24-hour exposure to 50 nM STSP was sufficient to induce processes in small cell lung carcinoma cells (SCLC) (Murmann et al., 2014) whereas a concentration of 316 nM was determined as the optimum concentration for inducing the greatest number of neurites without significant cell death in RGC-5 cells (Thompson and Levin, 2010). Concentrations of 10-100 nM were used for stimulating neurite growth in rat pheochromocytoma PC-12 cells

(Rasouly et al., 1994; Yao et al., 1997) and a concentration of 25 nM for 72 hours was used in inducing neurites in the neuroblastoma cell line SH-SY5Y. We determined that a concentration of 750 nM was optimum for generating processes in human dermal fibroblasts with the least toxicity to the cells (fig A.1, A.2, A.3). The mechanism of STSP-induced process formation is not well understood. PC-12 cells undergo neuronal differentiation in response to nerve growth factor that activates ERK1/2 pathway (extracellular signal-regulated kinase 1/2). STSP can mimic the effect of nerve growth factor in PC-12 cell without activating the ERK 1/2 pathway but through the activation of a c-Jun NH_2 terminal kinase (Yao et al., 1997). The induction of neurites is rapid and is reported to occur in as little as 60 seconds after STSP treatment (Frassetto et al., 2006) which points against the involvement of gene expression/protein synthesis (Murmann et al., 2014). Cellular protrusions are formed mainly through elongation of cytoskeletal elements such as actin and tubulin (Kohno et al., 2015). The polymerization and depolymerization of these cytoskeletal elements are regulated by complex molecular pathways within the cell (Kohno et al., 2015). Many of these regulatory pathways are modulated by protein phosphorylation (Govek et al., 2005). Therefore, Inhibition of these kinases can induce morphological changes as a result of the loss of regulation of polymerization/depolymerization of cytoskeletal elements (Kohno et al., 2015).

At present the only known *in vitro* neuronal model for LHON is the neural Ntera-2/D1 (NT2) human teratocarcinoma cell line that undergoes differentiation into neurons in response to retinoic acid treatment (Wong et al., 2002; Haroon et al., 2007; Schoeler et al., 2007). However, the cells require cybridization with LHON mitochondria prior to their use in LHON studies. NT2 cybrids carrying the 11778 and 3460 LHON mutations have shown an increase in ROS and a decrease in mtDNA/nDNA ratio following differentiation with retinoic acid (Wong et al., 2002) and also a decrease in the cellular glutathione pool (Schoeler et al., 2007). Currently there are no studies that have investigated mitochondrial dynamics in NT2 LHON cybrids. Due to the low yield of terminally differentiated LHON-neurons, the lengthy differentiation period (~4 weeks) and the heterogeneity of the differentiated cells, the use of NT2 LHON cybrids in LHON studies has been limited (Kirches, 2011).

Our chemically differentiated fibroblast model offers numerous advantages over current LHON cell models. Fibroblasts are primary cells that closely mimic normal cellular physiology and metabolism and are easy to grow in culture. Furthermore, the

use of patient fibroblasts containing the mutation eliminates the introduction of exogenous LHON mitochondria such as in cybrids. Our model also permits the investigation of mitochondrial movement along processes. The mitochondria appear discrete in the cellular processes of fibroblasts much like in dendrites and axons of neurons (fig 6) which makes the study of mitochondrial dynamics more feasible. In fibroblasts, microtubules are organized in a minus to plus orientation from the center to the periphery (Hirokawa, 1998; Müsch, 2004). The same microtubule orientation is found in axons of neurons which make it a more representative model of RGC axons. The importance of studying mitochondrial dynamics in LHON comes from existing evidence of mitochondrial accumulation in prelaminar region of the optic nerve in LHON patients (Carelli et al., 2002b) suggestive of mitochondrial trafficking defects as well as growing evidence of impaired mitochondrial dynamics in other neurodegenerative diseases (Chang et al., 2006; Baloh et al., 2007; Sasaki and Iwata, 2007; Du et al., 2010; Ishikawa et al., 2014).

4.2. Staurosporine treatment alters the mitochondrial network characteristics in WT but not in LHON fibroblasts under both glycolytic and OXPHOS conditions

Staurosporine is a broad-spectrum kinase inhibitor that can inhibit a range of different kinases including those that regulate mitochondrial morphology and dynamics. The Mitochondrial Network Analysis (MiNA) toolset (Valente et al., 2017) was used for evaluating the changes to the mitochondrial network morphology in response to STSP treatment in WT and LHON fibroblasts. This was done under both glycolytic and OXPHOS conditions. MiNA was developed to evaluate the extent of mitochondrial branching and therefore distinguish between discrete structures such as unbranched puncta and rods which are categorized as individual mitochondria and branched structures which are categorized as networks (Valente et al., 2017). In addition to identifying networks MiNA evaluates the extent of branching within individual networks and enables identification of networks that are highly branched (hyper-fused). Cells with highly fragmented or highly branched mitochondria have important implications in cell biology therefore the accurate identification of these states are critical (Valente et al., 2017).

Under glycolytic conditions STSP decreased the mean rod/branch length in WT fibroblasts (fig 17C). Lower rod/branch length points to mitochondrial remodeling which is a change in the mitochondrial shape characterized by a reduction in mitochondrial length that occur independent of fission and fusion events (Deheshi et al., 2015). Deheshi et al. (2015) reported that STSP primarily cause an increase in mitochondrial fission and not remodeling based on mitochondrial counts pre- and post STSP treatment. However, in the present study there was no significant change in the number of individual mitochondria and number of mitochondrial networks which together with the decreased rod/branch length points to mitochondrial remodeling as the more dominant effect of STSP in WT cells as opposed to mitochondrial fragmentation caused by increased fission (fig 17). The inconsistency between the results observed in the present study and Deheshi et al. (2015) can be explained by the differences in the cell type, concentration of STSP and incubation times. Nevertheless, mitochondrial remodeling has been shown to protect cells from apoptosis by maintaining mitochondrial membrane potential and also decreasing mitochondrial calcium uptake (Deheshi 2015).

Under OXPHOS conditions, STSP caused a significant reduction in the number of individual mitochondria and number of networks per cell in WT fibroblasts (fig 18A&B). This is an indication that individual mitochondria and smaller networks are joining together to form a single network. However, the mean rod/branch length and number of branches per mitochondrial network were not significantly different which suggest that the increase in mitochondrial networking was only partial. This is in contrast to the mitochondrial network morphology of STSP-treated WT fibroblasts under glycolytic conditions which showed remodeling. One possible explanation is an activation of a protective mechanism by the WT fibroblasts in response to STSP. STSP treatment can act as a stressor to which mitochondria respond by increasing fusion of the network for an uninterrupted electron transport chain (ETC) function under conditions where the mitochondrial OXPHOS is activated. Conversely, the decrease in individual mitochondria and number of networks may also implicate the activation of mitophagy. Metabolic conditions that promote increased mitochondrial function are also associated with increased mitophagy (Melser et al., 2013). When mitochondrial OXPHOS is upregulated, bulk mitophagy is also enhanced due to mitochondrial damage caused by increased ROS production (Mishra and Chan, 2016). STSP is also known to increase ROS levels

(Kruman et al., 1998) therefore, mitophagy might be enhanced in STSP-treated WT cells under OXPHOS conditions.

In contrast to WT fibroblasts, STSP had no effect on the mitochondrial network morphology of STSP-treated LHON fibroblasts in either glycolytic or OXPHOS conditions (fig 17, 18). It is unknown why the mitochondrial network did not show any significant changes to STSP treatment. It appears that mitochondria in WT fibroblasts were more sensitive to STSP treatment compared LHON fibroblasts. Conversely, it is possible that LHON mitochondria display a weaker adaptive response to changes in cellular physiology compared to WT mitochondria. This impairment of morphological plasticity in LHON mitochondria is a unique finding and requires further investigation.

4.3. OXPHOS conditions cause a decrease in mitochondrial movement in LHON fibroblasts but not in WT fibroblasts

Although STSP-treated fibroblasts resemble neurons in their morphology, in terms of energy metabolism, fibroblasts are primarily glycolytic when cultured under high glucose conditions (McKay et al., 1983; Guillery et al., 2008). This is due to the rapid activation of glycolysis resulting in faster generation of ATP compared to the slower ATP production by OXPHOS (Del Rey et al., 2017). So even under normoxic conditions fibroblasts exhibit high rates of glycolytic metabolism (Del Rey et al., 2017). In contrast, neurons rely on oxidative metabolism to meet their energy demands as OXPHOS provides 87% (26 out of 30 molecules) of the ATP generated per molelcule of glucose (Hall et al., 2012). Most of this energy goes into maintaining and restoring ion gradients (dissipated during post synaptic and action potentials) and also for the uptake and recycling of neurotransmitters (Attwell and Laughlin, 2001; Alle et al., 2009). However, it is possible to switch the energy metabolism of fibroblasts from glycolysis to OXPHOS by changing the energy-substrate in the culture media from glucose to galactose. While glycolytic metabolism of glucose yields 2 net ATP, the production of pyruvate via glycolytic metabolism of galactose yields no net ATP, forcing cells to have an increased reliance on OXPHOS for energy (Aguer et al., 2011). So, by switching to galactose media we were able to activate the OXPHOS machinery and mimic the energy metabolism of neurons in our experimental model and more importantly expose the LHON G11778A mutational effects on our measured variables which would otherwise be masked by compensatory glycolysis.

We first compared mitochondrial movement between STSP-treated fibroblasts carrying the LHON G11778A mutation and WT STSP-treated fibroblasts. Here we use an excel macro to quantify the bulk movement of mitochondria (Rintoul et al., 2003). Bulk movement is the measure of non-directional movement of mitochondria based on the changes in mitochondrial edge detection between successive frames. Mitochondrial bulk movement is expressed as a movement ratio which represents the changes in mitochondrial pixel intensity between a pair of successive images divided by the total mitochondrial pixels. The mean movement ratio is then calculated by averaging the movement ratio for each pair of successive images in a 26-frame time lapse movie spanning 2 minutes. The mitochondrial movement ratio was lower in LHON cells when the cellular energy dependency was shifted from glycolysis towards OXPHOS (fig 19). In contrast WT cells did not show a difference in the mitochondrial movement ratio when their energy dependency was switched to OXPHOS. Furthermore, the mitochondrial movement ratio of LHON cells was lower than that of WT cells under conditions that induce OXPHOS. These results point to a reduction in mitochondrial movement in fibroblasts containing the G11778A LHON mutation when mitochondrial OXPHOS is activated. Therefore, based on our cell model, we speculate a mitochondrial movement defect is present in LHON cells. A mitochondrial trafficking defect would lead to negative consequences especially in cells such as RGCs and their long axons.

Evidence in support of mitochondrial trafficking defects is quite limited in LHON, however, Sadun et al. (1994) showed clumps of mitochondria in spared axons in the retrolaminar region of the optic nerve, accumulations of multi-vesicular bodies and debris, and cytoskeletal changes in autopsies of LHON patients. Evidence for mitochondrial trafficking defects has been implicated in other neurodegenerative diseases. The evidence has mostly come from autopsied material and experimental models. In autopsied material from Alzheimer's disease patients, defects in axonal trafficking of organelles including mitochondria were inferred from the observations of axonal swellings containing vesicles, vacuoles and mitochondria in the nucleus basalis of Meynert (Stokin et al., 2005). Marked accumulation of mitochondria in the somata of anterior horn neurons was reported in patients with amyotrophic lateral sclerosis (ALS) (Sasaki and Iwata, 2007). Mitochondrial trafficking defects are more commonly reported in experimental models of familial forms of neurodegenerative disorders. In an experimental model, of autosomal dominant Perry syndrome, mutations in the

P150glued subunit of the dynactin complex caused mitochondrial entrapment in inclusions of misfolded protein aggregates (Levy et al., 2006; Ishikawa et al., 2014). Similarly, mutant HTT aggregates, the main pathological feature of Huntington's disease, acted as physical barriers for mitochondrial transport in cortical neuronal processes (Chang et al., 2006). Expression of mutant HTT in transgenic mice impaired trafficking of vesicles and mitochondria (Trushina et al., 2004). Mutant MFN2 which causes Type II Charcot-Marie-tooth disease (CMT), when expressed in cultured dorsal root ganglion neurons induced abnormal clustering of fragmented mitochondria, as well as impaired axonal transport of mitochondria (Baloh et al., 2007). Fibroblasts from sporadic Alzheimer's disease (AD) patients showed perinuclear clustering of mitochondria while a mouse model of AD showed decrease in both anterograde and retrograde mitochondrial motility (Du et al., 2010). Altered mitochondrial trafficking was also reported in familial ALS linked mouse models (Kong and Xu, 1998; Higgins et al., 2003). Aggregation of mitochondria and mutant proteins, accumulation of damaged mitochondria, dysfunction in the machinery involved in mitochondrial fusion and fission, defects in mitochondrial motors and adaptors are some of the ways in which the mitochondrial movement is altered in these disease states. However, we did not find evidence of mitochondrial clustering and accumulation in STSP-treated LHON fibroblasts under culture conditions of both glycolytic metabolism and oxidative metabolism. Since mitochondrial trafficking is an energy dependent process it is possible that under forced OXPHOS conditions, LHON cells do not produce enough ATP to drive processes such as mitochondrial trafficking.

4.4. No difference in cytosolic ATP between LHON and WT fibroblasts under OXPHOS conditions

The primary pathogenic mutations causing LHON occur in subunits that make up complex I (NADH dehydrogenase) of the electron transport chain. Therefore, it is possible that a movement defect is directly or indirectly associated with impaired OXPHOS due to a defective complex I. Evidence for OXPHOS defects causing mitochondrial movement impairment is rare. The induction of early Parkinson's disease like phenotypes by chronic treatment with low concentrations of complex I inhibitor, rotenone in differentiated SH-SY5Y neuroblastoma cells showed reduction in the dynamic movement of mitochondria in neurites (Lee et al., 2006). A dysfunction in

OXPHOS can be in the form of reduced complex I enzyme activity, loss of mitochondrial membrane potential, increased production of ROS or reduced ATP synthesis all of which can contribute to a movement defect. We investigated relative cytosolic ATP levels as ATP is required to drive the mitochondrial motors. A decrease in ATP has been demonstrated in cybrids carrying all three of the primary LHON mutations when grown in galactose media (Zanna et al., 2005).

We used a FRET-based ATP probe, ATeam, to monitor the relative levels of ATP in neurons in real time. When ATP is bound to the probe, a conformational change occurs which permits the efficient transfer of resonant energy from the CFP fluorochrome to the YFP fluorochrome (Imamura et al., 2009). Therefore, in the presence of ATP there is a higher 535nm/465nm emission ratio. Our results do not show any significant difference in relative cytosolic ATP levels between WT and LHON fibroblasts under glycolytic and OXPHOS conditions (fig 20). The unchanged cytosolic ATP levels may suggest an adaptive program where ATP is directed away from mitochondrial movement to more critical processes within the cell in LHON fibroblasts under OXPHOS conditions. Conversely, intra-mitochondrial, but not overall cellular ATP level might be more relevant to mitochondrial trafficking.

4.5. OXPHOS conditions cause higher degree of branching of the mitochondrial network in WT cells but not in LHON cells

Mitochondrial morphology is governed by the steady-state equilibrium between continuous and antagonistic fission and fusion reactions (Guillery et al., 2008). This equilibrium may be shifted by physiological, pathological or environmental factors resulting in a change in the overall mitochondrial morphology of the cell (Knott et al., 2008; Willems et al., 2009; Court and Coleman, 2012; Labbé et al., 2014; Mishra and Chan, 2014). Multiple lines of evidence have emerged that show a strong link between mitochondrial metabolism and dynamics (Benard and Rossignol, 2008; Mitra et al., 2009; Rambold et al., 2011; Mishra et al., 2014). We measured changes in the mitochondrial morphology and the network in STSP-treated WT and LHON fibroblasts under OXPHOS and glycolytic conditions using the Mitochondrial Network Analysis (MiNA) toolset (Valente et al., 2017). The macro allowed the characterization of the mitochondrial morphology and network in a cell based on the parameters; number of

individual mitochondria, number of mitochondrial networks, mean mitochondrial rod/branch length and number of branches per mitochondrial network. Networks are mitochondrial structures with at least a single node and three branches (in a skeletonized image) and individual mitochondria are punctate (a single pixel in a skeletonized image) and rod structures (unbranched structures with two or more pixels in a skeletonized image).

There is often a link between mitochondrial morphology and the energetic state of the cell (Mishra and Chan, 2016). Culture conditions that force increased OXPHOS activity are accompanied by elongation of the mitochondrial network in yeast cells (Egner et al., 2002; Jakobs et al., 2003), which was replicated in human cells grown in galactose media (Rossignol et al., 2004). It has been shown that elongated and highly branched mitochondrial networks are more efficient at energy generation and capable of distributing energy through long distances (Amchenkova et al., 1988; Skulachev, 2001). There was no evidence of elongation as there was no significant difference in mean mitochondrial rod/branch length between WT and LHON cells under OXPHOS conditions (fig 21C). However, our results for STSP-treated WT fibroblasts showed an increase in the number of branches per network when the energy dependency was switched from glycolysis to OXPHOS (fig 21D). In contrast, this increase in number of branches per network was not observed in LHON fibroblasts where the number of branches per mitochondrial network was significantly lower compared to WT fibroblasts under OXPHOS conditions (21D). This shows that mitochondria in LHON fibroblasts were not as efficient as mitochondria in WT fibroblasts at remodeling the mitochondrial network to adapt to conditions of high energy demand.

The greater than 2-fold increase in the number of branches per mitochondrial network in WT fibroblasts under OXPHOS conditions compared to glycolytic conditions shows a shift in the mitochondrial dynamics towards increased fusion (fig 21D). However, this was not observed in LHON fibroblasts where the number of branches per mitochondrial network remained unchanged under glycolytic and OXPHOS conditions. One explanation for reduced mitochondrial fusion observed in LHON fibroblasts under OXPHOS conditions is the decrease in bulk movement demonstrated by mitochondria in LHON fibroblasts under the same conditions (fig 19). One consequence of reduced mitochondrial movement is a reduced probability of mitochondrial fusion. Therefore, reduced fusion under energetically demanding conditions may cause an energy deficit

which can have a negative impact on the cell. Evidence for neurodegeneration resulting from impaired fusion machinery has been shown in mutations in the outer membrane fusion protein, MFN2 causing Charcot-Marie-Tooth disease type 2A, a peripheral neuropathy affecting long motor and sensory neurons (Züchner et al., 2004) and mutations in the inner membrane fusion protein OPA1 causing dominant optic atrophy, a blindness caused by degeneration of RGCs and is clinically regarded as the sister disease of LHON (Carelli et al., 2007). Increased OXPHOS activity stimulates mitochondrial fusion to cause elongation (Mishra and Chan, 2016). This is mediated by the metalloprotease YME1L1 which activates OPA1 by proteolytic cleavage into a soluble short form thus stimulating its fusion activity. YME1L1 is an ATP dependent protease and therefore OXPHOS or ATP stimulates OPA1 cleavage enhancing inner membrane fusion in response to metabolic signals (Mishra et al., 2014). YME1L1 may directly sense ATP generation by the electron transport chain (ETC) through its interactions with complex V subunits (Stiburek et al., 2012). Cybrids containing the G3460A LHON mutation in the ND1 subunit of complex I or a premature stop codon at nucleotide 6390 in the cytochrome c oxidase subunit I of complex IV showed lower cleavage activity of OPA1 by YME1L1. This shows that in pathogenic mtDNA mutations that cause defects in OXPHOS result in secondary defects in mitochondrial inner-membrane fusion (Mishra et al., 2014).

Conversely an increase in mitochondrial fission in LHON cells can also result in a reduced branching of mitochondria under OXPHOS conditions. A study by Guillery et al. (2008) reported that cybrids carrying G11778A LHON mutation appeared fragmented. Drugs that inhibit mitochondrial OXPHOS are generally associated with enhanced fission such as mitochondrial uncouplers (e.g. CCCP and FCCP) which cause rapid and dramatic fragmentation of the mitochondrial network (Mishra and Chan, 2016). However, the effects induced by such drugs are non-physiological and may not be representative of the actual pathophysiology even in the cases of severe OXPHOS gene mutations. The dramatic changes induced by pharmacological challenges are more reflective of acute toxicity rather than the milder, progressive impairments induced by pathogenic OXPHOS mutations like those underlying LHON. Nevertheless, mild mitochondrial fragmentation caused by inhibitors of the different OXPHOS complexes may point towards slight but critical changes to the mitochondrial morphology in pathogenic OXPHOS mutations.

Chapter 5. Conclusion

Despite the identification of the genetic cause of LHON as mutations in the mitochondrial DNA encoding components of the OXPHOS machinery, limited progress has been made in figuring out the pathophysiological mechanism that leads to RGC degeneration. One of the major hurdles in our understanding of the pathophysiological mechanism of LHON is the lack of a suitable model system. The current disease models only allow limited aspects of LHON pathophysiology to be studied such as complex I activity, ATP production, ROS imbalance, apoptosis. These studies have either produced contradictory results or have not been sufficient at explaining the unique features of LHON such as tissue specificity and gender bias. There is a growing body of evidence implicating the role of mitochondrial dynamics in neurodegeneration. So, there is need for a better model system for studying mitochondrial dynamics in LHON. Furthermore, researchers have also shown a strong link between mitochondrial metabolism and mitochondrial dynamics. The goal of this project was to create a cell model that enables the study of mitochondrial dynamics such as mitochondrial trafficking, fission and fusion in LHON. In our study, we provide preliminary evidence of altered mitochondrial dynamics in our LHON cell model.

By treating dermal fibroblasts cultures with a low concentration of STSP, we were able to induce formation of cytoplasmic protrusions which resemble neurites morphologically. The STSP-induced changes to the cell morphology were consistent for both WT fibroblasts and fibroblasts carrying the LHON G11778A mutation. However, STSP-induced changes to the mitochondrial morphology and network characteristics were different between WT and LHON fibroblasts. The generation of cytoplasmic processes by STSP allowed for easier observation of discrete mitochondria and analysis of their movement, a task which is challenging in fibroblasts due to their complex reticular mitochondrial networks.

We showed that mitochondrial movement was reduced in STSP-treated LHON fibroblasts under conditions that mimic the energy metabolism of RGCs (OXPHOS pathway). The movement defect could not be attributed to a reduction in cytosolic ATP levels. Other OXPHOS defects such as reduced mitochondrial membrane potential or increased ROS production could be other potential candidates for the observed

movement defect in LHON cells. Under OXPHOS conditions LHON fibroblasts also showed a lower degree of mitochondrial networking compared to WT cells. We propose that an OXPHOS defect ensuing from the LHON G11778A mutation causes impaired mitochondrial movement which in turn leads to reduced mitochondrial fusion under metabolic stress. Conversely it is possible that a decrease in fusion or an increase in fission precedes a decrease in movement due to the reciprocal interaction that exists between fission/fusion and trafficking machinery (Baloh et al., 2007; Chen et al., 2007; Misko et al., 2010; Sheng and Cai, 2012). A third scenario is that an OXPHOS defect causes both trafficking and fission/fusion decrease independently under metabolic stress (i.e. galactose). Regardless of the sequence of events, the inability of mitochondria to adapt to changes in metabolic state due to disrupted mitochondrial dynamics may have detrimental effect on the cell, especially if the cell is an RGC. The morphological state of the mitochondria has been linked to their energy production capacity (Bach et al., 2003; Chen et al., 2005; Benard and Rossignol, 2008) as well as cell health and cell death mechanisms (Cheung et al., 2007; Detmer and Chan, 2007; Jahani-Asl et al., 2007; Rintoul and Reynolds, 2010). In RGCs mitochondrial trafficking defects will cause decreased recycling and lead to accumulation of damaged mitochondria in regions of high energy demand. Decreased fusion will prevent the exchange of proteins, metabolites and diminish mtDNA repair mechanisms which normally serve a protective function. Further studies are required to determine the cause of the altered mitochondrial dynamics of LHON fibroblasts under OXPHOS conditions. Protonophores such as CCCP which completely dissipate the mitochondrial membrane potential only cause a mild decrease in ATP but induce severe mitochondrial fragmentation (Guillery et al., 2008). ROS may also play a role in mitochondrial fragmentation in a Ca^{2+}-independent manner (Tian et al., 2009). ROS can also reversibly decrease mitochondrial motility (Debattisti et al., 2017). Therefore, mitochondrial membrane potential, ROS as well as mitochondrial ATP levels should be investigated in the future.

However, despite being a useful model for evaluating mitochondrial dynamics, it does come with its flaws and limitations. The STSP-treated fibroblasts only resemble neurons in their morphology and not in function. Neurons possess specialized structural and functional domains and have a different protein expression profile from fibroblasts. The mitochondrial trafficking machinery as well as the regulatory mechanisms involved in trafficking is different between neurons and fibroblasts. Future research should look

into identifying the cytoskeletal components that make up the STSP induced processes as well as the molecular machinery involved in mitochondrial trafficking in fibroblasts in order to make direct comparisons. Staurosporine is a broad-spectrum kinase inhibitor therefore can affect a range of cellular processes including those that regulate mitochondrial dynamics. Therefore, it is important to take into account the effects of STSP on mitochondrial dynamics when evaluating mitochondrial function and dynamics in STSP-treated fibroblasts model. The new technique involving the trans-differentiation fibroblasts to functional neurons is a potential alternative for mitochondrial dynamics as well as other aspects of LHON (Vierbuchen et al., 2010; Caiazzo et al., 2011; Yoo et al., 2011; Richner et al., 2015).

Nevertheless, our model provides preliminary evidence of altered mitochondrial dynamics in LHON fibroblasts under OXPHOS conditions. This study warrants further investigation to an area of LHON that has received little attention and may provide a link between OXPHOS defect and RGC degeneration.

References

Abercrombie M (1978) The cells. J Clin Pathol 12:1–6.

Abu-Amero KK, Jaber M, Hellani A, Bosley TM (2010) Genome-wide expression profile of LHON patients with the 11778 mutation. Br J Ophthalmol 94:256–259.

Aguer C, Gambarotta D, Mailloux RJ, Moffat C, Dent R, McPherson R, Harper M-E (2011) Galactose enhances oxidative metabolism and reveals mitochondrial dysfunction in human primary muscle cells. PLoS One 6:e28536.

Aizawa H, Sekine Y, Takemura R, Zhang Z, Nangaku M, Hirokawa N (1992) Kinesin family in murine central nervous system. J Cell Biol 119:1287–1296.

Algvere P V., Marshall J, Seregard S (2006) Age-related maculopathy and the impact of blue light hazard. Acta Ophthalmol Scand 84:4–15.

Alle H, Roth A, Geiger JRP (2009) Energy-Efficient Action Potentials in Hippocampal Mossy Fibers. Science (80-) 325:1405–1408.

Amchenkova AA, Bakeeva LE, Chentsov YS, Skulachev VP, Zorov DB (1988) Coupling membranes as energy-transmitting cables. I. Filamentous mitochondria in fibroblasts and mitochondrial clusters in cardiomyocytes. J Cell Biol 107:481–495.

Anderson S, Bankier AT, Barrell BG, de Bruijn MHL, Coulson AR, Drouin J, Eperon IC, Nierlich DP, Roe BA, Sanger F, Schreier PH, Smith AJH, Staden R, Young IG (1981) Sequence and organization of the human mitochondrial genome. Nature 290:457–465.

Andrews RM, Griffiths PG, Johnson MA, Turnbull DM (1999) Histochemical localisation of mitochondrial enzyme activity in human optic nerve and retina. Br J Ophthalmol 83:231 LP-235.

Attwell D, Laughlin SB (2001) An Energy Budget for Signaling in the Grey Matter of the Brain. J Cereb Blood Flow Metab 21:1133–1145.

Bach D, Pich S, Soriano FX, Vega N, Baumgartner B, Oriola J, Daugaard JR, Lloberas J, Camps M, Zierath JR, Rabasa-Lhoret R, Wallberg-Henriksson H, Laville M, Palacín M, Vidal H, Rivera F, Brand M, Zorzano A (2003) Mitofusin-2 determines mitochondrial network architecture and mitochondrial metabolism. A novel regulatory mechanism altered in obesity. J Biol Chem 278:17190–17197.

Baloh RH, Schmidt RE, Pestronk A, Milbrandt J (2007) Altered axonal mitochondrial transport in the pathogenesis of Charcot-Marie-Tooth disease from mitofusin 2 mutations. J Neurosci 27:422–430.

Baracca A, Solaini G, Sgarbi G, Lenaz G, Baruzzi A, Schapira AH V, Martinuzzi A, Carelli V (2005) Severe impairment of complex I-driven adenosine triphosphate synthesis in leber hereditary optic neuropathy cybrids. Arch Neurol 62:730–736.

Barbiroli B, Montagna P, Cortelli P, Iotti S, Lodi R, Barboni P, Monari L, Lugaresi E, Frassineti C, Zaniol P (1995) Defective brain and muscle energy metabolism shown by in vivo 31P magnetic resonance spectroscopy in nonaffected carriers of 11778 mtDNA mutation. Neurology 45:1364–1369.

Barboni P, Carbonelli M, Savini G, Ramos C do VF, Carta A, Berezovsky A, Salomao SR, Carelli V, Sadun AA (2010) Natural History of Leber's Hereditary Optic Neuropathy: Longitudinal Analysis of the Retinal Nerve Fiber Layer by Optical Coherence Tomography. Ophthalmology 117:623–627.

Barron MJ, Griffiths P, Turnbull DM, Bates D, Nichols P (2004) The distributions of mitochondria and sodium channels reflect the specific energy requirements and conduction properties of the human optic nerve head. Br J Ophthalmol 88:286–290.

Baxter GD, Lavin MF (1992) Specific protein dephosphorylation in apoptosis induced by ionizing radiation and heat shock in human lymphoid tumor lines. J Immunol 148:1949–1954.

Beatty S, Koh H-H, Phil M, Henson D, Boulton M (2000) The Role of Oxidative Stress in the Pathogenesis of Age-Related Macular Degeneration. Curr Res Surv Ophthalmol Surv Ophthalmol 45:115–134.

Bell J (1931) The Treasury of Human Inheritance: Nettleship Memorial Volume. Anomalies and Diseases of the Eye. Hereditary Optic Atrophy (Leber's Disease). Cambridge University Press.

Benard G, Rossignol R (2008) Ultrastructure of the Mitochondrion and Its Bearing on Function and Bioenergetics. Antioxid Redox Signal 10:1313–1342.

Beretta S, Mattavelli L, Sala G, Tremolizzo L, Schapira AHV, Martinuzzi A, Carelli V, Ferrarese C (2004) Leber hereditary optic neuropathy mtDNA mutations disrupt glutamate transport in cybrid cell lines. Brain 127:2183–2192.

Bi R, Logan I, Yao Y-G (2016) Leber Hereditary Optic Neuropathy: A Mitochondrial Disease Unique in Many Ways. In, pp 309–336. Springer, Cham.

Bianco A, Bisceglia L, Russo L, Palese LL, D'Agruma L, Emperador S, Montoya J, Guerriero S, Petruzzella V (2017) High Mitochondrial DNA Copy Number Is a Protective Factor From Vision Loss in Heteroplasmic Leber's Hereditary Optic Neuropathy (LHON). Investig Opthalmology Vis Sci 58:2193.

Bindoff LA, Desnuelle C, Birch-Machin MA, Pellissier JF, Serratrice G, Dravet C, Bureau M, Howell N, Turnbull DM (1991) Multiple defects of the mitochondrial respiratory chain in a mitochondrial encephalopathy (MERRF): a clinical, biochemical and molecular study. J Neurol Sci 102:17–24.

Bonda DJ, Wang X, Perry G, Smith MA, Zhu X (2010) Mitochondrial Dynamics in Alzheimer's Disease. Drugs Aging 27:181–192.

Borland MK, Trimmer P a, Rubinstein JD, Keeney PM, Mohanakumar K, Liu L, Bennett JP (2008) Chronic, low-dose rotenone reproduces Lewy neurites found in early stages of Parkinson's disease, reduces mitochondrial movement and slowly kills differentiated SH-SY5Y neural cells. Mol Neurodegener 3:21.

Boulet L, Karpati G, Shoubridge EA (1992) Distribution and threshold expression of the tRNA(Lys) mutation in skeletal muscle of patients with myoclonic epilepsy and ragged-red fibers (MERRF). Am J Hum Genet 51:1187–1200.

Boulton M, Rózanowska M, Rózanowski B (2001) Retinal photodamage. J Photochem Photobiol B 64:144–161.

Bourgeron T, Chretien D, Rötig A, Munnich A, Rustin P (1993) Fate and expression of the deleted mitochondrial DNA differ between human heteroplasmic skin fibroblast and Epstein-Barr virus-transformed lymphocyte cultures. J Biol Chem 268:19369–19376.

Bower SP, Hawley I, Mackey DA (1992) Cardiac arrhythmia and Leber's hereditary optic neuropathy. Lancet (London, England) 339:1427–1428.

Braak H, Ghebremedhin E, Rüb U, Bratzke H, Del Tredici K (2004) Stages in the development of Parkinson's disease-related pathology. Cell Tissue Res 318:121–134.

Brickley K, Smith MJ, Beck M, Stephenson FA (2005) GRIF-1 and OIP106, Members of a Novel Gene Family of Coiled-Coil Domain Proteins. J Biol Chem 280:14723–14732.

Bristow EA, Griffiths PG, Andrews RM, Johnson MA, Turnbull DM (2002) The distribution of mitochondrial activity in relation to optic nerve structure. Arch Ophthalmol (Chicago, Ill 1960) 120:791–796.

Brown, MD (1994) Spectrum of mitochondrial DNA mutations in Leber's hereditary optic neuropathy. Clin Neurosci 2:138–145.

Brown MD, Sun F, Wallace DC (1997) Clustering of Caucasian Leber hereditary optic neuropathy patients containing the 11778 or 14484 mutations on an mtDNA lineage. Am J Hum Genet 60:381–387.

Brown MD, Trounce IA, Jun AS, Allen JC, Wallace DC (2000) Functional Analysis of Lymphoblast and Cybrid Mitochondria Containing the 3460, 11778, or 14484 Leber's Hereditary Optic Neuropathy Mitochondrial DNA Mutation. J Biol Chem 275:39831–39836.

Bu X, Rotter JI (1992) Leber hereditary optic neuropathy: estimation of number of embryonic precursor cells and disease threshold in heterozygous affected females at the X-linked locus. Clin Genet 42:143–148.

Bu XD, Rotter JI (1991) X chromosome-linked and mitochondrial gene control of Leber hereditary optic neuropathy: evidence from segregation analysis for dependence on X chromosome inactivation. Proc Natl Acad Sci U S A 88:8198–8202.

Caiazzo M, Dell'Anno MT, Dvoretskova E, Lazarevic D, Taverna S, Leo D, Sotnikova TD, Menegon A, Roncaglia P, Colciago G, Russo G, Carninci P, Pezzoli G, Gainetdinov RR, Gustincich S, Dityatev A, Broccoli V (2011) Direct generation of functional dopaminergic neurons from mouse and human fibroblasts. Nature 476:224–227.

Calkins MJ, Manczak M, Mao P, Shirendeb U, Reddy PH (2011) Impaired mitochondrial biogenesis, defective axonal transport of mitochondria, abnormal mitochondrial dynamics and synaptic degeneration in a mouse model of Alzheimer's disease. Hum Mol Genet 20:4515–4529.

Carelli V et al. (2006) Haplogroup Effects and Recombination of Mitochondrial DNA: Novel Clues from the Analysis of Leber Hereditary Optic Neuropathy Pedigrees. Am J Hum Genet 78:564–574.

Carelli V, Ghelli A, Bucchi L, Montagna P, De Negri A, Leuzzi V, Carducci C, Lenaz G, Lugaresi E, Degli Esposti M (1999) Biochemical features of mtDNA 14484 (ND6/M64V) point mutation associated with Leber's hereditary optic neuropathy. Ann Neurol 45:320–328.

Carelli V, Ghelli A, Ratta M, Bacchilega E, Sangiorgi S, Mancini R, Leuzzi V, Cortelli P, Montagna P, Lugaresi E, Degli Esposti M (1997) Leber's hereditary optic neuropathy: biochemical effect of 11778/ND4 and 3460/ND1 mutations and correlation with the mitochondrial genotype. Neurology 48:1623–1632.

Carelli V, La Morgia C, Iommarini L, Carroccia R, Mattiazzi M, Sangiorgi S, Farne' S, Maresca A, Foscarini B, Lanzi L, Amadori M, Bellan M, Valentino ML (2007) Mitochondrial optic neuropathies: How two genomes may kill the same cell type? Biosci Rep 27:173–184.

Carelli V, Napoli E, Valente L, Valentino L, Martinuzzi A (2002a) ROS production in cybrids carrying the three primary mutations associated with Leber's hereditary optic neuropathy. In: Neurology, pp A507–A507. LIPPINCOTT WILLIAMS & WILKINS 530 WALNUT ST, PHILADELPHIA, PA 19106-3621 USA.

Carelli V, Ross-Cisneros FN, Sadun A a. (2004a) Mitochondrial dysfunction as a cause of optic neuropathies. Prog Retin Eye Res 23:53–89.

Carelli V, Ross-Cisneros FN, Sadun AA (2002b) Optic nerve degeneration and mitochondrial dysfunction: genetic and acquired optic neuropathies. Neurochem Int 40:573–584.

Carelli V, Rugolo M, Sgarbi G, Ghelli A, Zanna C, Baracca A, Lenaz G, Napoli E, Martinuzzi A, Solaini G (2004b) Bioenergetics shapes cellular death pathways in Leber's hereditary optic neuropathy: a model of mitochondrial neurodegeneration. Biochim Biophys Acta - Bioenerg 1658:172–179.

Carelli V, Vergani L, Bernazzi B, Zampieron C, Bucchi L, Valentino M, Rengo C, Torroni A, Martinuzzi A (2002c) Respiratory function in cybrid cell lines carrying European mtDNA haplogroups: implications for Leber's hereditary optic neuropathy. Biochim Biophys Acta 1588:7–14.

Case JT, Wallace DC (1981) Maternal inheritance of mitochondrial DNA polymorphisms in cultured human fibroblasts. Somatic Cell Genet 7:103–108.

Chalmers RM, Davis MB, Sweeney MG, Wood NW, Harding AE (1996a) Evidence against an X-linked visual loss susceptibility locus in Leber hereditary optic neuropathy. Am J Hum Genet 59:103–108.

Chalmers RM, Gown GG, Schapira AH V, Harding AE (1996b) HLA class I genotypes in Leber's hereditary optic neuropathy. J Neurol Sci 135:173–175.

Chalmers RM, Harding AE (1996) A case-control study of Leber's hereditary optic neuropathy. Brain 119:1481–1486.

Chan NC, Salazar AM, Pham AH, Sweredoski MJ, Kolawa NJ, Graham RLJ, Hess S, Chan DC (2011) Broad activation of the ubiquitin-proteasome system by Parkin is critical for mitophagy. Hum Mol Genet 20:1726–1737.

Chang C-R, Blackstone C (2007) Cyclic AMP-dependent Protein Kinase Phosphorylation of Drp1 Regulates Its GTPase Activity and Mitochondrial Morphology. J Biol Chem 282:21583–21587.

Chang DTW, Rintoul GL, Pandipati S, Reynolds IJ (2006) Mutant huntingtin aggregates impair mitochondrial movement and trafficking in cortical neurons. Neurobiol Dis 22:388–400.

Charlmers RM, Harding AE (1996) A case-control study of Leber's hereditary optic neuropathy. Brain 119 (Pt 5:1481–1486.

Chen H, Chan DC (2009) Mitochondrial dynamics-fusion, fission, movement, and mitophagy-in neurodegenerative diseases. Hum Mol Genet 18:169–176.

Chen H, Chomyn A, Chan DC (2005) Disruption of fusion results in mitochondrial heterogeneity and dysfunction. J Biol Chem 280:26185–26192.

Chen H, Detmer SA, Ewald AJ, Griffin EE, Fraser SE, Chan DC (2003) Mitofusins Mfn1 and Mfn2 coordinately regulate mitochondrial fusion and are essential for embryonic development. J Cell Biol 160:189–200.

Chen H, McCaffery JM, Chan DC (2007) Mitochondrial fusion protects against neurodegeneration in the cerebellum. Cell 130:548–562.

Cheung ECC, McBride HM, Slack RS (2007) Mitochondrial dynamics in the regulation of neuronal cell death. Apoptosis 12:979–992.

Chevalier-Larsen E, Holzbaur ELF (2006) Axonal transport and neurodegenerative disease. Biochim Biophys Acta - Mol Basis Dis 1762:1094–1108.

Chevrollier A, Guillet V, Loiseau D, Gueguen N, Pou de Crescenzo M-A, Verny C, Ferre M, Dollfus H, Odent S, Milea D, Goizet C, Amati-Bonneau P, Procaccio V, Bonneau D, Reynier P (2008) Hereditary optic neuropathies share a common mitochondrial coupling defect. Ann Neurol 63:794–798.

Chinnery PF, Andrews RM, Turnbull DM, Howell NN (2001) Leber hereditary optic neuropathy: Does heteroplasmy influence the inheritance and expression of the G11778A mitochondrial DNA mutation? Am J Med Genet 98:235–243.

Chung KW, Kim SB, Park KD, Choi KG, Lee JH, Eun HW, Suh JS, Hwang JH, Kim WK, Seo BC, Kim SH, Son IH, Kim SM, Sunwoo IN, Choi BO (2006) Early onset severe and late-onset mild Charcot-Marie-Tooth disease with mitofusin 2 (MFN2) mutations. Brain 129:2103–2118.

Cipolat S, Rudka T, Hartmann D, Costa V, Serneels L, Craessaerts K, Metzger K, Frezza C, Annaert W, D'Adamio L, Derks C, Dejaegere T, Pellegrini L, D'Hooge R, Scorrano L, De Strooper B (2006) Mitochondrial Rhomboid PARL Regulates Cytochrome c Release during Apoptosis via OPA1-Dependent Cristae Remodeling. Cell 126:163–175.

Clark IE, Dodson MW, Jiang C, Cao JH, Huh JR, Seol JH, Yoo SJ, Hay BA, Guo M (2006) Drosophila pink1 is required for mitochondrial function and interacts genetically with parkin. Nature 441:1162–1166.

Clayton DA (1982) Replication of animal mitochondrial DNA. Cell 28:693–705.

Cock HR, Cooper JM, Schapira AH (1995) The 14484 ND6 mtDNA mutation in Leber hereditary optic neuropathy does not affect fibroblast complex I activity. Am J Hum Genet 57:1501–1502.

Cock HR, Cooper JM, Schapira AH (1999) Functional consequences of the 3460-bp mitochondrial DNA mutation associated with Leber's hereditary optic neuropathy. J Neurol Sci 165:10–17.

Cortelli P, Montagna P, Avoni P, Sangiorgi S, Bresolin N, Moggio M, Zaniol P, Mantovani V, Barboni P, Barbiroli B (1991) Leber's hereditary optic neuropathy: genetic, biochemical, and phosphorus magnetic resonance spectroscopy study in an Italian family. Neurology 41:1211–1215.

Court FA, Coleman MP (2012) Mitochondria as a central sensor for axonal degenerative stimuli. Trends Neurosci 35:364–372.

Curcio CA, Allen KA (1990) Topography of ganglion cells in human retina. J Comp Neurol 300:5–25.

Danielson SR, Carelli V, Tan G, Martinuzzi A, Schapira AH V., Savontaus M-L, Cortopassi GA (2005) Isolation of transcriptomal changes attributable to LHON mutations and the cybridization process. Brain 128:1026–1037.

Danielson SR, Wong A, Carelli V, Martinuzzi A, Schapira AH V., Cortopassi GA (2002) Cells Bearing Mutations Causing Leber's Hereditary Optic Neuropathy Are Sensitized to Fas-induced Apoptosis. J Biol Chem 277:5810–5815.

de Brito OM, Scorrano L (2008) Mitofusin 2 tethers endoplasmic reticulum to mitochondria. Nature 456:605–610.

De Vries DD, Went LN, Bruyn GW, Scholte HR, Hofstra RM, Bolhuis PA, van Oost BA (1996) Genetic and biochemical impairment of mitochondrial complex I activity in a family with Leber hereditary optic neuropathy and hereditary spastic dystonia. Am J Hum Genet 58:703–711.

Debattisti V, Gerencser AA, Saotome M, Das S, Rgy G, Czky H (2017) ROS Control Mitochondrial Motility through p38 and the Motor Adaptor Miro/Trak. CellReports 21:1667–1680.

Deheshi S, Dabiri B, Fan S, Tsang M, Rintoul GL (2015) Changes in mitochondrial morphology induced by calcium or rotenone in primary astrocytes occur predominantly through ros-mediated remodeling. J Neurochem.

Del Rey MJ, Valín Á, Usategui A, García-Herrero CM, Sánchez-Aragó M, Cuezva JM, Galindo M, Bravo B, Cañete JD, Blanco FJ, Criado G, Pablos JL (2017) Hif-1α Knockdown Reduces Glycolytic Metabolism and Induces Cell Death of Human Synovial Fibroblasts Under Normoxic Conditions. Sci Rep 7:3644.

Delettre C, Lenaers G, Griffoin JM, Gigarel N, Lorenzo C, Belenguer P, Pelloquin L, Grosgeorge J, Turc-Carel C, Perret E, Astarie-Dequeker C, Lasquellec L, Arnaud B, Ducommun B, Kaplan J, Hamel CP (2000) Nuclear gene OPA1, encoding a mitochondrial dynamin-related protein, is mutated in dominant optic atrophy. Nat Genet 26:207–210.

Deng H, Dodson MW, Huang H, Guo M (2008) The Parkinson's disease genes pink1 and parkin promote mitochondrial fission and/or inhibit fusion in Drosophila. Proc Natl Acad Sci 105:14503–14508.

Detmer SA, Chan DC (2007) Functions and dysfunctions of mitochondrial dynamics. Nat Rev Mol Cell Biol 8:870–879.

DiMauro S, Hirano M (2003) MERRF. GeneReviews:1 Available at: http://www.ncbi.nlm.nih.gov/pubmed/20301693 [Accessed March 3, 2018].

DiMauro S, Hirano M (2013) MELAS. University of Washington, Seattle.

DiMauro S, Schon EA (2003) Mitochondrial Respiratory-Chain Diseases. N Engl J Med 348:2656–2668.

Dorfman LJ, Nikoskelainen E, Rosenthal AR, Sogg RL (1977) Visual evoked potentials in Leber's hereditary optic neuropathy. Ann Neurol 1:565–568.

Downing KH, Nogales E (1998) Tubulin and microtubule structure. Curr Opin Cell Biol 10:16–22.

Du H, Guo L, Yan S, Sosunov AA, McKhann GM, Yan SS (2010) Early deficits in synaptic mitochondria in an Alzheimer's disease mouse model. Proc Natl Acad Sci U S A 107:18670–18675.

Dudkina N V., Eubel H, Keegstra W, Boekema EJ, Braun H-P (2005) Structure of a mitochondrial supercomplex formed by respiratory-chain complexes I and III. Proc Natl Acad Sci 102:3225–3229.

Ebneth A, Godemann R, Stamer K, Illenberger S, Trinczek B, Mandelkow E (1998) Overexpression of tau protein inhibits kinesin-dependent trafficking of vesicles, mitochondria, and endoplasmic reticulum: implications for Alzheimer's disease. J Cell Biol 143:777–794.

Egner A, Jakobs S, Hell SW (2002) Fast 100-nm resolution three-dimensional microscope reveals structural plasticity of mitochondria in live yeast. Proc Natl Acad Sci U S A 99:3370–3375.

Eilaghi A, Flanagan JG, Tertinegg I, Simmons CA, Wayne Brodland G, Ross Ethier C (2010) Biaxial mechanical testing of human sclera. J Biomech 43:1696–1701.

Elachouri G, Vidoni S, Zanna C, Pattyn A, Boukhaddaoui H, Gaget K, Yu-Wai-Man P, Gasparre G, Sarzi E, Delettre C, Olichon A, Loiseau D, Reynier P, Chinnery PF, Rotig A, Carelli V, Hamel CP, Rugolo M, Lenaers G (2011) OPA1 links human mitochondrial genome maintenance to mtDNA replication and distribution. Genome Res 21:12–20.

Enriquez JA, Chomyn A, Attardi G (1995) MtDNA mutation in MERRF syndrome causes defective aminoacylation of tRNALys and premature translation termination. Nat Genet 10:47–55.

Fabricius C, Berthold CH, Rydmark M (1993) Axoplasmic organelles at nodes of Ranvier. II. Occurrence and distribution in large myelinated spinal cord axons of the adult cat. J Neurocytol 22:941–954.

Falabella M, Forte E, Magnifico MC, Santini P, Arese M, Giuffrè A, Radić K, Chessa L, Coarelli G, Buscarinu MC, Mechelli R, Salvetti M, Sarti P (2016) Evidence for Detrimental Cross Interactions between Reactive Oxygen and Nitrogen Species in Leber's Hereditary Optic Neuropathy Cells. Oxid Med Cell Longev 2016:1–9.

Falk MJ, Sondheimer N (2010) Mitochondrial genetic diseases. Curr Opin Pediatr 22:711–716.

Floreani M, Napoli E, Martinuzzi A, Pantano G, De Riva V, Trevisan R, Bisetto E, Valente L, Carelli V, Dabbeni-Sala F (2005) Antioxidant defences in cybrids harboring mtDNA mutations associated with Leber's hereditary optic neuropathy. FEBS J 272:1124–1135.

Fontaine E, Eriksson O, Ichas F, Bernardi P (1998) Regulation of the permeability transition pore in skeletal muscle mitochondria. Modulation By electron flow through the respiratory chain complex i. J Biol Chem 273:12662–12668.

Fransson Å, Ruusala A, Aspenström P (2006) The atypical Rho GTPases Miro-1 and Miro-2 have essential roles in mitochondrial trafficking. Biochem Biophys Res Commun 344:500–510.

Frassetto LJ, Schlieve CR, Lieven CJ, Utter AA, Jones M V., Agarwal N, Levin LA (2006) Kinase-dependent differentiation of a retinal ganglion cell precursor. Investig Ophthalmol Vis Sci 47:427–438.

Fujii T, Hattori H, Higuchi Y, Tsuji M, Mitsuyoshi I (1998) Phenotypic differences between T-->C and T-->G mutations at nt 8993 of mitochondrial DNA in Leigh syndrome. Pediatr Neurol 18:275–277.

Fukuhara N, Tokiguchi S, Shirakawa K, Tsubaki T (1980) Myoclonus epilepsy associated with ragged-red fibres (mitochondrial abnormalities): disease entity or a syndrome? Light-and electron-microscopic studies of two cases and review of literature. J Neurol Sci 47:117–133.

Gabaldón T, Huynen MA (2007) From Endosymbiont to Host-Controlled Organelle: The Hijacking of Mitochondrial Protein Synthesis and Metabolism. PLoS Comput Biol 3:e219.

Galkina SI, Stadnichuk VI, Molotkovsky JG, Romanova JM, Sud'ina GF, Klein T (2010) Microbial alkaloid staurosporine induces formation of nanometer-wide membrane tubular extensions (cytonemes, membrane tethers) in human neutrophils. Cell Adhes Migr 4:32–38.

Galloway CA, Yoon Y (2013) Mitochondrial Morphology in Metabolic Diseases. Antioxid Redox Signal 19:415–430.

Gandre-Babbe S, van der Bliek AM (2008) The Novel Tail-anchored Membrane Protein Mff Controls Mitochondrial and Peroxisomal Fission in Mammalian Cells. Mol Biol Cell 19:2402–2412.

Ghelli A, Zanna C, Porcelli AM, Schapira AH V, Martinuzzi A, Carelli V, Rugolo M (2003) Leber's hereditary optic neuropathy (LHON) pathogenic mutations induce mitochondrial-dependent apoptotic death in transmitochondrial cells incubated with galactose medium. J Biol Chem 278:4145–4150.

Giles RE, Blanc H, Cann HM, Wallace DC (1980) Maternal inheritance of human mitochondrial DNA. Proc Natl Acad Sci U S A 77:6715–6719.

Giordano C et al. (2014) Efficient mitochondrial biogenesis drives incomplete penetrance in Leber's hereditary optic neuropathy. Brain 137:335–353.

Giordano C, Montopoli M, Perli E, Orlandi M, Fantin M, Ross-Cisneros FN, Caparrotta L, Martinuzzi A, Ragazzi E, Ghelli A, Sadun AA, d'Amati G, Carelli V (2011) Oestrogens ameliorate mitochondrial dysfunction in Leber's hereditary optic neuropathy. Brain 134:220–234.

Giordano L et al. (2015) Cigarette toxicity triggers Leber's hereditary optic neuropathy by affecting mtDNA copy number, oxidative phosphorylation and ROS detoxification pathways. Cell Death Dis 6:e2021.

Glater EE, Megeath LJ, Stowers RS, Schwarz TL (2006) Axonal transport of mitochondria requires milton to recruit kinesin heavy chain and is light chain independent. J Cell Biol 173:545–557.

Glickman RD (2002) Phototoxicity to the Retina: Mechanisms of Damage. Int J Toxicol 21:473–490.

Godley BF, Shamsi FA, Liang F-Q, Jarrett SG, Davies S, Boulton M (2005) Blue Light Induces Mitochondrial DNA Damage and Free Radical Production in Epithelial Cells. J Biol Chem 280:21061–21066.

Gorman GS, Schaefer AM, Ng Y, Gomez N, Blakely EL, Alston CL, Feeney C, Horvath R, Yu-Wai-Man P, Chinnery PF, Taylor RW, Turnbull DM, McFarland R (2015) Prevalence of nuclear and mitochondrial DNA mutations related to adult mitochondrial disease. Ann Neurol 77:753–759.

Goto Y, Horai S, Matsuoka T, Koga Y, Nihei K, Kobayashi M, Nonaka I (1992) Mitochondrial myopathy, encephalopathy, lactic acidosis, and stroke-like episodes (MELAS): a correlative study of the clinical features and mitochondrial DNA mutation. Neurology 42:545–550.

Goto Y, Nonaka I, Horai S (1990) A mutation in the tRNALeu(UUR) gene associated with the MELAS subgroup of mitochondrial encephalomyopathies. Nature 348:651–653.

Govan GG, Smith PR, Kellar-Wood H, Schapira AH, Harding AE (1994) HLA class II genotypes in Leber's hereditary optic neuropathy. J Neurol Sci 126:193–196.

Govek E-E, Newey SE, Van Aelst L (2005) The role of the Rho GTPases in neuronal development. Genes Dev 19:1–49.

Gray MW (1998) Rickettsia, typhus and the mitochondrial connection. Nature 396:109–110.

Gray MW (2012) Mitochondrial evolution. Cold Spring Harb Perspect Biol 4:a011403.

Greene JC, Whitworth AJ, Kuo I, Andrews LA, Feany MB, Pallanck LJ (2003) Mitochondrial pathology and apoptotic muscle degeneration in Drosophila parkin mutants. Proc Natl Acad Sci 100:4078–4083.

Gropman A, Chen T-J, Perng C-L, Krasnewich D, Chernoff E, Tifft C, Wong L-JC (2004) Variable clinical manifestation of homoplasmic G14459A mitochondrial DNA mutation. Am J Med Genet 124A:377–382.

Guillery O, Malka F, Frachon P, Milea D, Rojo M, Lombès A (2008) Modulation of mitochondrial morphology by bioenergetics defects in primary human fibroblasts. Neuromuscul Disord 18:319–330.

Gunawardena S, Her L-S, Brusch RG, Laymon RA, Niesman IR, Gordesky-Gold B, Sintasath L, Bonini NM, Goldstein LSB (2003) Disruption of axonal transport by loss of huntingtin or expression of pathogenic polyQ proteins in Drosophila. Neuron 40:25–40.

Guo B, Zhai D, Cabezas E, Welsh K, Nouraini S, Satterthwait AC, Reed JC (2003) Humanin peptide suppresses apoptosis by interfering with Bax activation. Nature 423:456–461.

Hall CN, Klein-Flügge MC, Howarth C, Attwell D (2012) Oxidative phosphorylation, not glycolysis, powers presynaptic and postsynaptic mechanisms underlying brain information processing. J Neurosci 32:8940–8951.

Handoko HY, Wirapati PJ, Sudoyo HA, Sitepu M, Marzuki S (1998) Meiotic breakpoint mapping of a proposed X linked visual loss susceptibility locus in Leber's hereditary optic neuropathy. J Med Genet 35:668–671.

Harding AE, Sweeney MG, Govan GG, Riordan-Eva P (1995) Pedigree analysis in Leber hereditary optic neuropathy families with a pathogenic mtDNA mutation. Am J Hum Genet 57:77–86.

Harding AE, Sweeney MG, Miller DH, Mumford CJ, Kellar-Wood H, Menard D, McDonald WI, Compston DA (1992) Occurrence of a multiple sclerosis-like illness in women who have a Leber's hereditary optic neuropathy mitochondrial DNA mutation. Brain 115 (Pt 4):979–989.

Haroon MF, Fatima A, Schöler S, Gieseler A, Horn TFW, Kirches E, Wolf G, Kreutzmann P (2007) Minocycline, a possible neuroprotective agent in Leber's hereditary optic neuropathy (LHON): Studies of cybrid cells bearing 11778 mutation.

Hashimoto S, Hagino A (1989) Staurosporine-induced neurite outgrowth in PC12h cells. Exp Cell Res 184:351–359.

Hashimoto Y, Niikura T, Tajima H, Yasukawa T, Sudo H, Ito Y, Kita Y, Kawasumi M, Kouyama K, Doyu M, Sobue G, Koide T, Tsuji S, Lang J, Kurokawa K, Nishimoto I (2001) A rescue factor abolishing neuronal cell death by a wide spectrum of familial Alzheimer's disease genes and A. Proc Natl Acad Sci 98:6336–6341.

Hayflick L (1965) The limited in vitro lifetime of human diploid cell strains. Exp Cell Res 37:614–636.

Helm M, Florentz C, Chomyn A, Attardi G (1999) Search for differences in post-transcriptional modification patterns of mitochondrial DNA-encoded wild-type and mutant human tRNALys and tRNALeu(UUR). Nucleic Acids Res 27:756–763.

Henry C, Patel N, Shaffer W, Murphy L, Park J, Spieler B (2017) Mitochondrial Encephalomyopathy With Lactic Acidosis and Stroke-Like Episodes-MELAS Syndrome. Ochsner J 17:296–301.

Higgins CMJ, Jung C, Xu Z (2003) ALS-associated mutant SOD1G93A causes mitochondrial vacuolation by expansion of the intermembrane space and by involvement of SOD1 aggregation and peroxisomes. BMC Neurosci 4:16.

Hirokawa N (1998) Kinesin and dynein superfamily proteins and the mechanism of organelle transport. Science (80-) 279:519–526.

Hirokawa N, Niwa S, Tanaka Y (2010) Molecular motors in neurons: transport mechanisms and roles in brain function, development, and disease. Neuron 68:610–638.

Hirokawa N, Takemura R (2004) Molecular motors in neuronal development, intracellular transport and diseases. Curr Opin Neurobiol 14:564–573.

Hofmann S, Jaksch M, Bezold R, Mertens S, Aholt S, Paprotta A, Gerbitz KD (1997) Population genetics and disease susceptibility: characterization of central European haplogroups by mtDNA gene mutations, correlation with D loop variants and association with disease. Hum Mol Genet 6:1835–1846.

Holländer H, Makarov F, Stefani FH, Stone J (1995) Evidence of constriction of optic nerve axons at the lamina cribrosa in the normotensive eye in humans and other mammals. Ophthalmic Res 27:296–309.

Hollenbeck PJ (1996) The pattern and mechanism of mitochondrial transport in axons. Front Biosci 1:d91-102.

Holt IJ, Harding AE, Morgan-Hughes JA (1988) Deletions of muscle mitochondrial DNA in patients with mitochondrial myopathies. Nature 331:717–719.

Holt IJ, Harding AE, Petty RK, Morgan-Hughes JA (1990) A new mitochondrial disease associated with mitochondrial DNA heteroplasmy. Am J Hum Genet 46:428–433.

Howell N (1997) Leber Hereditary Optic Neuropathy: How Do Mitochondrial DNA Mutations Cause Degeneration of the Optic Nerve? J Bioenerg Biomembr 29:165–173.

Howell N (1999) Human mitochondrial diseases: answering questions and questioning answers. Int Rev Cytol 186:49–116.

Howell N, Bindoff LA, McCullough DA, Kubacka I, Poulton J, Mackey D, Taylor L, Turnbull DM (1991a) Leber hereditary optic neuropathy: identification of the same mitochondrial ND1 mutation in six pedigrees. Am J Hum Genet 49:939–950.

Howell N, Ghosh SS, Fahy E, Bindoff LA (2000) Longitudinal analysis of the segregation of mtDNA mutations in heteroplasmic individuals. J Neurol Sci 172:1–6.

Howell N, Herrnstadt C, Shults C, Mackey DA (2003) Low penetrance of the 14484 LHON mutation when it arises in a non-haplogroup J mtDNA background. Am J Med Genet 119A:147–151.

Howell N, Kubacka I, Xu M, McCullough DA (1991b) Leber hereditary optic neuropathy: involvement of the mitochondrial ND1 gene and evidence for an intragenic suppressor mutation. Am J Hum Genet 48:935–942.

Howell N, Mackey DA (1998) Low-penetrance branches in matrilineal pedigrees with Leber hereditary optic neuropathy. Am J Hum Genet 63:1220–1224.

Howell N, Xu M, Halvorson S, Bodis-Wollner I, Sherman J, Gerdes J, Becker M (1994) A heteroplasmic LHON family: tissue distribution and transmission of the 11778 mutation. Am J Hum Genet 55:203–206.

Hudson G et al. (2007a) Clinical Expression of Leber Hereditary Optic Neuropathy Is Affected by the Mitochondrial DNA–Haplogroup Background. Am J Hum Genet 81:228–233.

Hudson G, Carelli V, Horvath R, Zeviani M, Smeets HJ, Chinnery PF (2007b) X-Inactivation patterns in females harboring mtDNA mutations that cause Leber hereditary optic neuropathy. Mol Vis 13:2339–2343.

Hudson G, Keers S, Man PYW, Griffiths P, Huoponen K, Savontaus M-L, Nikoskelainen E, Zeviani M, Carrara F, Horvath R, Karcagi V, Spruijt L, de Coo IFM, Smeets HJM, Chinnery PF (2005) Identification of an X-Chromosomal Locus and Haplotype Modulating the Phenotype of a Mitochondrial DNA Disorder. Am J Hum Genet 77:1086–1091.

Huoponen K, Vilkki J, Aula P, Nikoskelainen EK, Savontaus ML (1991) A new mtDNA mutation associated with Leber hereditary optic neuroretinopathy. Am J Hum Genet 48:1147–1153.

Ikonen M, Liu B, Hashimoto Y, Ma L, Lee K-W, Niikura T, Nishimoto I, Cohen P (2003) Interaction between the Alzheimer's survival peptide humanin and insulin-like growth factor-binding protein 3 regulates cell survival and apoptosis. Proc Natl Acad Sci U S A 100:13042–13047.

Imai Y, Moriwaki D (1936) A probable case of cytoplasmic inheritance in man: A critique of leber's disease. J Genet 33:163–167.

Imamura H, Huynh Nhat KP, Togawa H, Saito K, Iino R, Kato-Yamada Y, Nagai T, Noji H (2009) Visualization of ATP levels inside single living cells with fluorescence resonance energy transfer-based genetically encoded indicators. Proc Natl Acad Sci 106:15651–15656.

Iommarini L, Maresca A, Caporali L, Valentino ML, Liguori R, Giordano C, Carelli V (2012) Revisiting the issue of mitochondrial DNA content in optic mitochondriopathies. Neurology 79:1517–1519.

Ishikawa K, Funayama T, Ohde H, Inagaki Y, Mashima Y (2005) Genetic variants of TP53 and EPHX1 in Leber's hereditary optic neuropathy and their relationship to age at onset. Jpn J Ophthalmol 49:121–126.

Ishikawa KI, Saiki S, Furuya N, Yamada D, Imamichi Y, Li Y, Kawajiri S, Sasaki H, Koike M, Tsuboi Y, Hattori N (2014) P150Glued-Associated Disorders Are Caused By Activation of Intrinsic Apoptotic Pathway. PLoS One 9.

Jacobi FK, Leo-Kottler B, Mittelviefhaus K, Zrenner E, Meyer J, Pusch CM, Wissinger B (2001) Segregation patterns and heteroplasmy prevalence in Leber's hereditary optic neuropathy. Invest Ophthalmol Vis Sci 42:1208–1214.

Jahani-Asl A, Cheung ECC, Neuspiel M, MacLaurin JG, Fortin A, Park DS, McBride HM, Slack RS (2007) Mitofusin 2 protects cerebellar granule neurons against injury-induced cell death. J Biol Chem 282:23788–23798.

Jakobs S, Martini N, Schauss AC, Egner A, Westermann B, Hell SW (2003) Spatial and temporal dynamics of budding yeast mitochondria lacking the division component Fis1p. J Cell Sci 116:2005–2014.

Jalava A, Akerman K, Heikkila J (1993) Protein kinase inhibitor, staurosporine, induces a mature neuronal phenotype in SH-SY5Y human neuroblastoma cells through an alpha-, beta- , and zeta-protein kinase C-independent pathway. J Cell Physiol 155:301–12.

James AM, Wei YH, Pang CY, Murphy MP (1996) Altered mitochondrial function in fibroblasts containing MELAS or MERRF mitochondrial DNA mutations. Biochem J 318 (Pt 2):401–407.

Jandova J, Janda J, Sligh JE (2013) Cyclophilin 40 alters UVA-induced apoptosis and mitochondrial ROS generation in keratinocytes. Exp Cell Res 319:750–760.

Jankauskaitė E, Bartnik E, Kodroń A (2017) Investigating Leber's hereditary optic neuropathy: Cell models and future perspectives. Mitochondrion 32:19–26.

Jansen PH, van der Knaap MS, de Coo IF (1996) Leber's hereditary optic neuropathy with the 11 778 mtDNA mutation and white matter disease resembling multiple sclerosis: clinical, MRI and MRS findings. J Neurol Sci 135:176–180.

Ji C, Yang B, Yang Z, Tu Y, Yang Y, He L, Bi Z-G (2012) Ultra-violet B (UVB)-induced skin cell death occurs through a cyclophilin D intrinsic signaling pathway. Biochem Biophys Res Commun 425:825–829.

Ji Y, Jia X, Li S, Xiao X, Guo X, Zhang Q (2010) Evaluation of the X-linked modifier loci for Leber hereditary optic neuropathy with the G11778A mutation in Chinese. Mol Vis 16:416–424.

Jia X, Li S, Xiao X, Guo X, Zhang Q (2006) Molecular epidemiology of mtDNA mutations in 903 Chinese families suspected with Leber hereditary optic neuropathy. J Hum Genet 51:851–856.

Jiang P, Wang J, Kang Z, Li D, Zhang D (2013) Porcine JAB1 significantly enhances apoptosis induced by staurosporine. Cell Death Dis 4:e823.

Johns DR (1990) Improved molecular-genetic diagnosis of Leber's hereditary optic neuropathy. N Engl J Med 323:1488–1489.

Johns DR, Heher KL, Miller NR, Smith KH (1993) Leber's hereditary optic neuropathy. Clinical manifestations of the 14484 mutation. Arch Ophthalmol (Chicago, Ill 1960) 111:495–498.

Johns DR, Neufeld MJ, Park RD (1992) An ND-6 mitochondrial DNA mutation associated with Leber hereditary optic neuropathy. Biochem Biophys Res Commun 187:1551–1557.

Jun AS, Brown MD, Wallace DC (1994) A mitochondrial DNA mutation at nucleotide pair 14459 of the NADH dehydrogenase subunit 6 gene associated with maternally inherited Leber hereditary optic neuropathy and dystonia. Proc Natl Acad Sci U S A 91:6206–6210.

Kanai Y, Okada Y, Tanaka Y, Harada A, Terada S, Hirokawa N (2000) KIF5C, a novel neuronal kinesin enriched in motor neurons. J Neurosci 20:6374–6384.

Kaplanová V, Zeman J, Hansíková H, Černá L, Houšťková H, Mišovicová N, Houštěk J (2004) Segregation pattern and biochemical effect of the G3460A mtDNA mutation in 27 members of LHON family. J Neurol Sci 223:149–155.

Karaman MW et al. (2008) A quantitative analysis of kinase inhibitor selectivity. Nat Biotechnol 26:127–132.

Kasamatsu H, Vinograd J (1974) Replication of Circular DNA in Eukaryotic Cells. Annu Rev Biochem 43:695–719.

Kellar-Wood H, Robertson N, Govan GG, Compston DAS, Harding AE (1994) Leber's hereditary optic neuropathy mitochondrial DNA mutations in multiple sclerosis. Ann Neurol 36:109–112.

Kerrison JB, Miller NR, Hsu F, Beaty TH, Maumenee IH, Smith KH, Savino PJ, Stone EM, Newman NJ (2000) A case-control study of tobacco and alcohol consumption in Leber hereditary optic neuropathy. Am J Ophthalmol 130:803–812.

Kijima K, Numakura C, Izumino H, Umetsu K, Nezu A, Shiiki T, Ogawa M, Ishizaki Y, Kitamura T, Shozawa Y, Hayasaka K (2004) Mitochondrial GTPase mitofusin 2 mutation in Charcot?Marie?Tooth neuropathy type 2A. Hum Genet 116:23–27.

Kim I, Rodriguez-Enriquez S, Lemasters JJ (2007) Selective degradation of mitochondria by mitophagy. Arch Biochem Biophys 462:245–253.

King A, Gottlieb E, Brooks DG, Murphy MP, Dunaief JL (2004) Mitochondria-derived reactive oxygen species mediate blue light-induced death of retinal pigment epithelial cells. Photochem Photobiol 79:470–475.

King MP, Attardi G (1989) Human cells lacking mtDNA: repopulation with exogenous mitochondria by complementation. Science 246:500–503.

King MP, Koga Y, Davidson M, Schon EA (1992) Defects in mitochondrial protein synthesis and respiratory chain activity segregate with the tRNA(Leu(UUR)) mutation associated with mitochondrial myopathy, encephalopathy, lactic acidosis, and strokelike episodes. Mol Cell Biol 12:480–490.

Kirches E (2011) LHON: Mitochondrial Mutations and More. Curr Genomics 12:44–54.

Kirkman MA, Yu-Wai-Man P, Korsten A, Leonhardt M, Dimitriadis K, De Coo IF, Klopstock T, Chinnery PF (2009) Gene-environment interactions in Leber hereditary optic neuropathy. Brain 132:2317–2326.

Kissová I, Deffieu M, Manon S, Camougrand N (2004) Uth1p is involved in the autophagic degradation of mitochondria. J Biol Chem 279:39068–39074.

Kitada T, Asakawa S, Hattori N, Matsumine H, Yamamura Y, Minoshima S, Yokochi M, Mizuno Y, Shimizu N (1998) Mutations in the parkin gene cause autosomal recessive juvenile parkinsonism. Nature 392:605–608.

Klivenyi P, Karg E, Rozsa C, Horvath R, Komoly S, Nemeth I, Turi S, Vecsei L (2001) alpha-Tocopherol/lipid ratio in blood is decreased in patients with Leber's hereditary optic neuropathy and asymptomatic carriers of the 11778 mtDNA mutation. J Neurol Neurosurg Psychiatry 70:359–362.

Knott AB, Perkins G, Schwarzenbacher R, Bossy-Wetzel E (2008) Mitochondrial fragmentation in neurodegeneration. Nat Rev Neurosci 9:505–518.

Kohno T, Ninomiya T, Kikuchi S, Konno T, Kojima T (2015) Staurosporine Induces Formation of Two Types of Extra-Long Cell Protrusions: Actin-Based Filaments and Microtubule-Based Shafts. Mol Pharmacol 5:815–824.

Koilkonda RD, Guy J (2011) Leber's Hereditary Optic Neuropathy-Gene Therapy: From Benchtop to Bedside. J Ophthalmol 2011:179412.

Koirala S, Guo Q, Kalia R, Bui HT, Eckert DM, Frost A, Shaw JM (2013) Interchangeable adaptors regulate mitochondrial dynamin assembly for membrane scission. Proc Natl Acad Sci 110:E1342–E1351.

Kong J, Xu Z (1998) Massive mitochondrial degeneration in motor neurons triggers the onset of amyotrophic lateral sclerosis in mice expressing a mutant SOD1. J Neurosci 18:3241–3250.

Koopman WJH, Distelmaier F, Smeitink JAM, Willems PHGM (2013) OXPHOS mutations and neurodegeneration. EMBO J 32:9–29.

Koshiba T, Detmer SA, Kaiser JT, Chen H, McCaffery JM, Chan DC (2004) Structural basis of mitochondrial tethering by mitofusin complexes. Science 305:858–862.

Krishnamoorthy RR, Clark AF, Daudt D, Vishwanatha JK, Yorio T (2013) A forensic path to RGC-5 cell line identification: lessons learned. Invest Ophthalmol Vis Sci 54:5712–5719.

Kruman I, Guo Q, Mattson MP (1998) Calcium and reactive oxygen species mediate staurosporine- induced mitochondrial dysfunction and apoptosis in PC12 cells. J Neurosci Res 51:293–308.

La Morgia C, Ross-Cisneros FN, Sadun AA, Hannibal J, Munarini A, Mantovani V, Barboni P, Cantalupo G, Tozer KR, Sancisi E, Salomao SR, Moraes MN, Moraes-Filho MN, Heegaard S, Milea D, Kjer P, Montagna P, Carelli V (2010) Melanopsin retinal ganglion cells are resistant to neurodegeneration in mitochondrial optic neuropathies. Brain 133:2426–2438.

Labbé K, Murley A, Nunnari J (2014) Determinants and Functions of Mitochondrial Behavior. Annu Rev Cell Dev Biol 30:357–391.

Lagerström-Fermér M, Olsson C, Forsgren L, Syvänen AC (2001) Heteroplasmy of the human mtDNA control region remains constant during life. Am J Hum Genet 68:1299–1301.

Lam BL, Feuer WJ, Abukhalil F, Porciatti V, Hauswirth WW, Guy J (2010) Leber hereditary optic neuropathy gene therapy clinical trial recruitment: year 1. Arch Ophthalmol (Chicago, Ill 1960) 128:1129–1135.

Langford GM (1995) Actin- and microtubule-dependent organelle motors: interrelationships between the two motility systems. Curr Opin Cell Biol 7:82–88.

Larsson NG, Holme E, Kristiansson B, Oldfors A, Tulinius M (1990) Progressive increase of the mutated mitochondrial DNA fraction in Kearns-Sayre syndrome. Pediatr Res 28:131–136.

Lawson VH, Graham B V, Flanigan KM (2005) Clinical and electrophysiologic features of CMT2A with mutations in the mitofusin 2 gene. Neurology 65:197–204.

Leber T (1871) Ueber hereditäre und congenital-angelegte Sehnervenleiden. Albr von Græfe's Arch für Ophthalmol 17:249–291.

Lee C, Kim KH, Cohen P (2016) MOTS-c: A novel mitochondrial-derived peptide regulating muscle and fat metabolism. Free Radic Biol Med 100:182–187.

Lee C, Zeng J, Drew BG, Sallam T, Martin-Montalvo A, Wan J, Kim S-J, Mehta H, Hevener AL, de Cabo R, Cohen P (2015) The mitochondrial-derived peptide MOTS-c promotes metabolic homeostasis and reduces obesity and insulin resistance. Cell Metab 21:443–454.

Lee HJ, Khoshaghideh F, Lee S, Lee SJ (2006) Impairment of microtubule-dependent trafficking by overexpression of ??-synuclein. Eur J Neurosci 24:3153–3162.

Lee W-CM, Yoshihara M, Littleton JT (2004) Cytoplasmic aggregates trap polyglutamine-containing proteins and block axonal transport in a Drosophila model of Huntington's disease. Proc Natl Acad Sci 101:3224–3229.

Lemasters JJ (2005) Selective Mitochondrial Autophagy, or Mitophagy, as a Targeted Defense Against Oxidative Stress, Mitochondrial Dysfunction, and Aging. Rejuvenation Res 8:3–5.

Lenaers G, Hamel C, Delettre C, Amati-Bonneau P, Procaccio V, Bonneau D, Reynier P, Milea D (2012) Dominant optic atrophy. Orphanet J Rare Dis 7:46.

Levy JR, Sumner CJ, Caviston JP, Tokito MK, Ranganathan S, Ligon L a., Wallace KE, LaMonte BH, Harmison GG, Puls I, Fischbeck KH, Holzbaur ELF (2006) A motor neuron disease-associated mutation in p150Glued perturbs dynactin function and induces protein aggregation. J Cell Biol 172:733–745.

Li H, Li SH, Yu ZX, Shelbourne P, Li XJ (2001) Huntingtin aggregate-associated axonal degeneration is an early pathological event in Huntington's disease mice. J Neurosci 21:8473–8481.

Li Z, Okamoto K-I, Hayashi Y, Sheng M (2004) The Importance of Dendritic Mitochondria in the Morphogenesis and Plasticity of Spines and Synapses. Cell 119:873–887.

Lill R, Kispal G (2000) Maturation of cellular Fe–S proteins: an essential function of mitochondria. Trends Biochem Sci 25:352–356.

Lin CS, Sharpley MS, Fan W, Waymire KG, Sadun a. a., Carelli V, Ross-Cisneros FN, Baciu P, Sung E, McManus MJ, Pan BX, Gil DW, MacGregor GR, Wallace DC (2012) Mouse mtDNA mutant model of Leber hereditary optic neuropathy. Proc Natl Acad Sci 109:20065–20070.

Lodi R, Carelli V, Cortelli P, Iotti S, Valentino ML, Barboni P, Pallotti F, Montagna P, Barbiroli B (2002) Phosphorus MR spectroscopy shows a tissue specific in vivo distribution of biochemical expression of the G3460A mutation in Leber's hereditary optic neuropathy. J Neurol Neurosurg Psychiatry 72:805–807.

Lodi R, Montagna P, Cortelli P, Iotti S, Cevoli S, Carelli V, Barbiroli B (2000) `Secondary' 4216/ND1 and 13708/ND5 Leber's hereditary optic neuropathy mitochondrial DNA mutations do not further impair in vivo mitochondrial oxidative metabolism when associated with the 11778/ND4 mitochondrial DNA mutation. Brain 123:1896–1902.

Losón OC, Song Z, Chen H, Chan DC (2013) Fis1, Mff, MiD49, and MiD51 mediate Drp1 recruitment in mitochondrial fission Newmeyer DD, ed. Mol Biol Cell 24:659–667.

Lundsgaard R (1944) Leber's disease; a genealogic, genetic and clinical study of 101 cases of retrobulbar optic neuritis in 20 Danish families. Gyldendalske Boghandel, Nordisk Forlag.

Mackey D, Howell N (1992) A variant of Leber hereditary optic neuropathy characterized by recovery of vision and by an unusual mitochondrial genetic etiology. Am J Hum Genet 51:1218–1228.

Mackey DA, Fingert JH, Luzhansky JZ, McCluskey PJ, Howell N, Hall AJH, Pierce AB, Hoy JF (2003) Leber's hereditary optic neuropathy triggered by antiretroviral therapy for human immunodeficiency virus. Eye 17:312–317.

Mackey DA, Oostra RJ, Rosenberg T, Nikoskelainen E, Bronte-Stewart J, Poulton J, Harding AE, Govan G, Bolhuis PA, Norby S (1996) Primary pathogenic mtDNA mutations in multigeneration pedigrees with Leber hereditary optic neuropathy. Am J Hum Genet 59:481–485.

Macmillan C, Kirkham T, Fu K, Allison V, Andermann E, Chitayat D, Fortier D, Gans M, Hare H, Quercia N, Zackon D, Shoubridge EA (1998) Pedigree analysis of French Canadian families with T14484C Leber's hereditary optic neuropathy. Neurology 50:417–422.

Man PYW, Turnbull DM, Chinnery PF (2002) Leber hereditary optic neuropathy.

Manczak M, Calkins MJ, Reddy PH (2011) Impaired mitochondrial dynamics and abnormal interaction of amyloid beta with mitochondrial protein Drp1 in neurons from patients with Alzheimer's disease: implications for neuronal damage. Hum Mol Genet 20:2495–2509.

Manczak M, Reddy PH (2012) Abnormal interaction of VDAC1 with amyloid beta and phosphorylated tau causes mitochondrial dysfunction in Alzheimer's disease. Hum Mol Genet 21:5131–5146.

Martin M, Iyadurai SJ, Gassman A, Gindhart JG, Hays TS, Saxton WM (1999) Cytoplasmic dynein, the dynactin complex, and kinesin are interdependent and essential for fast axonal transport. Mol Biol Cell 10:3717–3728.

Mashima Y, Kigasawa K, Hasegawa H, Tani M, Oguchi Y (1996) High incidence of pre-excitation syndrome in Japanese families with Leber's hereditary optic neuropathy. Clin Genet 50:535–537.

Mashima Y, Kimura I, Yamamoto Y, Ohde H, Ohtake Y, Tanino T, Tomita G, Oguchi Y (2003) Optic disc excavation in the atrophic stage of Leber's hereditary optic neuropathy: comparison with normal tension glaucoma. Graefe's Arch Clin Exp Ophthalmol 241:75–80.

Mashima Y, Yamada K, Wakakura M, Kigasawa K, Kudoh J, Shimizu N, Oguchi Y (1998) Spectrum of pathogenic mitochondrial DNA mutations and clinical features in Japanese families with Leber's hereditary optic neuropathy. Curr Eye Res 17:403–408.

Matsuda N, Sato S, Shiba K, Okatsu K, Saisho K, Gautier CA, Sou Y, Saiki S, Kawajiri S, Sato F, Kimura M, Komatsu M, Hattori N, Tanaka K (2010) PINK1 stabilized by mitochondrial depolarization recruits Parkin to damaged mitochondria and activates latent Parkin for mitophagy. J Cell Biol 189:211–221.

McBride HM, Neuspiel M, Wasiak S (2006) Mitochondria: More Than Just a Powerhouse. Curr Biol 16:551–560.

McKay ND, Robinson B, Brodie R, Rooke-Allen N (1983) Glucose transport and metabolism in cultured human skin fibroblasts. Biochim Biophys Acta - Mol Cell Res 762:198–204.

Meeusen S, DeVay R, Block J, Cassidy-Stone A, Wayson S, McCaffery JM, Nunnari J (2006) Mitochondrial Inner-Membrane Fusion and Crista Maintenance Requires the Dynamin-Related GTPase Mgm1. Cell 127:383–395.

Meijer AJ, Lamers WH, Chamuleau RAFM (1990) Nitrogen Metabolism and Ornithine Cycle Function. Physiol Rev 70.

Meijering E, Jacob M, Sarria J-CF, Steiner P, Hirling H, Unser M (2004) Design and validation of a tool for neurite tracing and analysis in fluorescence microscopy images. Cytometry 58A:167–176.

Meire FM, Van Coster R, Cochaux P, Obermaier-Kusser B, Candaele C, Martin JJ (1995) Neurological disorders in members of families with Leber's hereditary optic neuropathy (LHON) caused by different mitochondrial mutations. Ophthalmic Genet 16:119–126.

Melser S, Chatelain EH, Lavie J, Mahfouf W, Jose C, Obre E, Goorden S, Priault M, Elgersma Y, Rezvani HR, Rossignol R, Bénard G (2013) Rheb regulates mitophagy induced by mitochondrial energetic status. Cell Metab 17:719–730.

Meng YX, Wilson GW, Avery MC, Varden CH, Balczon R (1997) Suppression of the Expression of a Pancreatic β-Cell Form of the Kinesin Heavy Chain by Antisense Oligonucleotides Inhibits Insulin Secretion from Primary Cultures of Mouse β-Cells [1]. Endocrinology 138:1979–1987.

Michaels GS, Hauswirth WW, Laipis PJ (1982) Mitochondrial DNA copy number in bovine oocytes and somatic cells. Dev Biol 94:246–251.

Miller WL (1995) Mitochondrial specificity of the early steps in steroidogenesis. J Steroid Biochem Mol Biol 55:607–616.

Minckler DS, McLean IW, Tso MO (1976) Distribution of axonal and glial elements in the rhesus optic nerve head studied by electron microscopy. Am J Ophthalmol 82:179–187.

Mishra P, Carelli V, Manfredi G, Chan DC (2014) Proteolytic Cleavage of Opa1 Stimulates Mitochondrial Inner Membrane Fusion and Couples Fusion to Oxidative Phosphorylation. Cell Metab 19:630–641.

Mishra P, Chan DC (2014) Mitochondrial dynamics and inheritance during cell division, development and disease. Nat Rev Mol Cell Biol 15:634–646.

Mishra P, Chan DC (2016) Metabolic regulation of mitochondrial dynamics. J Cell Biol 212:379–387.

Misko A, Jiang S, Wegorzewska I, Milbrandt J, Baloh RH (2010) Mitofusin 2 is necessary for transport of axonal mitochondria and interacts with the Miro/Milton complex. J Neurosci 30:4232–4240.

Mita S, Schmidt B, Schon EA, DiMauro S, Bonilla E (1989) Detection of "deleted" mitochondrial genomes in cytochrome-c oxidase-deficient muscle fibers of a patient with Kearns-Sayre syndrome. Proc Natl Acad Sci 86.

Mitra K, Wunder C, Roysam B, Lin G, Lippincott-Schwartz J (2009) A hyperfused mitochondrial state achieved at G1-S regulates cyclin E buildup and entry into S phase. Proc Natl Acad Sci U S A 106:11960–11965.

Moraes CT et al. (1989) Mitochondrial DNA Deletions in Progressive External Ophthalmoplegia and Kearns-Sayre Syndrome. N Engl J Med 320:1293–1299.

Moraes CT, Sciacco M, Ricci E, Tengan CH, Hao H, Bonilla E, Schon EA, DiMauro S (1995) Phenotype-genotype correlations in skeletal muscle of patients with mtDNA deletions. Muscle Nerve 18:S150–S153.

Morioka H, Ishihara M, Shibai H, Suzuki T (1985) Staurosporine-induced Differentiation in a Human Neuroblastoma Cell Line, NB-1. Agric Biol Chem 49:1959–1963.

Morris RL, Hollenbeck PJ (1993) The regulation of bidirectional mitochondrial transport is coordinated with axonal outgrowth. J Cell Sci 104 (Pt 3):917–927.

Moura ALA, Nagy B V., La Morgia C, Barboni P, Oliveira AGF, Salomão SR, Berezovsky A, de Moraes-Filho MN, Chicani CF, Belfort R, Carelli V, Sadun AA, Hood DC, Ventura DF (2013) The Pupil Light Reflex in Leber's Hereditary Optic Neuropathy: Evidence for Preservation of Melanopsin-Expressing Retinal Ganglion Cells. Investig Opthalmology Vis Sci 54:4471.

Murmann T, Carrillo-García C, Veit N, Courts C, Glassmann A, Janzen V, Madea B, Reinartz M, Harzen A, Nowak M, Perner S, Winter J, Probstmeier R (2014) Staurosporine and Extracellular Matrix Proteins Mediate the Conversion of Small Cell Lung Carcinoma Cells into a Neuron-Like Phenotype Kalinichenko V V., ed. PLoS One 9:e86910.

Müsch A (2004) Microtubule Organization and Function in Epithelial Cells. Traffic 5:1–9.

Nedergaard J, Cannon B (1992) Chapter 17 The uncoupling protein thermogenin and mitochondrial thermogenesis. New Compr Biochem 23:385–420.

Neuspiel M, Zunino R, Gangaraju S, Rippstein P, McBride H (2005) Activated mitofusin 2 signals mitochondrial fusion, interferes with Bax activation, and reduces susceptibility to radical induced depolarization. J Biol Chem 280:25060–25070.

Newman NJ (2005) Hereditary Optic Neuropathies: From the Mitochondria to the Optic Nerve. Am J Ophthalmol 140:517.e1-517.e9.

Newman NJ, Biousse V, Newman SA, Bhatti MT, Hamilton SR, Farris BK, Lesser RL, Turbin RE (2006) Progression of Visual Field Defects in Leber Hereditary Optic Neuropathy: Experience of the LHON Treatment Trial. Am J Ophthalmol 141:1061–1067.e1.

Newman NJ, Lott MT, Wallace DC (1991) The clinical characteristics of pedigrees of Leber's hereditary optic neuropathy with the 11778 mutation. Am J Ophthalmol 111:750–762.

Nightingale H, Pfeffer G, Bargiela D, Horvath R, Chinnery PF (2016) Emerging therapies for mitochondrial disorders. Brain 139:1633–1648.

Nijtmans LGJ, Henderson NS, Attardi G, Holt IJ (2001) Impaired ATP Synthase Assembly Associated with a Mutation in the Human ATP Synthase Subunit 6 Gene. J Biol Chem 276:6755–6762.

Nikoskelainen EK (1994) Clinical picture of LHON. Clin Neurosci 2:115–120.

Nikoskelainen EK, Marttila RJ, Huoponen K, Juvonen V, Lamminen T, Sonninen P, Savontaus ML (1995) Leber's "plus": neurological abnormalities in patients with Leber's hereditary optic neuropathy. J Neurol Neurosurg Psychiatry 59:160–164.

Nishioka T, Soemantri A, Ishida T (2004) mtDNA/nDNA ratio in 14484 LHON mitochondrial mutation carriers. J Hum Genet 49:701–705.

Ochs S, Hollingsworth D (1971) DEPENDENCE OF FAST AXOPLASMIC TRANSPORT IN NERVE ON OXIDATIVE METABOLISM. J Neurochem 18:107–114.

Oexle K, Zwirner A (1997) Advanced telomere shortening in respiratory chain disorders. Hum Mol Genet 6:905–908.

Oiwa K, Sakakibara H (2005) Recent progress in dynein structure and mechanism. Curr Opin Cell Biol 17:98–103.

Ojala D, Montoya J, Attardi G (1981) tRNA punctuation model of RNA processing in human mitochondria. Nature 290:470–474.

Olichon A, Baricault L, Gas N, Guillou E, Valette A, Belenguer P, Lenaers G (2003) Loss of OPA1 perturbates the mitochondrial inner membrane structure and integrity, leading to cytochrome c release and apoptosis. J Biol Chem 278:7743–7746.

Olichon A, Landes T, Arnauné-Pelloquin L, Emorine LJ, Mils V, Guichet A, Delettre C, Hamel C, Amati-Bonneau P, Bonneau D, Reynier P, Lenaers G, Belenguer P (2007) Effects of OPA1 mutations on mitochondrial morphology and apoptosis: Relevance to ADOA pathogenesis. J Cell Physiol 211:423–430.

Olsen NK, Hansen AW, Nørby S, Edal AL, Jørgensen JR, Rosenberg T (1995) Leber's hereditary optic neuropathy associated with a disorder indistinguishable from multiple sclerosis in a male harbouring the mitochondrial DNA 11778 mutation. Acta Neurol Scand 91:326–329.

Ong S-B, Hausenloy DJ (2010) Mitochondrial morphology and cardiovascular disease. Cardiovasc Res 88:16–29.

Oostra RJ, Bolhuis PA, Wijburg FA, Zorn-Ende G, Bleeker-Wagemakers EM (1994) Leber's hereditary optic neuropathy: correlations between mitochondrial genotype and visual outcome. J Med Genet 31:280–286.

Oostra RJ, Kemp S, Bolhuis PA, Bleeker-Wagemakers EM (1996) No evidence for "skewed" inactivation of the X-chromosome as cause of Leber's hereditary optic neuropathy in female carriers. Hum Genet 97:500–505.

Osawa S, Jukes TH, Watanabe K, Muto A (1992) Recent evidence for evolution of the genetic code. Microbiol Rev 56:229–264.

Otera H, Wang C, Cleland MM, Setoguchi K, Yokota S, Youle RJ, Mihara K (2010) Mff is an essential factor for mitochondrial recruitment of Drp1 during mitochondrial fission in mammalian cells. J Cell Biol 191:1141–1158.

Pagani L, Eckert A (2011) Amyloid-Beta interaction with mitochondria. Int J Alzheimers Dis 2011:925050.

Palmer CS, Osellame LD, Laine D, Koutsopoulos OS, Frazier AE, Ryan MT (2011) MiD49 and MiD51, new components of the mitochondrial fission machinery. EMBO Rep 12:565–573.

Pan BX, Ross-Cisneros FN, Carelli V, Rue KS, Salomao SR, Moraes-Filho MN, Moraes MN, Berezovsky A, Belfort R, Sadun AA (2012) Mathematically Modeling the Involvement of Axons in Leber's Hereditary Optic Neuropathy. Investig Opthalmology Vis Sci 53:7608.

Pegoraro E, Carelli V, Zeviani M, Cortelli P, Montagna P, Barboni P, Angelini C, Hoffman EP (1996) X-inactivation patterns in female Leber's hereditary optic neuropathy patients do not support a strong X-linked determinant. Am J Med Genet 61:356–362.

Pezzi PP, De Negri AM, Sadun F, Carelli V, Leuzzi V (1998) Childhood Leber's hereditary optic neuropathy (ND1/3460) with visual recovery. Pediatr Neurol 19:308–312.

Pfeffer G, Burke A, Yu-Wai-Man P, Compston DAS, Chinnery PF (2013) Clinical features of MS associated with Leber hereditary optic neuropathy mtDNA mutations. Neurology 81:2073–2081.

Phasukkijwatana N, Kunhapan B, Stankovich J, Chuenkongkaew WL, Thomson R, Thornton T, Bahlo M, Mushiroda T, Nakamura Y, Mahasirimongkol S, Tun AW, Srisawat C, Limwongse C, Peerapittayamongkol C, Sura T, Suthammarak W, Lertrit P (2010) Genome-wide linkage scan and association study of PARL to the expression of LHON families in Thailand. Hum Genet 128:39–49.

Pilling AD, Horiuchi D, Lively CM, Saxton WM (2006) Kinesin-1 and Dynein Are the Primary Motors for Fast Transport of Mitochondria in Drosophila Motor Axons. Mol Biol Cell 17:2057–2068.

Ponka P (1999) Cell Biology of Heme. Am J Med Sci 318:241–256.

Portugal J, Waring MJ (1988) Assignment of DNA binding sites for 4',6-diamidine-2-phenylindole and bisbenzimide (Hoechst 33258). A comparative footprinting study. Biochim Biophys Acta 949:158–168.

Puomila A, Hämäläinen P, Kivioja S, Savontaus M-L, Koivumäki S, Huoponen K, Nikoskelainen E (2007) Epidemiology and penetrance of Leber hereditary optic neuropathy in Finland. Eur J Hum Genet 15:1079–1089.

Puomila A, Viitanen T, Savontaus ML, Nikoskelainen E, Huoponen K (2002) Segregation of the ND4/11778 and the ND1/3460 mutations in four heteroplasmic LHON families. J Neurol Sci 205:41–45.

Pyakurel A, Savoia C, Hess D, Scorrano L (2015) Extracellular regulated kinase phosphorylates mitofusin 1 to control mitochondrial morphology and apoptosis. Mol Cell 58:244–254.

Qi X, Lewin AS, Hauswirth WW, Guy J (2003a) Optic Neuropathy Induced by Reductions in Mitochondrial Superoxide Dismutase. Investig Opthalmology Vis Sci 44:1088.

Qi X, Lewin AS, Hauswirth WW, Guy J (2003b) Suppression of complex I gene expression induces optic neuropathy. Ann Neurol 53:198–205.

Qi X, Sun L, Hauswirth WW, Lewin AS, Guy J (2007) Use of Mitochondrial Antioxidant Defenses for Rescue of Cells With a Leber Hereditary Optic Neuropathy–Causing Mutation. Arch Ophthalmol 125:268.

Raha S, Robinson BH (2001) Mitochondria, oxygen free radicals, and apoptosis. Am J Med Genet 106:62–70.

Rambold AS, Kostelecky B, Elia N, Lippincott-Schwartz J (2011) Tubular network formation protects mitochondria from autophagosomal degradation during nutrient starvation. Proc Natl Acad Sci U S A 108:10190–10195.

Rapp LM, Tolman BL, Dhindsa HS (1990) Separate mechanisms for retinal damage by ultraviolet-A and mid-visible light. Invest Ophthalmol Vis Sci 31:1186–1190.

Rasouly D, Rahamim E, Ringel I, Ginzburg I, Muarakata C, Matsuda Y, Lazarovici P (1994) Neurites induced by staurosporine in PC12 cells are resistant to colchicine and express high levels of tau proteins. Mol Pharmacol 45:29–35.

Ravikanth M, Soujanya P, Manjunath K, Saraswathi TR, Ramachandran CR (2011) Heterogenecity of fibroblasts. J Oral Maxillofac Pathol 15:247–250.

Reddy PH, Tripathi R, Troung Q, Tirumala K, Reddy TP, Anekonda V, Shirendeb UP, Calkins MJ, Reddy AP, Mao P, Manczak M (2012) Abnormal mitochondrial dynamics and synaptic degeneration as early events in Alzheimer's disease: implications to mitochondria-targeted antioxidant therapeutics. Biochim Biophys Acta 1822:639–649.

Reilly MM, Murphy SM, Laurá M (2011) Charcot-Marie-Tooth disease. J Peripher Nerv Syst 16:1–14.

Richner M, Victor MB, Liu Y, Abernathy D, Yoo AS (2015) MicroRNA-based conversion of human fibroblasts into striatal medium spiny neurons. Nat Protoc 10:1543–1555.

Rintoul GL, Filiano AJ, Brocard JB, Kress GJ, Reynolds IJ (2003) Glutamate decreases mitochondrial size and movement in primary forebrain neurons. J Neurosci 23:7881–7888.

Rintoul GL, Reynolds IJ (2010) Mitochondrial trafficking and morphology in neuronal injury. Biochim Biophys Acta - Mol Basis Dis 1802:143–150.

Riordan-Eva P, Harding AE (1995) Leber's hereditary optic neuropathy: the clinical relevance of different mitochondrial DNA mutations. J Med Genet 32:81–87.

Riordan-Eva P, Sanders MD, Govan GG, Sweeney MG, Costa J Da, Harding AE (1995) The clinical features of Leber's hereditary optic neuropathy defined by the presence of a pathogenic mitochondrial DNA mutation. Brain 118:319–337.

Rossignol R, Gilkerson R, Aggeler R, Yamagata K, Remigton SJ, Capaldi RA (2004) Energy substrate modulates mitochondrial structures and oxidative capacityin cancer cells. Cancer Res 64:985–993.

Rothe G, Valet G (1990) Flow cytometric analysis of respiratory burst activity in phagocytes with hydroethidine and 2',7'-dichlorofluorescin. J Leukoc Biol 47:440–448.

Rüegg UT, Burgess GM, R??egg UT, Gillian B (1989) Staurosporine, K-252 and UCN-01: potent but nonspecific inhibitors of protein kinases. Trends Pharmacol Sci 10:218–220.

Ryan KR, Jensen RE (1995) Protein translocation across mitochondrial membranes: What a long, strange trip it is. Cell 83:517–519.

Sabri MI, Ochs S (1972) RELATION OF ATP AND CREATINE PHOSPHATE TO FAST AXOPLASMIC TRANSPORT IN MAMMALIAN NERVE. J Neurochem 19:2821–2828.

Sadun A, Kashima Y, Wurdeman A, Dao J, Heller K SJ (1994) Morphological findings in the visual system in a case of Leber's hereditary optic neuropathy. Clin Neurosci 2:165–172.

Sadun A a., Morgia C La, Carelli V (2011) Leber's Hereditary Optic Neuropathy. Curr Treat Options Neurol 13:109–117.

Sadun AA, Carelli V, Salomao SR, Berezovsky A, Quiros PA, Sadun F, DeNegri AM, Andrade R, Moraes M, Passos A, Kjaer P, Pereira J, Valentino ML, Schein S, Belfort R (2003) Extensive investigation of a large Brazilian pedigree of 11778/haplogroup J Leber hereditary optic neuropathy. Am J Ophthalmol 136:231–238.

Sadun AA, Win PH, Ross-Cisneros FN, Walker SO, Carelli V (2000) Leber's hereditary optic neuropathy differentially affects smaller axons in the optic nerve. Trans Am Ophthalmol Soc 98:223-32; discussion 232-5.

Salomão SR, Berezovsky A, Andrade RE, Belfort R, Carelli V, Sadun AA (2004) Visual electrophysiologic findings in patients from an extensive Brazilian family with Leber's hereditary optic neuropathy. Doc Ophthalmol 108:147–155.

Santorelli FM, Shanske S, Jain KD, Tick D, Schon EA, DiMauro S (1994) A T-->C mutation at nt 8993 of mitochondrial DNA in a child with Leigh syndrome. Neurology 44:972–974.

Sasaki S, Iwata M (1996) Impairment of fast axonal transport in the proximal axons of anterior horn neurons in amyotrophic lateral sclerosis. Neurology 47:535–540.

Sasaki S, Iwata M (2007) Mitochondrial alterations in the spinal cord of patients with sporadic amyotrophic lateral sclerosis. J Neuropathol Exp Neurol 66:10–16.

Schoeler S, Winkler-Stuck K, Szibor R, Haroon MF, Gellerich FN, Chamaon K, Mawrin C, Kirches E (2007) Glutathione depletion in antioxidant defense of differentiated NT2-LHON cybrids. Neurobiol Dis 25:536–544.

Schon EA (2000) Mitochondrial genetics and disease. Trends Biochem Sci 25:555–560.

Schon EA, DiMauro S, Hirano M (2012) Human mitochondrial DNA: roles of inherited and somatic mutations. Nat Rev Genet 13:878–890.

Schon EA, Przedborski S (2011) Mitochondria: The Next (Neurode)Generation. Neuron 70:1033–1053.

Schousboe A, Bak LK, Waagepetersen HS (2013) Astrocytic Control of Biosynthesis and Turnover of the Neurotransmitters Glutamate and GABA. Front Endocrinol (Lausanne) 4:102.

Schwarz TL (2013) Mitochondrial trafficking in neurons. Cold Spring Harb Perspect Med 3:1–16.

Schweers RL, Zhang J, Randall MS, Loyd MR, Li W, Dorsey FC, Kundu M, Opferman JT, Cleveland JL, Miller JL, Ney PA (2007) NIX is required for programmed mitochondrial clearance during reticulocyte maturation. Proc Natl Acad Sci U S A 104:19500–19505.

Seedorff T (1985) The inheritance of Leber's disease. Acta Ophthalmol 63:135–145.

Seglen PO, Berg TO, Blankson H, Fengsrud M, Holen I, Strømhaug PE (1996) Structural aspects of autophagy. Adv Exp Med Biol 389:103–111.

Seiler MJ, Liu OL, Cooper NG, Callahan TL, Petry HM, Aramant RB (2000) Selective photoreceptor damage in albino rats using continuous blue light. A protocol useful for retinal degeneration and transplantation research. Graefes Arch Clin Exp Ophthalmol 238:599–607.

Seko Y, Pang J, Tokoro T, Ichinose S, Mochizuki M (2001) Blue light-induced apoptosis in cultured retinal pigment epithelium cells of the rat. Graefes Arch Clin Exp Ophthalmol 239:47–52.

Seog D-H, Lee D-H, Lee S-K (2004) Molecular motor proteins of the kinesin superfamily proteins (KIFs): structure, cargo and disease. J Korean Med Sci 19:1–7.

Shankar SP, Fingert JH, Carelli V, Valentino ML, King TM, Daiger SP, Salomao SR, Berezovsky A, Belfort R, Braun TA, Sheffield VC, Sadun AA, Stone EM (2008) Evidence for a Novel X-Linked Modifier Locus for Leber Hereditary Optic Neuropathy. Ophthalmic Genet 29:17–24.

Shea TB, Beermann ML (1991) Staurosporine-induced morphological differentiation of human neuroblastoma cells. Cell Biol Int Rep 15:161–168.

Sheng Z-H, Cai Q (2012) Mitochondrial transport in neurons: impact on synaptic homeostasis and neurodegeneration. Nat Rev Neurosci 13:77–93.

Shoffner JM, Lott MT, Lezza AMS, Seibel P, Ballinger SW, Wallace DC (1990) Myoclonic epilepsy and ragged-red fiber disease (MERRF) is associated with a mitochondrial DNA tRNALys mutation. Cell 61:931–937.

Shoffner JM, Lott MT, Voljavec AS, Soueidan SA, Costigan DA, Wallace DC (1989) Spontaneous Kearns-Sayre/chronic external ophthalmoplegia plus syndrome associated with a mitochondrial DNA deletion: a slip-replication model and metabolic therapy. Proc Natl Acad Sci U S A 86:7952–7956.

Shokolenko IN, Alexeyev MF (2015) Mitochondrial DNA: A disposable genome? Biochim Biophys Acta - Mol Basis Dis 1852:1805–1809.

Shuster RC, Rubenstein AJ, Wallace DC (1988) Mitochondrial DNA in anucleate human blood cells. Biochem Biophys Res Commun 155:1360–1365.

Silvestri G, Moraes CT, Shanske S, Oh SJ, DiMauro S (1992) A new mtDNA mutation in the tRNA(Lys) gene associated with myoclonic epilepsy and ragged-red fibers (MERRF). Am J Hum Genet 51:1213–1217.

Skulachev VP (2001) Mitochondrial filaments and clusters as intracellular power-transmitting cables. Trends Biochem Sci 26:23–29.

Smirnova E, Griparic L, Shurland DL, van der Bliek AM (2001) Dynamin-related protein Drp1 is required for mitochondrial division in mammalian cells. Mol Biol Cell 12:2245–2256.

Smith BT, Belani S, Ho AC (2005) Ultraviolet and near-blue light effects on the eye. Int Ophthalmol Clin 45:107–115.

Smith KH, Johns DR, Heher KL, Miller NR (1993) Heteroplasmy in Leber's hereditary optic neuropathy. Arch Ophthalmol (Chicago, Ill 1960) 111:1486–1490.

Smith PR, Cooper JM, Govan GG, Riordan-Eva P, Harding AE, Schapira AH (1995) Antibodies to human optic nerve in Leber's hereditary optic neuropathy. J Neurol Sci 130:134–138.

Song W-HH, Ballard JWO, Yi Y-JJ, Sutovsky P (2014) Regulation of mitochondrial genome inheritance by autophagy and ubiquitin-proteasome system: Implications for health, fitness, and fertility. Biomed Res Int 2014:1–16.

Song Z, Ghochani M, McCaffery JM, Frey TG, Chan DC (2009) Mitofusins and OPA1 mediate sequential steps in mitochondrial membrane fusion. Mol Biol Cell 20:3525–3532.

Spruijt L, Kolbach DN, de Coo RF, Plomp AS, Bauer NJ, Smeets HJ, de Die-Smulders CEM (2006) Influence of Mutation Type on Clinical Expression of Leber Hereditary Optic Neuropathy. Am J Ophthalmol 141:676–676.e8.

Stiburek L, Cesnekova J, Kostkova O, Fornuskova D, Vinsova K, Wenchich L, Houstek J, Zeman J (2012) YME1L controls the accumulation of respiratory chain subunits and is required for apoptotic resistance, cristae morphogenesis, and cell proliferation Fox TD, ed. Mol Biol Cell 23:1010–1023.

Stokin GB, Lillo C, Falzone TL, Brusch RG, Rockenstein E, Mount SL, Raman R, Davies P, Masliah E, Williams DS, Goldstein LSB (2005) Axonopathy and Transport Deficits Early in the Pathogenesis of Alzheimer's Disease. Science (80-) 307:1282–1288.

Stone EM, Newman NJ, Miller NR, Johns DR, Lott MT, Wallace DC (1992) Visual recovery in patients with Leber's hereditary optic neuropathy and the 11778 mutation. J Clin Neuroophthalmol 12:10–14.

Stowers RS, Megeath LJ, Górska-Andrzejak J, Meinertzhagen IA, Schwarz TL (2002) Axonal transport of mitochondria to synapses depends on milton, a novel Drosophila protein. Neuron 36:1063–1077.

Sweeney MG, Davis MB, Lashwood A, Brockington M, Toscano A, Harding AE (1992) Evidence against an X-linked locus close to DXS7 determining visual loss susceptibility in British and Italian families with Leber hereditary optic neuropathy. Am J Hum Genet 51:741–748.

Taanman J-W (1999) The mitochondrial genome: structure, transcription, translation and replication. Biochim Biophys Acta - Bioenerg 1410:103–123.

Tal R, Winter G, Ecker N, Klionsky DJ, Abeliovich H (2007) Aup1p, a Yeast Mitochondrial Protein Phosphatase Homolog, Is Required for Efficient Stationary Phase Mitophagy and Cell Survival. J Biol Chem 282:5617–5624.

Tanaka A, Cleland MM, Xu S, Narendra DP, Suen D-F, Karbowski M, Youle RJ (2010) Proteasome and p97 mediate mitophagy and degradation of mitofusins induced by Parkin. J Cell Biol 191:1367–1380.

Tanaka Y, Kanai Y, Okada Y, Nonaka S, Takeda S, Harada A, Hirokawa N (1998) Targeted disruption of mouse conventional kinesin heavy chain, kif5B, results in abnormal perinuclear clustering of mitochondria. Cell 93:1147–1158.

Tatuch Y, Robinson BH (1993) The Mitochondrial DNA Mutation at 8993 Associated with NARP Slows the Rate of ATP Synthesis in Isolated Lymphoblast Mitochondria. Biochem Biophys Res Commun 192:124–128.

Tharaphan P, Chuenkongkaew WL, Luangtrakool K, Sanpachudayan T, Suktitipat B, Suphavilai R, Srisawat C, Sura T, Lertrit P (2006) Mitochondrial DNA Haplogroup Distribution in Pedigrees of Southeast Asian G11778A Leber Hereditary Optic Neuropathy. J Neuro-Ophthalmology 26:264–267.

Thompson AF, Levin LA (2010) Neuronal differentiation by analogs of staurosporine. Neurochem Int 56:554–560.

Thorburn DR, Rahman J, Rahman S (1993) Mitochondrial DNA-Associated Leigh Syndrome and NARP. University of Washington, Seattle.

Tian C, Murrin LC, Zheng JC (2009) Mitochondrial Fragmentation Is Involved in Methamphetamine-Induced Cell Death in Rat Hippocampal Neural Progenitor Cells Cookson MR, ed. PLoS One 4:e5546.

Torroni A, Huoponen K, Francalacci P, Petrozzi M, Morelli L, Scozzari R, Obinu D, Savontaus M-L, Wallace DC (1996) Classification of European mtDNAs From an Analysis of Three European Populations. Genetics 144.

Toyama EQ, Herzig S, Courchet J, Lewis TL, Losón OC, Hellberg K, Young NP, Chen H, Polleux F, Chan DC, Shaw RJ, Shaw RJ (2016) Metabolism. AMP-activated protein kinase mediates mitochondrial fission in response to energy stress. Science 351:275–281.

Trounce I, Neill S, Wallace DC (1994) Cytoplasmic transfer of the mtDNA nt 8993 T-->G (ATP6) point mutation associated with Leigh syndrome into mtDNA-less cells demonstrates cosegregation with a decrease in state III respiration and ADP/O ratio. Proc Natl Acad Sci U S A 91:8334–8338.

Trushina E et al. (2004) Mutant Huntingtin Impairs Axonal Trafficking in Mammalian Neurons In Vivo and In Vitro Mutant Huntingtin Impairs Axonal Trafficking in Mammalian Neurons In Vivo and In Vitro. Mol Cell Biol 24:8195–8209.

Tsao K, Aitken PA, Johns DR (1999) Smoking as an aetiological factor in a pedigree with Leber's hereditary optic neuropathy. Br J Ophthalmol 83:577–581.

Tun AW, Chaiyarit S, Kaewsutthi S, Katanyoo W, Chuenkongkaew W, Kuwano M, Tomonaga T, Peerapittayamongkol C, Thongboonkerd V, Lertrit P (2014) Profiling the mitochondrial proteome of Leber's Hereditary Optic Neuropathy (LHON) in Thailand: down-regulation of bioenergetics and mitochondrial protein quality control pathways in fibroblasts with the 11778G>A mutation. Yao Y-G, ed. PLoS One 9:e106779.

Twig G, Elorza A, Molina AJA, Mohamed H, Wikstrom JD, Walzer G, Stiles L, Haigh SE, Katz S, Las G, Alroy J, Wu M, Py BF, Yuan J, Deeney JT, Corkey BE, Shirihai OS (2008) Fission and selective fusion govern mitochondrial segregation and elimination by autophagy. EMBO J 27:433–446.

Uckun FM, Tuel-Ahlgren L, Song CW, Waddick K, Myers DE, Kirihara J, Ledbetter JA, Schieven GL (1992) Ionizing radiation stimulates unidentified tyrosine-specific protein kinases in human B-lymphocyte precursors, triggering apoptosis and clonogenic cell death. Proc Natl Acad Sci U S A 89:9005–9009.

Vale RD (2003) The Molecular Motor Toolbox for Intracellular Transport. Cell 112:467–480.

Valente AJ, Maddalena LA, Robb EL, Moradi F, Stuart JA (2017) A simple ImageJ macro tool for analyzing mitochondrial network morphology in mammalian cell culture. Acta Histochem 119:315–326.

Valente EM et al. (2004) Hereditary early-onset Parkinson's disease caused by mutations in PINK1. Science 304:1158–1160.

Van Bergen NJ, Crowston JG, Craig JE, Burdon KP, Kearns LS, Sharma S, Hewitt AW, Mackey DA, Trounce IA (2015) Measurement of Systemic Mitochondrial Function in Advanced Primary Open-Angle Glaucoma and Leber Hereditary Optic Neuropathy Vavvas D, ed. PLoS One 10:e0140919.

Van Bergen NJ, Wood JPM, Chidlow G, Trounce IA, Casson RJ, Ju W-K, Weinreb RN, Crowston JG (2009) Recharacterization of the RGC-5 Retinal Ganglion Cell Line. Investig Opthalmology Vis Sci 50:4267.

van Kuijk FJ (1991) Effects of ultraviolet light on the eye: role of protective glasses. Environ Health Perspect 96:177–184.

Vandecasteele G, Szabadkai G, Rizzuto R (2002) Mitochondrial calcium homeostasis: Mechanisms and molecules. IUBMB Life 52:213–219.

Vanopdenbosch L, Dubois B, D'Hooghe MB, Meire F, Carton H (2000) Mitochondrial mutations of Leber's hereditary optic neuropathy: a risk factor for multiple sclerosis. J Neurol 247:535–543.

Vergani L, Martinuzzi A, Carelli V, Cortelli P, Montagna P, Schievano G, Carrozzo R, Angelini C, Lugaresi E (1995) MtDNA Mutations Associated with Leber′s Hereditary Optic Neuropathy: Studies on Cytoplasmic Hybrid (Cybrid) Cells. Biochem Biophys Res Commun 210:880–888.

Vierbuchen T, Ostermeier A, Pang ZP, Kokubu Y, Südhof TC, Wernig M (2010) Direct conversion of fibroblasts to functional neurons by defined factors. Nature 463:1035–1041.

Vilkki J, Ott J, Savontaus ML, Aula P, Nikoskelainen EK (1991) Optic atrophy in Leber hereditary optic neuroretinopathy is probably determined by an X-chromosomal gene closely linked to DXS7. Am J Hum Genet 48:486–491.

Vives-Bauza C, Zhou C, Huang Y, Cui M, de Vries RLA, Kim J, May J, Tocilescu MA, Liu W, Ko HS, Magrané J, Moore DJ, Dawson VL, Grailhe R, Dawson TM, Li C, Tieu K, Przedborski S (2010) PINK1-dependent recruitment of Parkin to mitochondria in mitophagy. Proc Natl Acad Sci U S A 107:378–383.

Wallace DC (1999) Mitochondrial diseases in man and mouse. Science 283:1482–1488.

Wallace DC, Brown MD, Lott MT (1999) Mitochondrial DNA variation in human evolution and disease. Gene 238:211–230.

Wallace DC, Singh G, Lott MT, Hodge JA, Schurr TG, Lezza AM, Elsas LJ, Nikoskelainen EK (1988a) Mitochondrial DNA mutation associated with Leber's hereditary optic neuropathy. Science 242:1427–1430.

Wallace DC, Zheng X, Lott MT, Shoffner JM, Hodge JA, Kelley RI, Epstein CM, Hopkins LC (1988b) Familial mitochondrial encephalomyopathy (MERRF): Genetic, pathophysiological, and biochemical characterization of a mitochondrial DNA disease. Cell 55:601–610.

Wan X, Pei H, Zhao M, Yang S, Hu W, He H, Ma S, Zhang G, Dong X, Chen C, Wang D, Li B (2016) Efficacy and Safety of rAAV2-ND4 Treatment for Leber's Hereditary Optic Neuropathy. Sci Rep 6:21587.

Wang C, Youle RJ (2009) The role of mitochondria in apoptosis*. Annu Rev Genet 43:95–118.

Wang L, Dong J, Cull G, Fortune B, Cioffi GA (2003) Varicosities of Intraretinal Ganglion Cell Axons in Human and Nonhuman Primates. Investig Opthalmology Vis Sci 44:2.

Wang X, Su B, Fujioka H, Zhu X (2008) Dynamin-Like Protein 1 Reduction Underlies Mitochondrial Morphology and Distribution Abnormalities in Fibroblasts from Sporadic Alzheimer's Disease Patients. Am J Pathol 173:470–482.

Wang X, Winter D, Ashrafi G, Schlehe J, Wong YLL, Selkoe D, Rice S, Steen J, LaVoie MJJ, Schwarz TLL (2011) PINK1 and Parkin target Miro for phosphorylation and degradation to arrest mitochondrial motility. Cell 147:893–906.

Wang ZX, Tan L, Yu JT (2014) Axonal Transport Defects in Alzheimer's Disease. Mol Neurobiol:1309–1321.

Westermann B (2010) Mitochondrial fusion and fission in cell life and death. Nat Rev Mol Cell Biol 11:872–884.

Willems PHGM, Smeitink JAM, Koopman WJH (2009) Mitochondrial dynamics in human NADH:ubiquinone oxidoreductase deficiency. Int J Biochem Cell Biol 41:1773–1782.

Williams KP, Sobral BW, Dickerman AW (2007) A robust species tree for the alphaproteobacteria. J Bacteriol 189:4578–4586.

Wolstenholme DR (1992) Animal Mitochondrial DNA: Structure and Evolution. Int Rev Cytol 141:173–216.

Wong A, Cavelier L, Collins-Schramm HE, Seldin MF, McGrogan M, Savontaus M-L, Cortopassi GA (2002) Differentiation-specific effects of LHON mutations introduced into neuronal NT2 cells. Hum Mol Genet 11:431–438.

Wong A, Cortopassi G (1997) mtDNA Mutations Confer Cellular Sensitivity to Oxidant Stress That Is Partially Rescued by Calcium Depletion and Cyclosporin A. Biochem Biophys Res Commun 239:139–145.

Wood JPM, Lascaratos G, Bron AJ, Osborne NN (2008) The influence of visible light exposure on cultured RGC-5 cells. Mol Vis 14:334–344.

Wredenberg A, Wibom R, Wilhelmsson H, Graff C, Wiener HH, Burden SJ, Oldfors A, Westerblad H, Larsson N-G (2002) Increased mitochondrial mass in mitochondrial myopathy mice. Proc Natl Acad Sci 99:15066–15071.

Xie L, Cheng L, Xu G, Zhang J, Ji X, Song E (2017) The novel cyclophilin D inhibitor compound 19 protects retinal pigment epithelium cells and retinal ganglion cells from UV radiation. Biochem Biophys Res Commun 487:807–812.

Y-W-Man P, Griffiths PG, Brown DT, Howell N, Turnbull DM, Chinnery PF (2003) The epidemiology of Leber hereditary optic neuropathy in the North East of England. Am J Hum Genet 72:333–339.

Yang D, Oyaizu Y, Oyaizu H, Olsen GJ, Woese CR (1985) Mitochondrial origins. Proc Natl Acad Sci U S A 82:4443–4447.

Yang Y, Gehrke S, Imai Y, Huang Z, Ouyang Y, Wang J-W, Yang L, Beal MF, Vogel H, Lu B (2006) Mitochondrial pathology and muscle and dopaminergic neuron degeneration caused by inactivation of Drosophila Pink1 is rescued by Parkin. Proc Natl Acad Sci U S A 103:10793–10798.

Yang Y, Ouyang Y, Yang L, Beal MF, McQuibban A, Vogel H, Lu B (2008) Pink1 regulates mitochondrial dynamics through interaction with the fission/fusion machinery. Proc Natl Acad Sci 105:7070–7075.

Yao R, Yoshihara M, Osada H (1997) Specific activation of a c-Jun NH2-terminal kinase isoform and induction of neurite outgrowth in PC-12 cells by staurosporine. J Biol Chem 272:18261–18266.

Yen M-Y, Chen C-S, Wang A-G, Wei Y-H (2002) Increase of mitochondrial DNA in blood cells of patients with Leber's hereditary optic neuropathy with 11778 mutation. Br J Ophthalmol 86:1027–1030.

Yen M-Y, Wang A-G, Wei Y-H (2006) Leber's hereditary optic neuropathy: a multifactorial disease. Prog Retin Eye Res 25:381–396.

Yen MY, Lee JF, Liu JH, Wei YH (1998) Energy charge is not decreased in lymphocytes of patients with Leber's hereditary optic neuropathy with the 11,778 mutation. J Neuroophthalmol 18:84–85.

Yiu E, Tai G, Peverill R, Lee K, Croft K, Mori T, Stephenson S, Lockhart P, Sarsero J, Churchyard A, Evans-Galea M, Ryan M, Corben L, Delatycki M (2013) An Open Label Clinical Pilot Study of Resveratrol as a Treatment for Friedreich Ataxia (S43.006). Neurology 80.

Yoo AS, Sun AX, Li L, Shcheglovitov A, Portmann T, Li Y, Lee-Messer C, Dolmetsch RE, Tsien RW, Crabtree GR (2011) MicroRNA-mediated conversion of human fibroblasts to neurons. Nature 476:228–231.

Yoon Y, Krueger EW, Oswald BJ, McNiven MA (2003) The mitochondrial protein hFis1 regulates mitochondrial fission in mammalian cells through an interaction with the dynamin-like protein DLP1. Mol Cell Biol 23:5409–5420.

Youle RJ, Bliek AM Van Der, Complementation FP, Mitochondria BD, Fusion M, Proteins F (2012) REVIEW Mitochondrial Fission, Fusion, and Stress. Science (80-) 337:1062–1065.

Youle RJ, Narendra DP (2011) Mechanisms of mitophagy. Nat Rev Mol Cell Biol 12:9–14.

Young RW (1988) Solar radiation and age-related macular degeneration. Surv Ophthalmol 32:252–269.

Yu-Wai-Man P, Griffiths PG, Hudson G, Chinnery PF (2008) Inherited mitochondrial optic neuropathies. J Med Genet 46:145–158.

Yu-Wai-Man P, Griffiths PG, Hudson G, Chinnery PF (2009) Inherited mitochondrial optic neuropathies. J Med Genet 46:145–158.

Yu-Wai-Man P, Votruba M, Moore AT, Chinnery PF (2014) Treatment strategies for inherited optic neuropathies: past, present and future. Eye (Lond) 28:521–537.

Zakharov IA, Yarovoy BP (1977) Cytoduction as a new tool in studying the cytoplasmic heredity in yeast. Mol Cell Biochem 14:15–18.

Zanna C, Ghelli A, Porcelli AM, Carelli V, Martinuzzi A, Rugolo M (2003) Apoptotic cell death of cybrid cells bearing Leber's hereditary optic neuropathy mutations is caspase independent. Ann N Y Acad Sci 1010:213–217.

Zanna C, Ghelli A, Porcelli AM, Karbowski M, Youle RJ, Schimpf S, Wissinger B, Pinti M, Cossarizza A, Vidoni S, Valentino ML, Rugolo M, Carelli V (2008) OPA1 mutations associated with dominant optic atrophy impair oxidative phosphorylation and mitochondrial fusion. Brain 131:352–367.

Zanna C, Ghelli A, Porcelli AM, Martinuzzi A, Carelli V, Rugolo M (2005) Caspase-independent death of Leber's hereditary optic neuropathy cybrids is driven by energetic failure and mediated by AIF and Endonuclease G. Apoptosis 10:997–1007.

Zeviani M, Moraes CT, DiMauro S, Nakase H, Bonilla E, Schon EA, Rowland LP (1988) Deletions of mitochondrial DNA in Kearns-Sayre syndrome. Neurology 38:1339–1346.

Zhang A-M, Jia X, Zhang Q, Yao Y-G (2010) No association between the SNPs (rs3749446 and rs1402000) in the PARL gene and LHON in Chinese patients with m.11778G>A. Hum Genet 128:465–468.

Zhang X, Jones D, Gonzalez-Lima F (2002) Mouse model of optic neuropathy caused by mitochondrial complex I dysfunction. Neurosci Lett 326:97–100.

Zhang Y, Huang H, Wei S, Gong Y, Li H, Dai Y, Zhao S, Wang Y, Yan H (2014) Characterization of macular thickness changes in Leber's hereditary optic neuropathy by optical coherence tomography. BMC Ophthalmol 14:105.

Ziccardi L, Sadun F, De Negri AM, Barboni P, Savini G, Borrelli E, Morgia C La, Carelli V, Parisi V (2013) Retinal Function and Neural Conduction Along the Visual Pathways in Affected and Unaffected Carriers With Leber's Hereditary Optic Neuropathy. Investig Opthalmology Vis Sci 54:6893.

Züchner S et al. (2004) Mutations in the mitochondrial GTPase mitofusin 2 cause Charcot-Marie-Tooth neuropathy type 2A. Nat Genet 36:449–451.

Appendix.

Supplementary figures

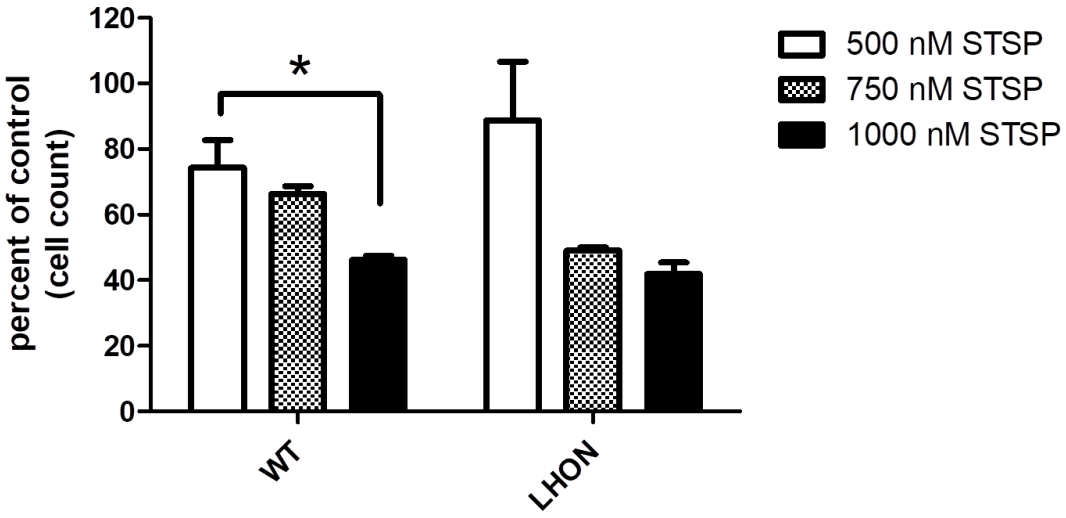

Figure A.1 Greater cell viability in WT fibroblasts treated with 500 nM STSP compared to 1000 nM and no difference in cell viability in LHON fibroblasts for the three concentrations of STSP tested in glucose media.

WT and LHON fibroblasts grown in glucose media were treated with 0 (vehicle control), 500, 750 and 1000 nM STSP for 24 hours and cell viability was measured by averaging the counts of Hoechst stained nuclei in four representative 100x fields (4-5 replicates) per coverslip where n represents the number of coverslips which is then expressed as a percent of vehicle treated (0.04% ethyl acetate) controls. Data are presented as Means ± Standard Error of Mean. There was a significant effect of STSP concentration on cell viability in WT fibroblasts ($F(2, 4) = 9.599$, $p = 0.0297$. Post hoc comparisons using Bonferroni's multiple comparison test showed the mean cell count (percent of vehicle control) of WT fibroblasts treated with 500 nM STSP (74.35 ± 8.425, n = 2) was significantly greater than WT fibroblasts treated with 1000 nM (46.26 ± 1.220, n = 2). However the mean cell count of WT fibroblasts treated with 750 nM STSP (66.37 ± 2.329, n = 3) was not significantly different from WT fibroblasts treated with either 500 nM (74.35 ± 8.425, n = 2) or 1000 nM (46.26 ± 1.220, n = 2). There was no significant effect of STSP concentration on cell viability in LHON fibroblasts ($F(2, 3) = 5.812$, $p = 0.0929$).

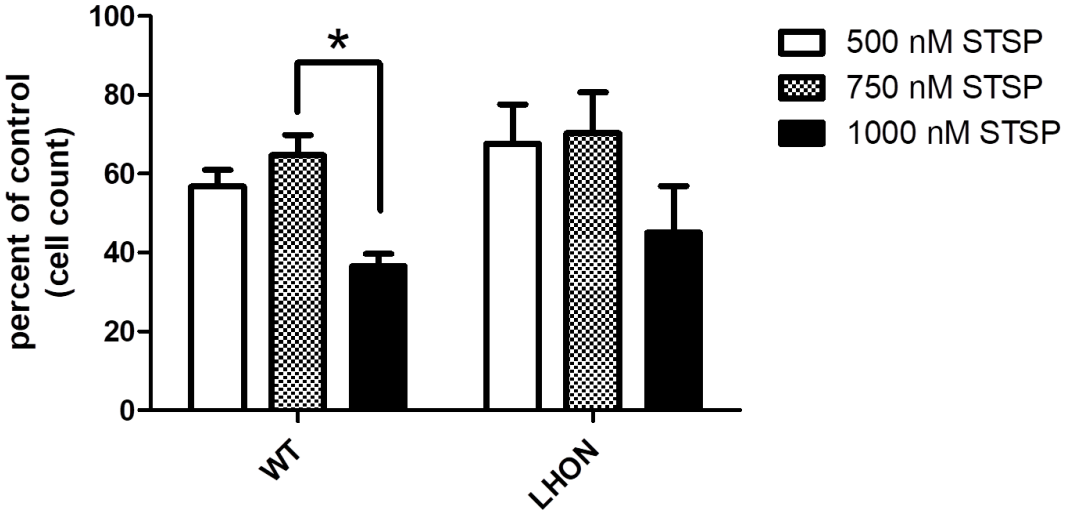

Figure A.2 Greater cell viability in WT fibroblasts treated with 750 nM compared to 1000 nM and no difference in cell viability in LHON fibroblasts for the three concentrations of STSP tested in glucose-free galactose media.

WT and LHON fibroblasts grown in glucose-free galactose media were treated with 0 (vehicle control), 500, 750 and 1000 nM STSP for 24 hours and cell viability was measured by averaging the counts of Hoechst stained nuclei in four representative 100x fields (4-5 replicates) per coverslip where n represents the number of coverslips which is then expressed as a percent of vehicle treated (0.04% ethyl acetate) controls. Data are presented as Means ± Standard Error of Mean. There was a significant effect of STSP concentration on cell viability in WT fibroblasts ($F(2, 5) = 12.47$, $p = 0.0114$. Post hoc comparisons using Bonferroni's multiple comparison test showed the mean cell count (percent of vehicle control) of WT fibroblasts treated with 750 nM STSP (64. 73 ± 5.111, n = 3) was significantly greater than WT fibroblasts treated with 1000 nM STSP (36.58 ± 3.149, n = 3). However, the mean cell count of WT fibroblasts treated with 500 nM STSP (56.83 ± 4.097, n = 2) was not significantly different from WT fibroblasts treated with either 750 nM (64. 73 ± 5.111, n = 3) or 1000 nM (36.58 ± 3.149, n = 3). There was no significant effect of STSP concentration on cell viability in LHON fibroblasts ($F(2, 6) = 1.275$, $p = 0.3457$.

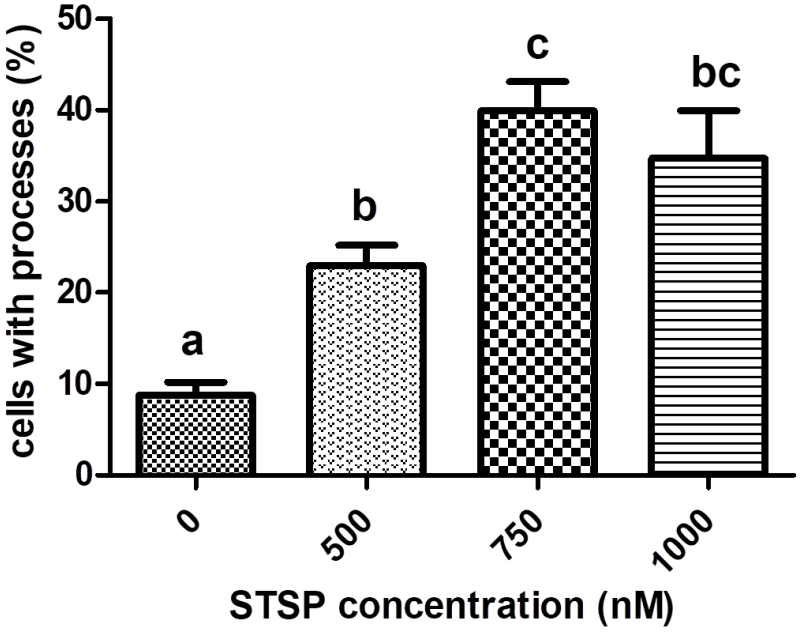

Figure A.3 Percentage of WT fibroblasts with processes were significantly greater for cells treated with 750 nM STSP compared to 0 nM (vehicle control) and 500 nM STSP but was not signficantly different from cells treated with 1000 nM STSP in glucose media.

WT and LHON fibroblasts grown in glucose media were treated with 0 (vehicle control), 500, 750 and 1000 nM STSP for 24 hours and stained with H_2DCFDA and Hoechst 33342, 1-hour following STSP treatment termination. There was a significant effect on STSP concentration on the percentage of cells containing processes ($F(3, 14) = 15.72$, $p < 0.0001$. Post hoc comparisons using Bonferroni's multiple comparison test showed the percentage of cells with processes were significantly greater for cells treated with all three concentrations of STSP compared to vehicle controls (8.780 ± 1.146, n = 5). Furthermore, the percentage of cells with processes were significantly greater for cells treated with 750 nM STSP (39.94 ± 3.153, n = 3) compared to 500 nM STSP (22.94 ± 2.234, n = 5) but was not significantly different from cells treated with 1000 nM STSP (34.74 ± 5.181, n = 5). However, there was no significant difference in the percentage of cells with processes in cells treated with 500 nM STSP (22.94 ± 2.234, n = 5) and the cells treated with 1000 nM STSP (34.74 ± 5.181, n = 5).